NASA TECHNICAL NOTE

NASA TN D-5686

c. 1

NASA TN D-5686

WIND-TUNNEL INVESTIGATION OF THE AERODYNAMIC PRESSURES ON THE APOLLO LAUNCH ESCAPE VEHICLE CONFIGURATION

by William C. Moseley, Jr., and B. J. Wells

Manned Spacecraft Center
Houston, Texas

NATIONAL AERONAUTICS AND SPACE ADMINISTRATION • WASHINGTON, D. C. • APRIL 1970

1. REPORT NO.	2. GOVERNMENT ACCESSION NO.	3. RECIPIENT'S CAT
NASA TN D-5686		

4. TITLE AND SUBTITLE
WIND-TUNNEL INVESTIGATION OF THE AERODYNAMIC PRESSURES ON THE APOLLO LAUNCH ESCAPE VEHICLE CONFIGURATION

5. REPORT DATE
April 1970

6. PERFORMING ORGANIZATION CODE

7. AUTHOR(S)
William C. Moseley, Jr., MSC, and
B. J. Wells, Federal Electric Corp.

8. PERFORMING ORGANIZATION REPORT NO.
MSC S-230

9. PERFORMING ORGANIZATION NAME AND ADDRESS
Manned Spacecraft Center
Houston, Texas 77058

10. WORK UNIT NO.
914-50-10-03-72

11. CONTRACT OR GRANT NO.

12. SPONSORING AGENCY NAME AND ADDRESS
National Aeronautics and Space Administration
Washington, D. C. 20546

13. REPORT TYPE AND PERIOD COVERED
Technical Note

14. SPONSORING AGENCY CODE

15. SUPPLEMENTARY NOTES

16. ABSTRACT
A program of wind-tunnel tests was conducted at Mach numbers from 0.4 to 9.08 to determine the pressure distribution on the Apollo launch escape vehicle. Data are presented for the angle-of-attack range from 0° to 136°. The data are plotted as the pressure coefficient versus the physical position of the pressure orifice to show some effects of the flow separator, of the escape-tower length, and of the angle of attack on the pressure distribution over the command module in the presence of the escape tower.

17. KEY WORDS (SUPPLIED BY AUTHOR)
* Aerodynamic Characteristics
* Launch Escape Vehicle
* Manned Spacecraft
* Pressure Coefficient
* Apollo
* Wind Tunnel
* Command Module
* Scale Model

18. DISTRIBUTION STATEMENT
Unclassified - Unlimited

19. SECURITY CLASSIFICATION (THIS REPORT)	20. SECURITY CLASSIFICATION (THIS PAGE)	21. NO. OF PAGES	22. PRICE*
None	None	71	$3.00

*For sale by the Clearinghouse for Federal Scientific and Technical Information
Springfield, Virginia 22151

CONTENTS

TABLES

FIGURES

WIND-TUNNEL INVESTIGATION OF THE AERODYNAMIC PRESSURES ON THE APOLLO LAUNCH ESCAPE VEHICLE CONFIGURATION

By William C. Moseley, Jr., and B. J. Wells*
Manned Spacecraft Center

SUMMARY

Wind-tunnel tests were conducted to determine the effects of the tower length and the flow separator on the pressure distribution over the Apollo launch escape vehicle configuration at Mach numbers from 0.4 to 9.08 and at an angle-of-attack range from 0° to 136°. The data are presented as the pressure coefficient versus the physical position of the pressure orifice.

From the data, aerodynamic loads on the Apollo launch escape vehicle can be determined by the analysis of the pressure distribution over the surface of the command module.

INTRODUCTION

In late 1959, personnel from several NASA Centers recommended a circumlunar flight and an earth-orbiting laboratory program to be called the Apollo Program. The program was initiated and assigned to the NASA Space Task Group. On May 25, 1961, the Apollo Program was reoriented to achieve a manned lunar landing, as part of the continuing program of space exploration following Project Mercury and the Gemini Program.

In the formulation of the design criteria, the guidelines established by NASA personnel were developed around certain stipulations. With these stipulations and with the aerodynamic limitations, many possible types of configurations were considered. The basic configuration chosen for development was the one that was determined to be most practical for the development of the state of the art at that time.

The launch escape vehicle (LEV) provides an escape capability in the event of a malfunction of the booster or spacecraft (refs. 1 and 2). The LEV is used only during the atmospheric portion of the ascent trajectory and is composed of an escape rocket, the escape tower, and the command module (CM). After the atmospheric portion of the ascent trajectory is completed, the escape tower and rocket are jettisoned.

*ITT Federal Electric Corp.

The basic design of the Apollo spacecraft had to be evaluated thoroughly. One method used to evaluate the basic design was the Apollo wind-tunnel testing program (AWTTP), which is discussed more thoroughly in reference 3. Some of the early wind-tunnel studies that were used to support and verify the design are reported in references 4 to 7.

The AWTTP incorporated tests that were designed to gather data necessary for the study of atmospheric abort situations involving the LEV from the launch pad through atmospheric flight. Also, investigations were made to determine the aerodynamic pressures on the LEV configuration. From these tests, the load distribution was determined and was used to define the criteria for the structural design of the vehicle.

The purposes of this paper are to present the pressure distributions on the LEV and to indicate the effects of the tower length and the flow separator on the pressure distribution. Pressure distribution data will be presented with minimal analysis and discussion because the static and dynamic stability characteristics of the LEV configurations have been discussed in references 1 and 2.

Pressure coefficients have been determined at Mach numbers from 0.4 to 9.08 and at an angle-of-attack range from 0° to 136°. The data are presented in plotted form as the pressure coefficient versus the physical position of the pressure orifice.

SYMBOLS

Some of the symbols defined in this section are illustrated in figure 1, where the positive directions of the body axes system are also shown.

C_p pressure coefficient, $\frac{P_x - P_\infty}{q_\infty}$

D maximum diameter of CM (154 in., full scale)

M Mach number

P_x orifice pressure

P_∞ free-stream static pressure

q_∞ free-stream dynamic pressure, $\left(\frac{1}{2}\right)\rho V^2$

R radius of CM corners, in.

R_A radius of CM apex, in.

R_C radius of CM corner, in.

R_O radius of CM aft heat shield, in.

Re Reynolds number, $\frac{\rho}{\mu}VD$ (based on maximum diameter of CM)

r radius of CM at maximum diameter, in.

s distance to orifice from center of launch face (CM apex) of the model measured along the surface of the model, in.

V velocity

X, Y, Z body reference axes

α angle of attack in the X-Z plane, deg

λ angle of instrumentation plane relative to pitch plane, deg

μ coefficient of viscosity of the fluid

ρ air density

MODELS AND TEST TECHNIQUES

The model nomenclature and full-scale dimensions are presented in table I. The 0.045- and the 0.02-scale static pressure models were tested. The test conditions are presented in table II.

The body axes system is presented in figure 1, and sketches of the test models are presented in figure 2. The basic rocket configurations are shown in figures 2(a), 2(b), and 2(c); the shorter rocket shown in figure 2(a) was tested early in the AWTTP. The longer rocket (figs. 2(b) and 2(c)) represents a later configuration as the design developed. The escape-rocket towers shown in figures 2(d) and 2(e) represent early configurations before the nominal 120-inch length was selected (fig 2(f)). The tower bracing was modified later to the hour-glass configuration to preclude escape-rocket impingement on the upper portion of the tower. The apex radius of the basic CM design, configuration C, was decreased for the final CM design, configuration C_2 (fig. 2(g)).

Sketches of the models which define the pressure-orifice location that were used in the different wind tunnels are shown in figure 3. These static pressure orifices are located over the surface of the Apollo CM. The physical position of the individual orifice is indicated by the ratio of s/r and λ (fig. 3) for the various models tested.

Each orifice is connected to a calibrated transducer and a known reference pressure is used. The data are presented as pressure coefficients and are defined by $C_p = \frac{P_x - P_\infty}{q_\infty}$.

FACILITIES

The broad range of expected flight conditions (M, Re, and α) and the limitations of any single wind tunnel to simulate all these conditions required the use of a number of test facilities. The wind-tunnel test facilities used to obtain pressure distributions of the LEV configuration, along with the tunnel size and capability, are listed in table III.

TEST CONDITIONS AND ACCURACY

The test conditions for each facility are given in table II.

In the North American Aviation 7- by 7-Foot Trisonic Wind Tunnel (NAA-TWT), the C_p was repeated to within ± 0.012, based on transducer sensitivities and the repeatability of the data system. The pressure measuring accuracy of the Jet Propulsion Laboratory 20-Inch Supersonic Wind Tunnel (JPL-20SWT) and the Jet Propulsion Laboratory 21-Inch Hypersonic Wind Tunnel (JPL-21HWT) is ± 0.25 percent of the full-scale transducer capability or approximately ± 0.008 C_p.

SUMMARY OF RESULTS

The stability and dynamic characteristics of the Apollo LEV configuration (with the power on and off) were investigated; the results are presented in reference 1. The results of a configuration investigation during the development of the LEV configuration are presented in reference 2.

The pressure-coefficient data presented as plotted data in this paper represent measurements over the CM in the presence of the escape tower and rocket. Limited data were determined for orifice locations on the escape rocket. These data are presented in table IV for Mach numbers of 0.4, 1.05, and 1.34. The orifice locations for the escape-rocket measurements are defined in figure 3(c). Limited measurements were made both with and without the flow separator.

Effects of the flow separator on the CM pressure distribution are shown in figure 4. Data are given for $\lambda = 0°$ only. Data for the same data plane are given in figure 5 to show some of the effects that varying the escape-tower length has on the pressure distribution. Data for nominal tower lengths of 85 and 119 inches are presented.

The data presented in figures 6 to 19 are for the nominal tower length of 120 inches. Although the tower bracing was modified later to the hour-glass spacing to preclude escape-rocket impingement at the upper braces of the tower, the data presented are considered indicative of the final flight configuration. These figures present data for the three data planes ($\lambda = 0°$, $\lambda = 45°$, and $\lambda = 90°$) at angles of attack from 0° to 136° and at Mach numbers from 0.4 to 9.08.

Manned Spacecraft Center
National Aeronautics and Space Administration
Houston, Texas, December 22, 1969
914-50-10-03-72

REFERENCES

1. Moseley, William C., Jr.; and Hondros, James G.: Aerodynamic Stability Characteristics of the Apollo Launch Escape Vehicle. NASA TN D-3964, 1967.

2. Moseley, William C., Jr.; and Bowen, Francis Evans: Aerodynamic Characteristics Determined During Development of the Apollo Launch Escape Vehicle Configuration. NASA TN D-5208, 1969.

3. Moseley, William C., Jr.; and Martino, Joseph C.: Apollo Wind Tunnel Testing Program — Historical Development of General Configurations. NASA TN D-3748, 1967.

4. Morgan, James R.; and Fournier, Roger H.: Static Longitudinal Characteristics of a 0.07-Scale Model of a Proposed Apollo Spacecraft at Mach Numbers of 1.57 to 4.65. NASA TM X-603, 1961.

5. Pearson, Albin O.: Wind-Tunnel Investigation of the Static Longitudinal Aerodynamic Characteristics of Models of Reentry and Atmospheric-Abort Configurations of a Proposed Apollo Spacecraft at Mach Numbers from 0.30 to 1.20. NASA TM X-604, 1961.

6. Pearson, Albin O.: Wind-Tunnel Investigation of the Static Longitudinal Aerodynamic Characteristics of a Modified Model of a Proposed Apollo Atmospheric-Abort Configuration at Mach Numbers from 0.30 to 1.20. NASA TM X-686, 1962.

7. Fournier, Roger H.; and Corlett, William A.: Aerodynamic Characteristics in Pitch of Several Models of the Apollo Abort System from Mach 1.57 to 2.16. NASA TM X-910, 1964.

TABLE I. - MODEL FULL-SCALE DIMENSIONS

(a) Command module

Parameters	Command module	
	C	C_2
Maximum diameter, in.	154.0	154.0
Radius of spherical blunt end, in.	184.8	184.8
Corner radius, in.	7.7	7.7
Nose-cone semiangle, deg	33	33
Nose-cone vertex radius, in.	15.4	9.19

(b) Tower structure

Parameters	Tower structure		
	T_7	T_8 [a]	T_{14} [b]
Total length, in.	119.0	82.75	114.62
Number of longitudinal members	4	4	4
Diameter of longitudinal members, in.	3.2	3.2	3.51
Diameter of cross braces, in.	2.5	3.2	2.51
Distance between attach points at CM			
Plan view, in.	52.0	52.0	50.67
Side view, in.	52.0	52.0	46.84
Distance between attach points at escape motor, in.	12.0	30.0	36.06

[a]Tower structure T_8 has a stiffener gusset at the base of the tower; the height of the stiffener plate is 18 inches.

[b]Tower structure T_{14} has stiffener gussets at the base and the top of the tower; the height of the stiffener plate at the base is 4.44 inches.

(c) Escape motor

Parameters	Escape motor		
	E_{10}	E_{53} [a]	E_{54} [b]
Total length (including jettison motor), in.	226.9	279.67	279.67
Length of jettison motor, in.	48.0	48.00	48.00
Diameter of escape and jettison motor, in.	26.0	26.00	26.00
Nose-included angle, deg	30	30	30
Diameter of escape-rocket base, in.	47.0	54.60	54.60
Skirt flare angle, deg: min	30	36.55	34

[a]The skirt of model E_{53} has a 28.89-inch-diameter ring installed at the interface of the skirt and the rocket.

[b]Model E_{54} has a 65.0-inch-diameter disk located 18 inches forward of the rocket base with a 51.07-inch-diameter fairing extending aft from the disk to the intersection of the flared skirt.

TABLE II. - TEST CONDITIONS

Figure no.	Facility	Configuration	Scale, percent	Mach no.	Re × 10^{-6}
4	NAA-TWT[a]	$E_{53/54}T_{14}C_2$	0.045	0.4 1.05 1.34	0.87 1.01 1.09
5	JPL-20SWT[b]	$E_{10}T_{7/8}C$	.02	1.48	1.68
6	NAA-TWT	$E_{53}T_{14}C_2$	.045	.4	.87
7	NAA-TWT	$E_{53}T_{14}C_2$	.045	.7	.91
8	NAA-TWT	$E_{53}T_{14}C_2$	.045	.9	.96
9	NAA-TWT	$E_{53}T_{14}C_2$	.045	.95	.98
10	NAA-TWT	$E_{53}T_{14}C_2$	.045	1.05	1.01
11	NAA-TWT	$E_{53}T_{14}C_2$	.045	1.20	1.06
12	NAA-TWT	$E_{53}T_{14}C_2$	.045	1.34	1.099
13	JPL-20SWT	$E_{10}T_7C$	.02	1.48	1.68
14	JPL-20SWT	$E_{10}T_7C$	.02	2.01	1.71
15	JPL-20SWT	$E_{10}T_7C$	.02	3.01	.98
16	JPL-20SWT	$E_{10}T_7C$	.02	3.99	.75
17	JPL-20SWT	$E_{10}T_7C$	.02	5.01	.76
18	JPL-21HWT[c]	$E_{10}T_7C$	.02	7.35	.748
19	JPL-21HWT	$E_{10}T_7C$	.02	9.08	.456

[a]North America Aviation-Trisonic Wind Tunnel.

[b]Jet Propulsion Laboratory 20-inch Supersonic Wind Tunnel.

[c]Jet Propulsion Laboratory 21-inch Hypersonic Wind Tunnel.

TABLE III. - TEST FACILITIES

Facility	Size of test section	Mach no. range	Re range $\times 10^{-6}$/ft
Continuous tunnels			
JPL-20SWT	18 by 20 in.	1.3 to 5	0.4 to 6
JPL-21HWT	21 by 15 to 28 in.	5 to 9.5	.25 to 36
Intermittent tunnel			
NAA-TWT	7 ft^2	0.2 to 3.5	5 to 14

TABLE IV.- PRESSURE COEFFICIENTS OF THE ESCAPE ROCKET

(a) Configuration E_{54}

α, deg	Mach no.	Pressure coefficients				
		Orifice 2	Orifice 3	Orifice 4	Orifice 5	Orifice 6
0	0.4	0.5982	-0.1121	-0.1321	-0.1567	0.4761
5	.4	.6978	-.2167	-.1597	-.1603	.4682
10	.4	.9374	-.3158	-.2979	-.2807	.4692
15	.4	1.0064	-.4402	-.4820	-.3728	.8610
20	.4	.9708	-.4937	-.5352	-.4249	.7484
0	1.05	.7042	.0303	.0250	.0175	.6579
5	1.05	.9330	-.0089	.0441	-.0024	.5825
10	1.05	.9168	-.0071	.0392	-.0037	.5718
20	1.05	1.1970	-.1997	-.2265	-.1611	1.0006
0	1.34	.5962	.1875	.2366	.1888	.4827
5	1.34	1.0514	.1138	.2019	.1158	.5311
10	1.34	1.4811	.0679	.0843	.0625	.9251
15	1.34	1.4762	-.0127	-.0449	.0229	1.1442
20	1.34	1.4091	-.0514	-.0651	-.0306	1.1402

(b) Configuration E_{53}

α, deg	Mach no.	Pressure coefficients				
		Orifice 8	Orifice 7	Orifice 4	Orifice 9	Orifice 10
0	0.4	0.5446	0.5804	-0.0012	0.5506	0.5242
5	.4	.6105	.6312	-.1001	.4950	.4535
10	.4	.5880	.6062	-.1793	.4127	.3709
15	.4	.5956	.6249	-.2465	.3219	.3568
20	.4	.5652	.5762	-.2794	.2605	.2867
0	1.05	.7187	.7840	.2126	.7699	.7036
5	1.05	.8603	.8806	.1869	.6642	.5631
10	1.05	.8519	.8785	.0839	.6405	.6364
20	1.05	.8184	.8435	.0029	.4859	.5026
0	1.34	.6157	.7545	.3315	.7344	.5557
5	1.34	1.2298	1.2571	.3043	.4755	.5311
10	1.34	1.1411	1.1686	.2454	.6531	.7182
15	1.34	1.0631	1.0905	.1304	.7280	.7859
20	1.34	1.0148	1.0435	.0949	.6985	.7507

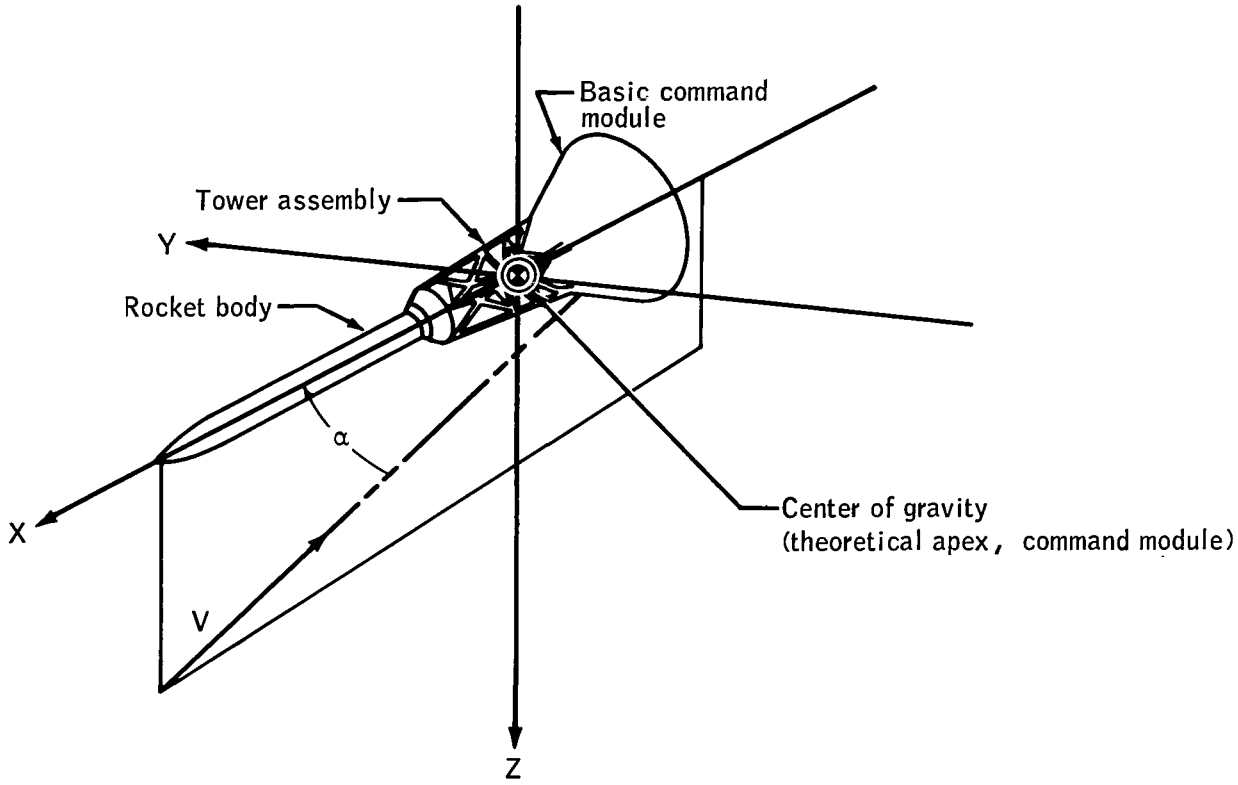

Figure 1.- Sketch showing system of body axes. Arrows indicate positive directions.

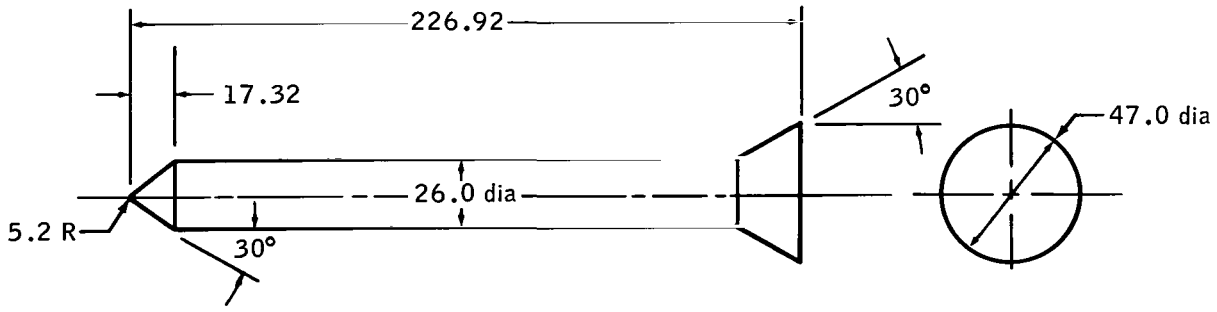

Full scale dimensions in inches
Drawing not to scale

(a) Escape rocket E_{10}.

Figure 2.- Test models.

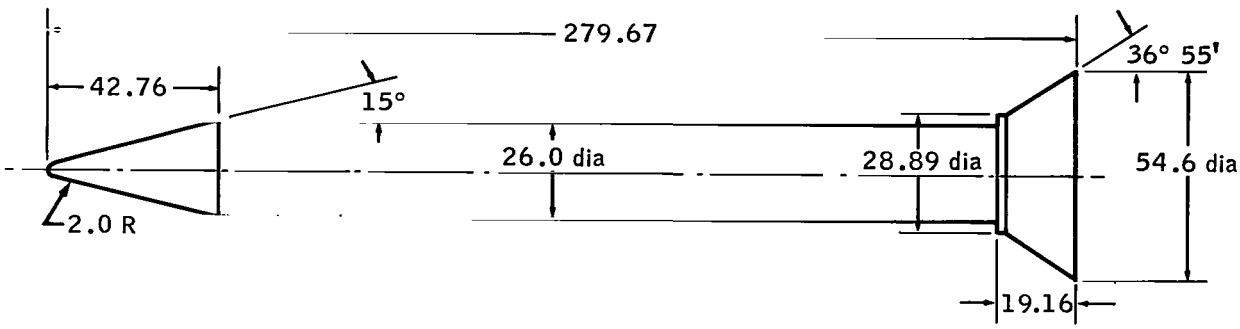

(b) Escape rocket E_{53}.

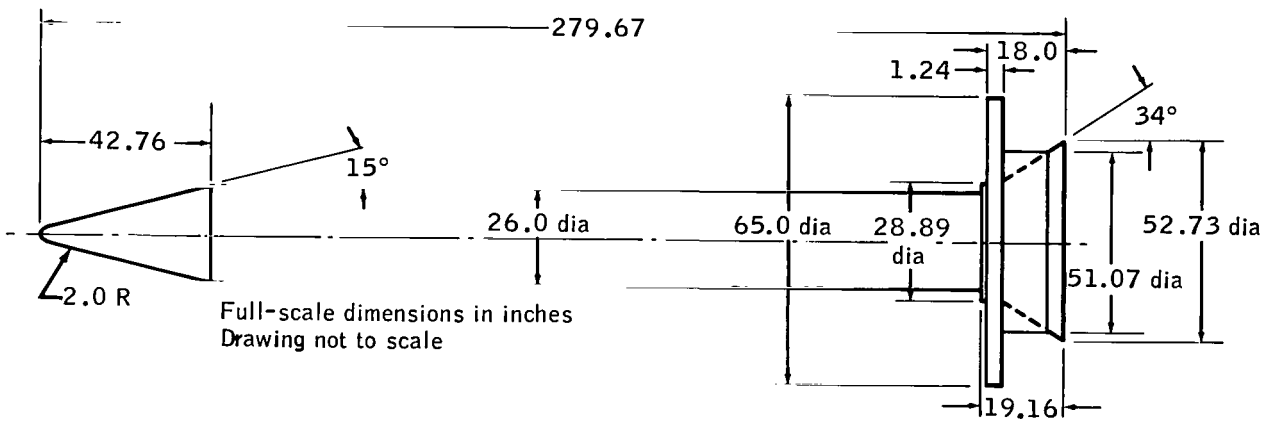

(c) Escape rocket E_{54}.

Figure 2. - Continued.

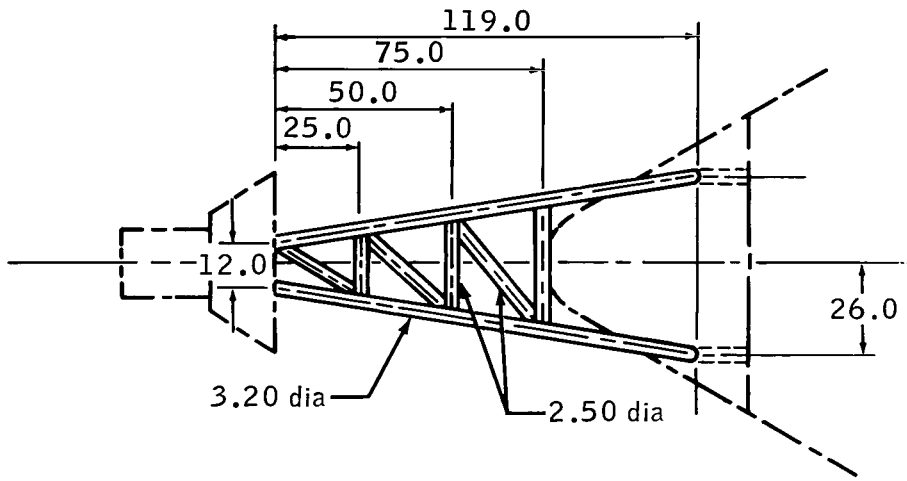

(d) Escape-tower structure T_7.

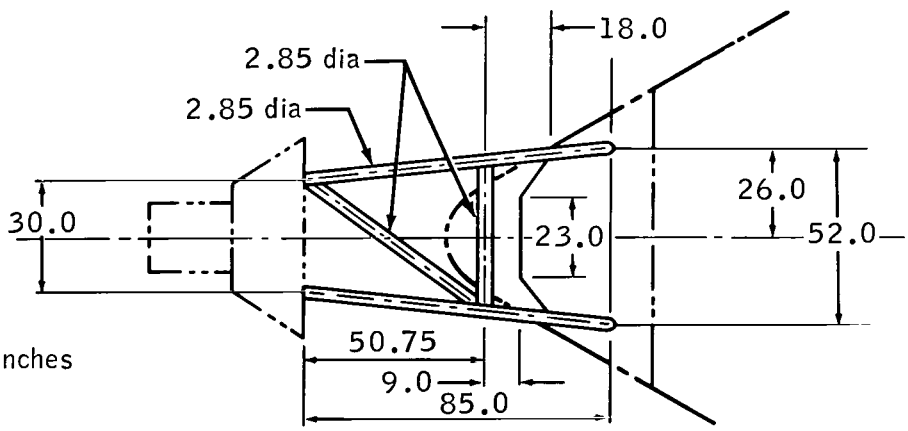

Full-scale dimensions in inches
Drawing not to scale

(e) Escape-tower structure T_8.

Figure 2. - Continued.

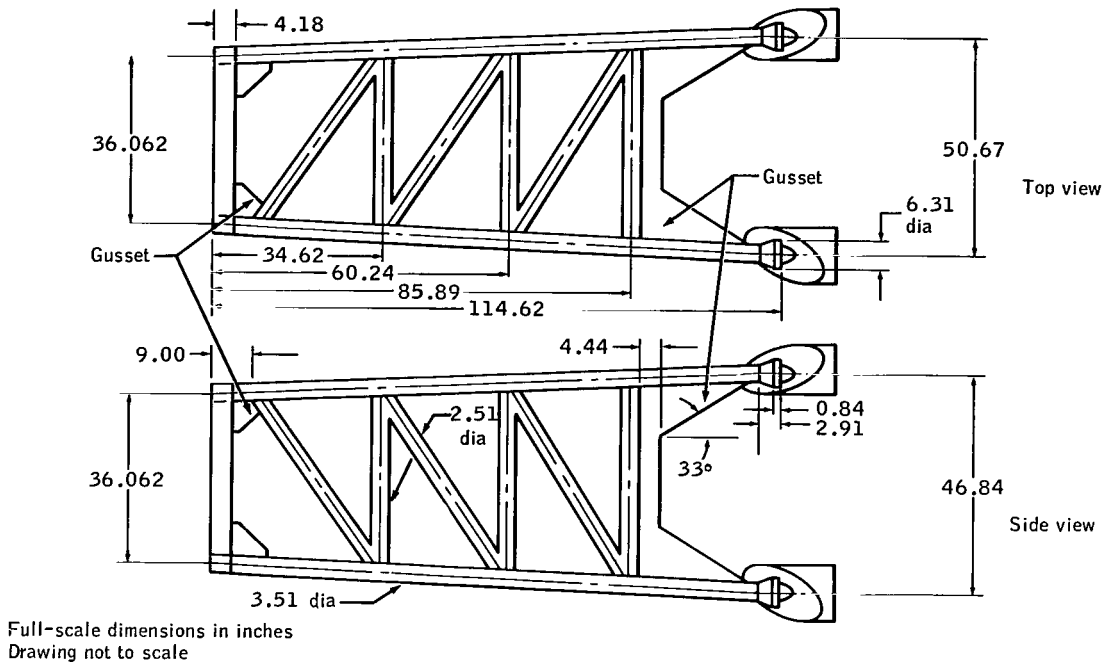

(f) Escape-tower structure T_{14}.

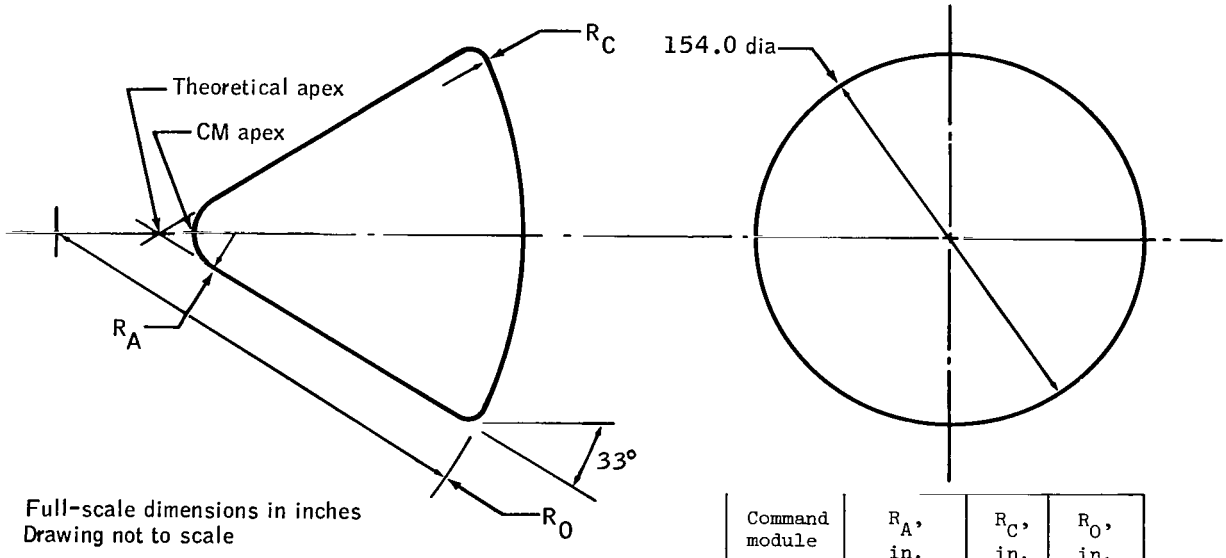

Command module	R_A, in.	R_C, in.	R_O, in.
C_1	15.4	7.7	184.8
C_2	9.152	7.7	184.8

(g) Command modules.

Figure 2. - Concluded.

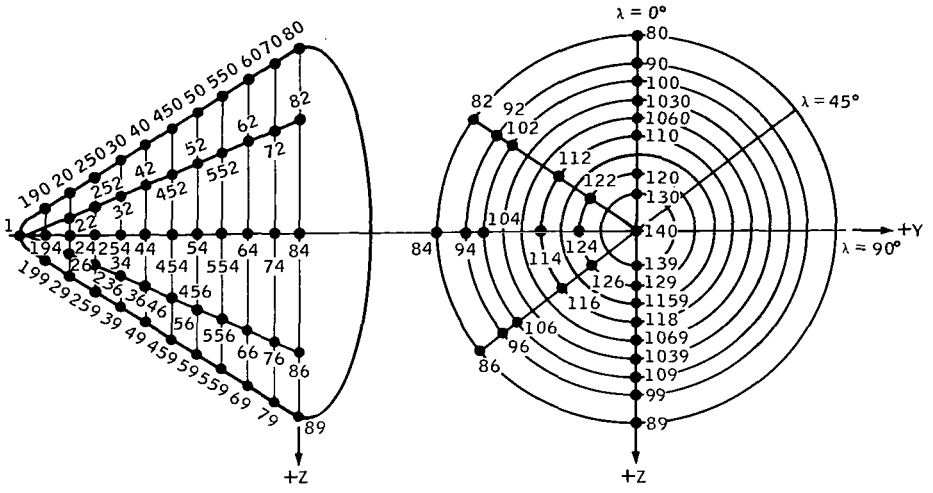

Model orifice no.	λ, deg	Apex forward, s/r	Model orifice no.	λ, deg	Apex forward, s/r
1	0	0.000	45	45	-0.497
190	0	-.064	452	45	-1.046
20	0	-.118	52	45	-1.155
250	0	-.208	552	45	-1.372
30	0	-.289	62	45	-1.589
40	0	-.497	72	45	-1.742
450	0	-.936	82	45	-1.797
50	0	-1.155	92	45	-1.854
550	0	-1.372	102	45	-1.918
60	0	-1.589	112	45	-2.085
70	0	-1.742	122	45	-2.354
80	0	-1.797	140	45	2.886
90	0	-1.854	126	45	2.354
100	0	-1.918	116	45	2.085
1030	0	-1.979	106	45	1.918
1060	0	-2.034	96	45	1.854
110	0	-2.085	86	45	1.797
120	0	-2.354	76	45	1.742
130	0	-2.626	66	45	1.589
140	0	2.886	556	45	1.372
139	0	2.626	56	45	1.155
129	0	2.354	456	45	.936
1159	0	2.143	46	45	.497
119	0	2.085	36	45	.289
1069	0	2.034	256	45	.208
1039	0	1.979	26	45	.118
109	0	1.918	1	90	.000
99	0	1.854	194	90	.064
89	0	1.797	24	90	.118
79	0	1.742	254	90	.208
69	0	1.589	34	90	.289
559	0	1.372	44	90	.497
59	0	1.155	454	90	.936
459	0	.936	54	90	1.155
49	0	.497	554	90	1.372
39	0	.289	64	90	1.589
259	0	.208	74	90	1.742
29	0	.118	84	90	1.797
199	0	.064	94	90	1.854
1	45	-.000	104	90	1.918
22	45	-.118	114	90	2.085
252	45	-.208	124	90	2.354
32	45	-.289	140	90	2.886

(a) Configuration C 0.02-scale pressure model. Apex forward: positive s in positive Z-direction.

Figure 3.- Pressure-orifice locations.

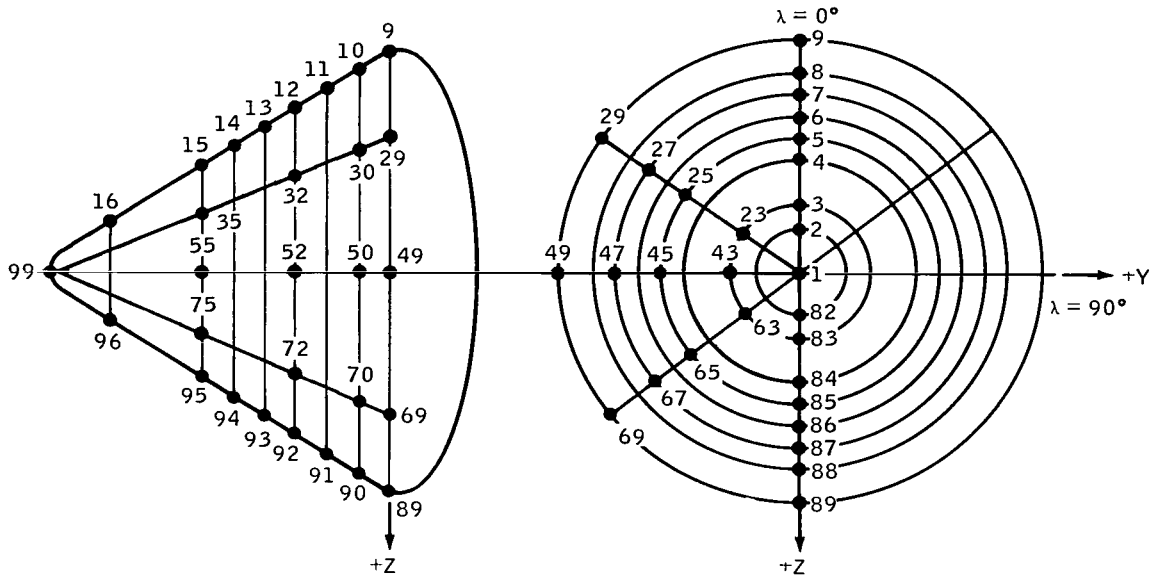

Model orifice no.	λ, deg	Apex forward, s/r	Model orifice no.	λ, deg	Apex forward, s/r
99	0	0.000	94	0	0.686
16	0	-.253	95	0	.470
15	0	-.470	96	0	.253
14	0	-.686	99	45	.000
13	0	-.902	35	45	-.470
12	0	-1.118	32	45	-1.118
11	0	-1.334	30	45	-1.550
10	0	-1.550	29	45	-1.765
9	0	-1.765	27	45	-2.052
8	0	-1.914	25	45	-2.322
7	0	-2.052	23	45	-2.586
6	0	-2.118	1	45	2.846
5	0	-2.322	63	45	2.586
4	0	-2.455	65	45	2.322
3	0	-2.586	67	45	2.052
2	0	-2.716	69	45	1.765
1	0	2.846	70	45	1.550
82	0	2.716	72	45	1.118
83	0	2.586	75	45	.470
84	0	2.455	99	90	.000
85	0	2.322	55	90	.470
86	0	2.188	52	90	1.118
87	0	2.052	50	90	1.550
88	0	1.914	49	90	1.765
89	0	1.765	47	90	2.052
90	0	1.550	45	90	2.322
91	0	1.334	43	90	2.586
92	0	1.118	1	90	2.846
93	0	.902			

(b) Configuration C_2 0.045-scale pressure model. Apex forward: positive s in positive Z-direction.

Figure 3.- Continued.

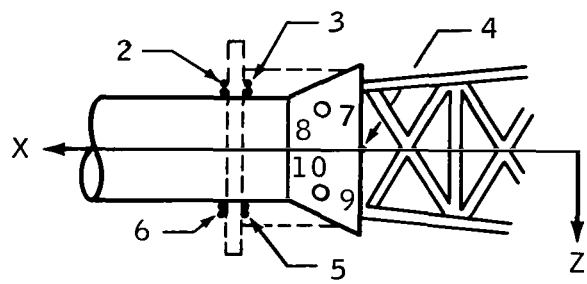

Note: E_{54} configuration taps 2, 3, 6, and 5 become taps 8, 7, 10, and 9 in the E_{53} configuration. Taps 8 and 10 are on the left side of the rocket.

(c) Escape-rocket motor.

Figure 3. - Concluded.

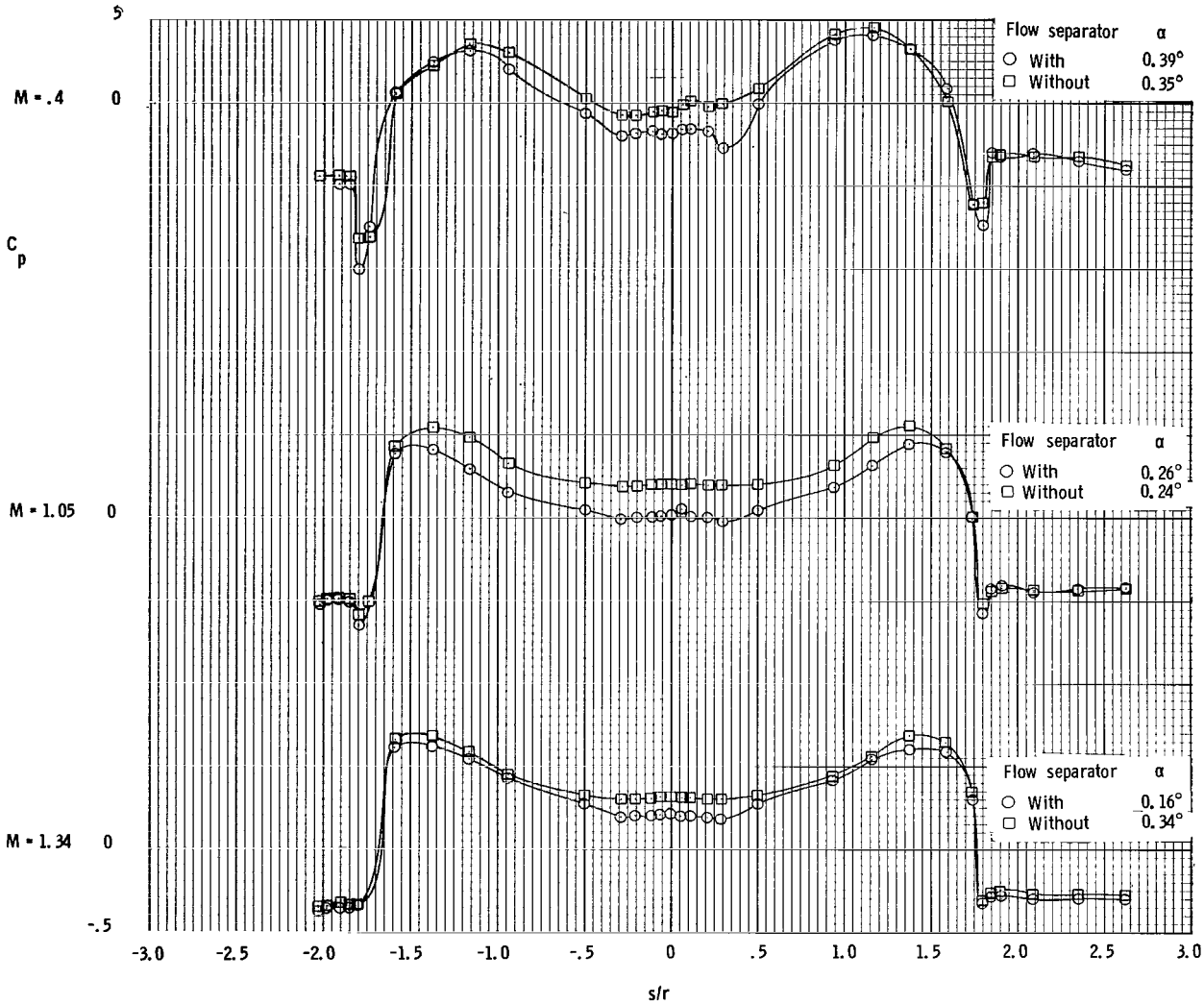

(a) α range is from 0.16° to 0.39°.

Figure 4. - Effect of flow separator on C_p with increasing Mach number at $\lambda = 0°$. Data are for the command module only, in the presence of the escape tower and the rocket.

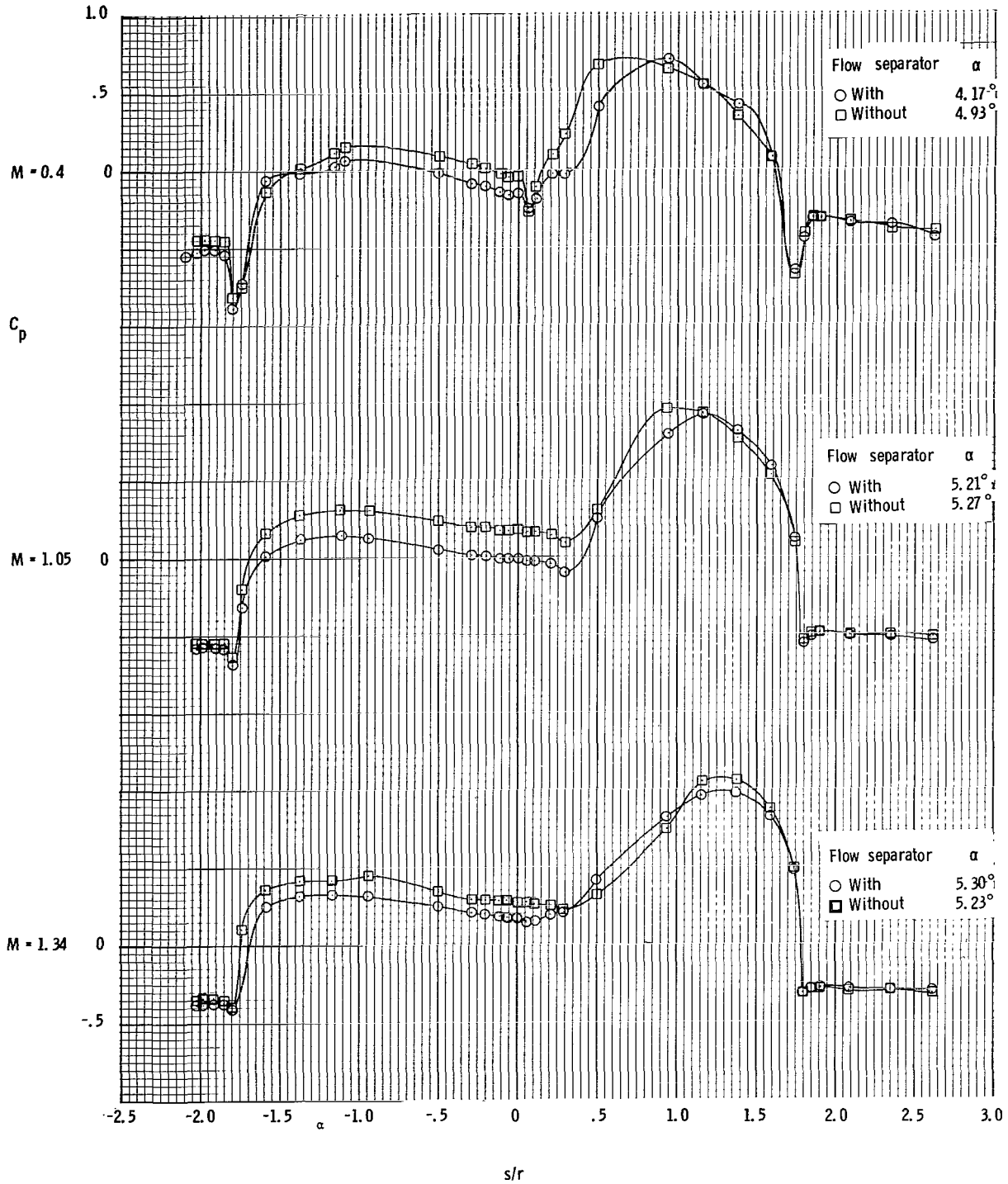

(b) α range is from 4.17° to 5.30°.

Figure 4. - Continued.

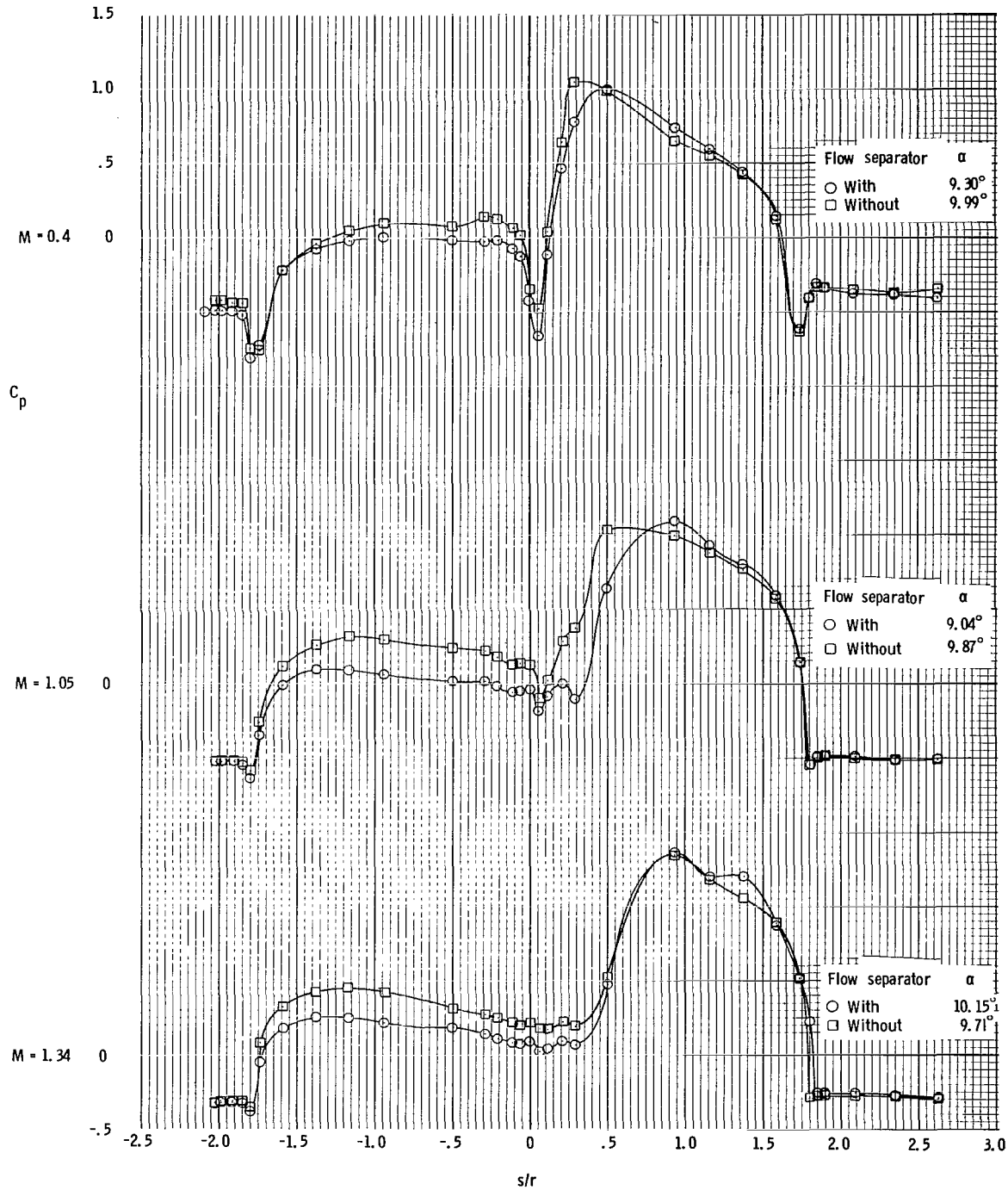

(c) α range is from 9.04° to 10.15°.

Figure 4. - Continued.

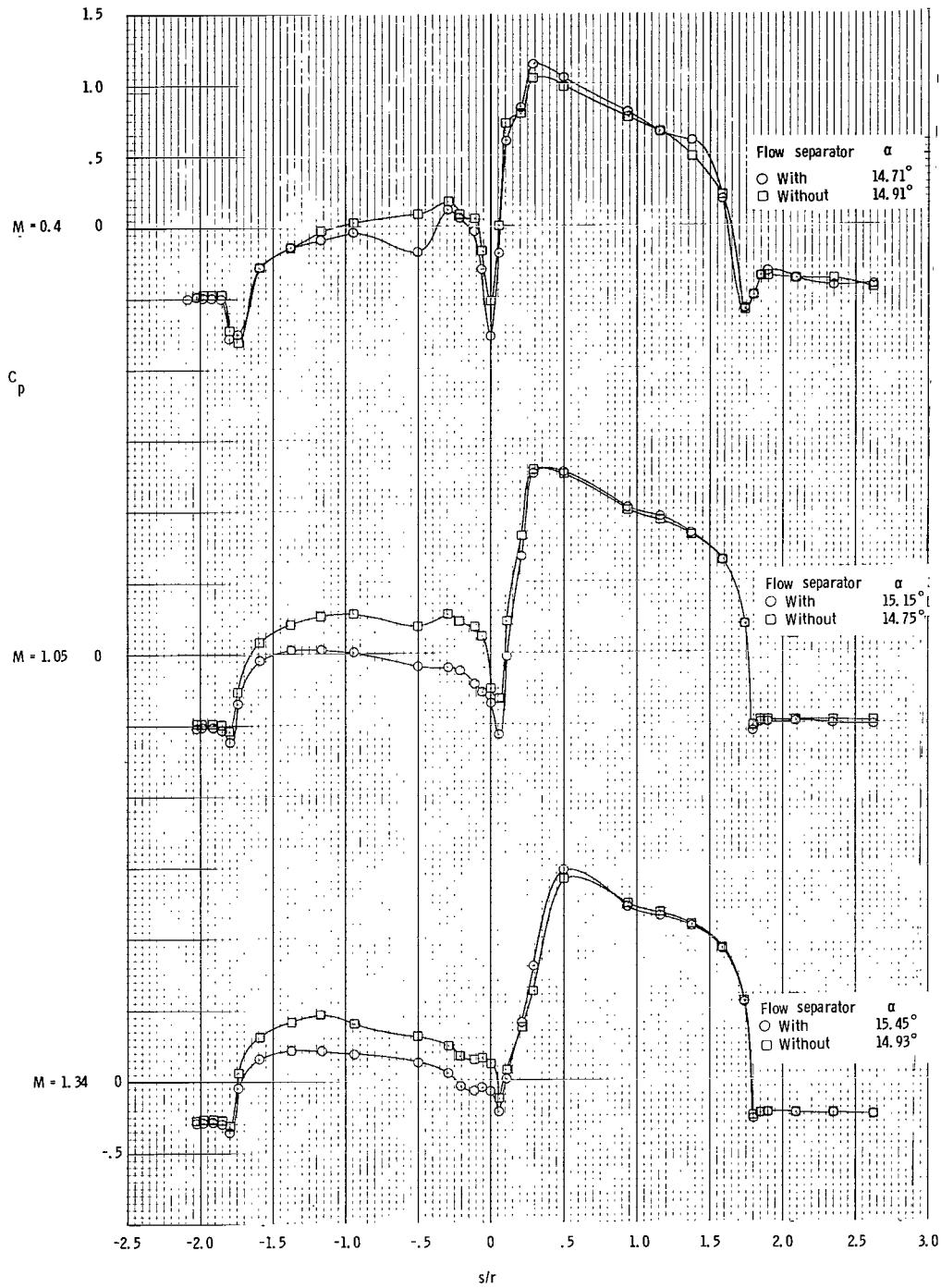

(d) α range is from 14.71° to 15.45°.

Figure 4. - Continued.

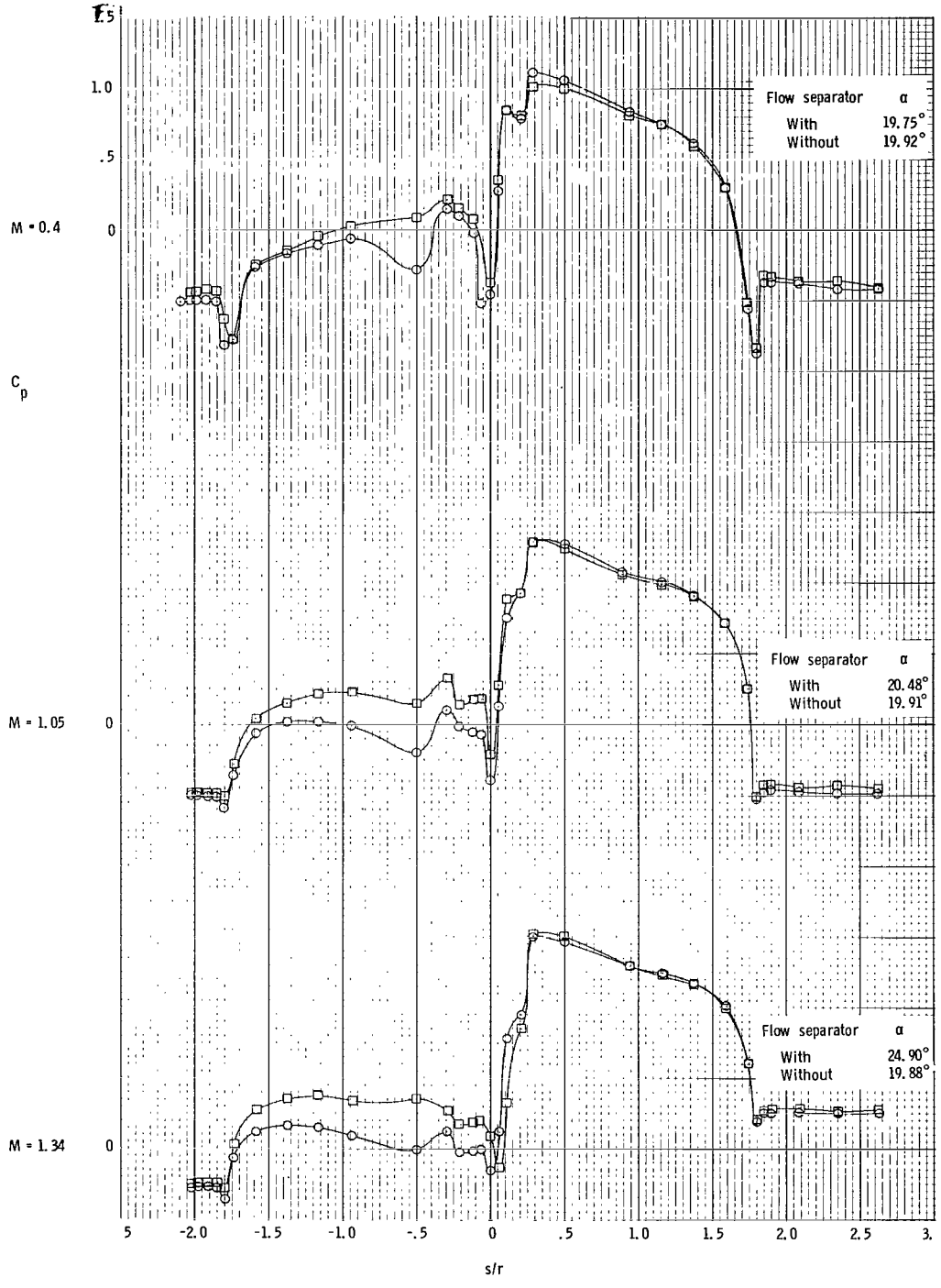

(e) α range is from 19.75° to 24.90°.

Figure 4. - Concluded.

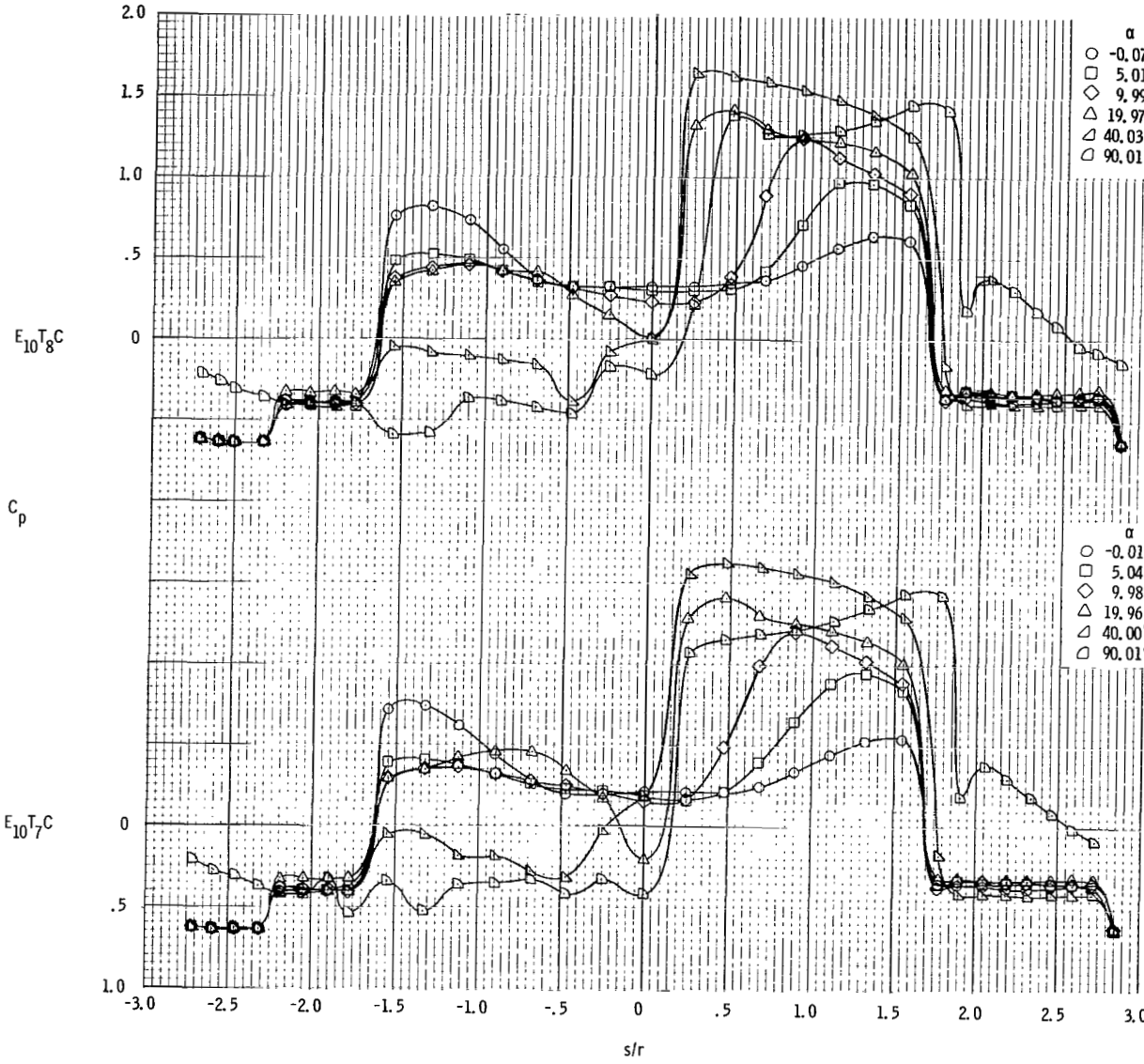

Figure 5. - Effect of tower length on C_p at $\lambda = 0°$ when $M = 1.48$ and the α range is from 0° to 90°. Data are for the command module only, in the presence of the escape tower and the rocket.

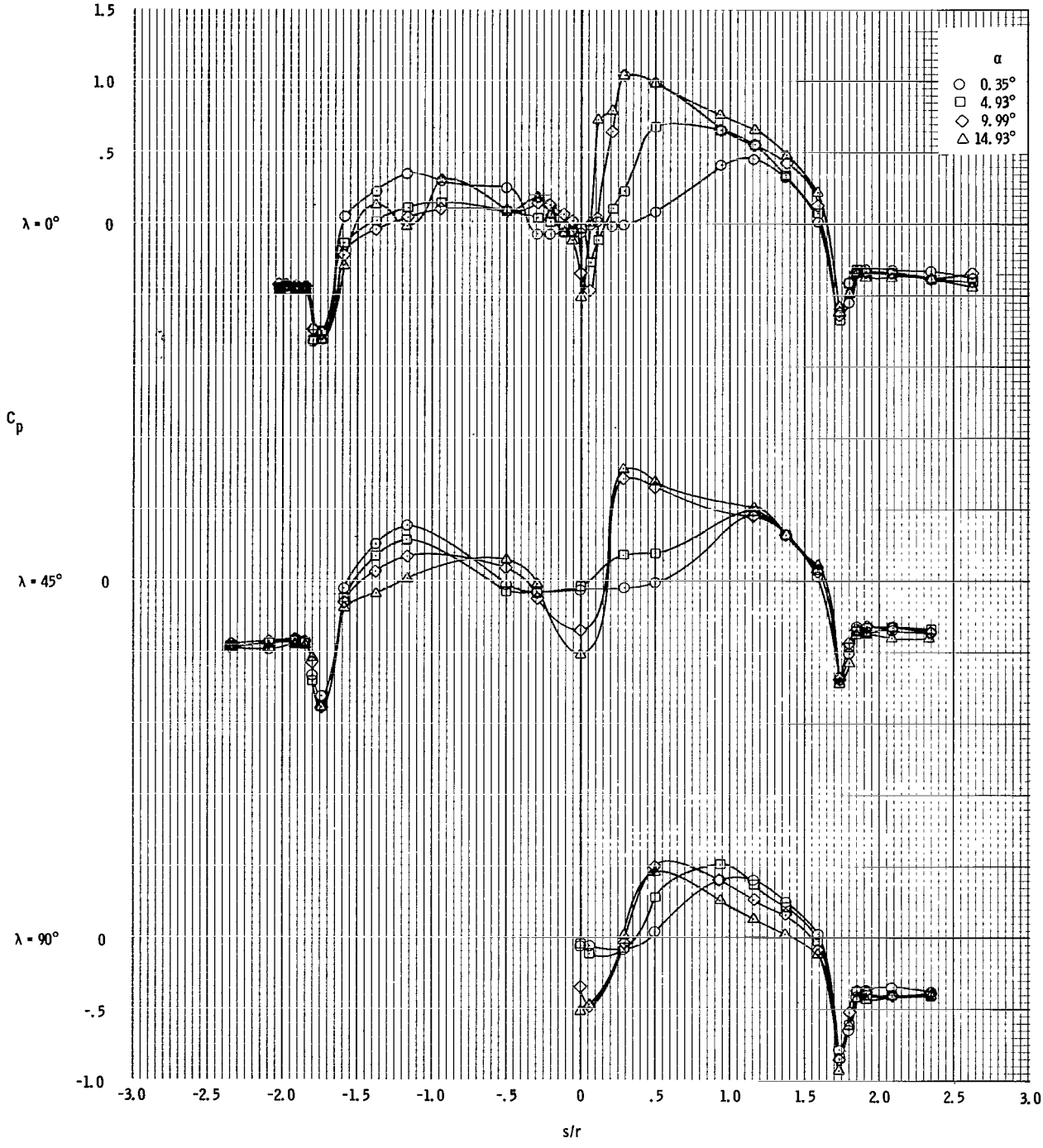

(a) α range is from 0° to 15°.

Figure 6. - Variation of C_p with increasing α at $\lambda = 0°$, $\lambda = 45°$, and $\lambda = 90°$ at $M = 0.4$. Data are for the command module only, in the presence of the escape tower and the rocket.

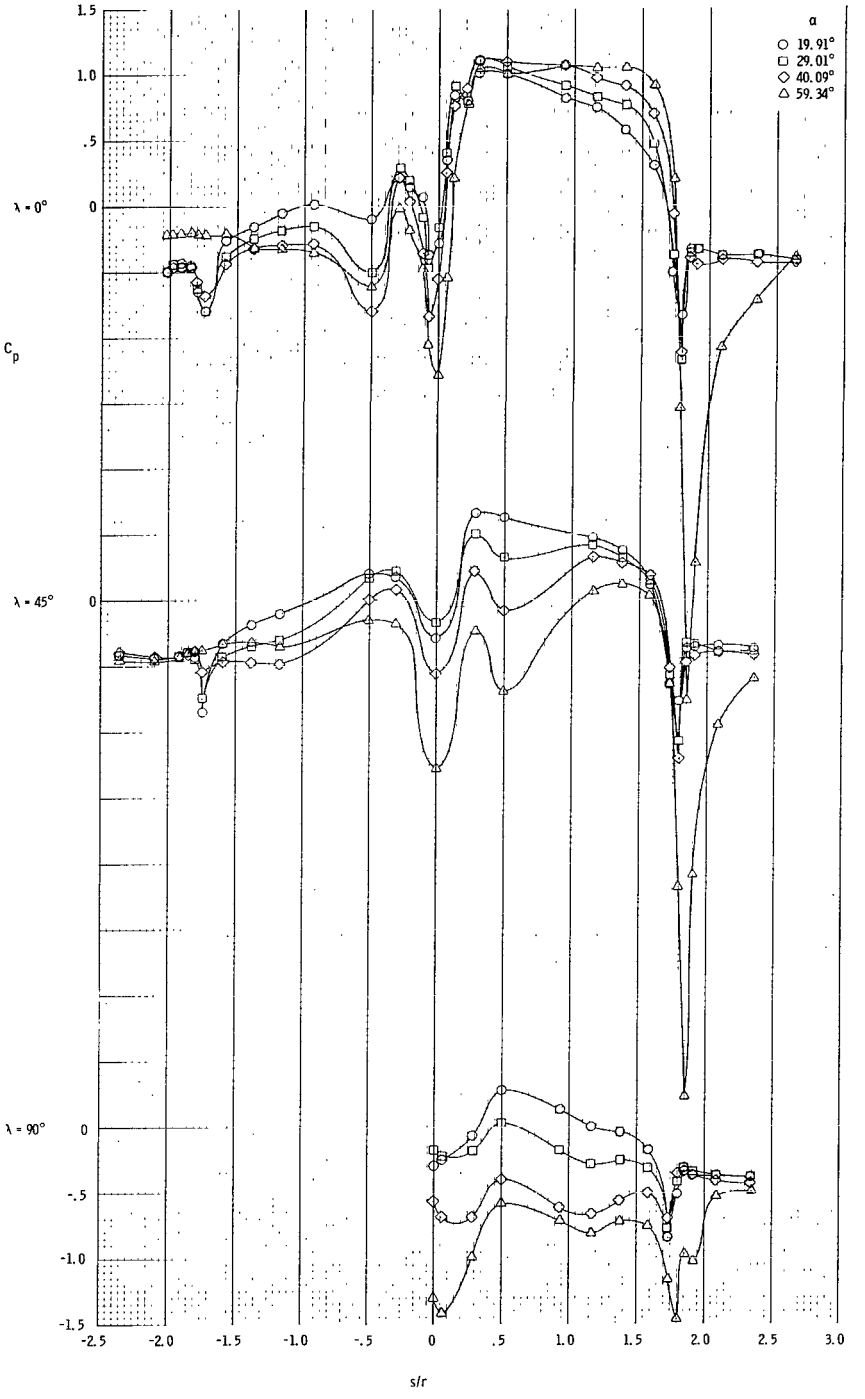

(b) α range is from 20° to 60°.

Figure 6. - Continued.

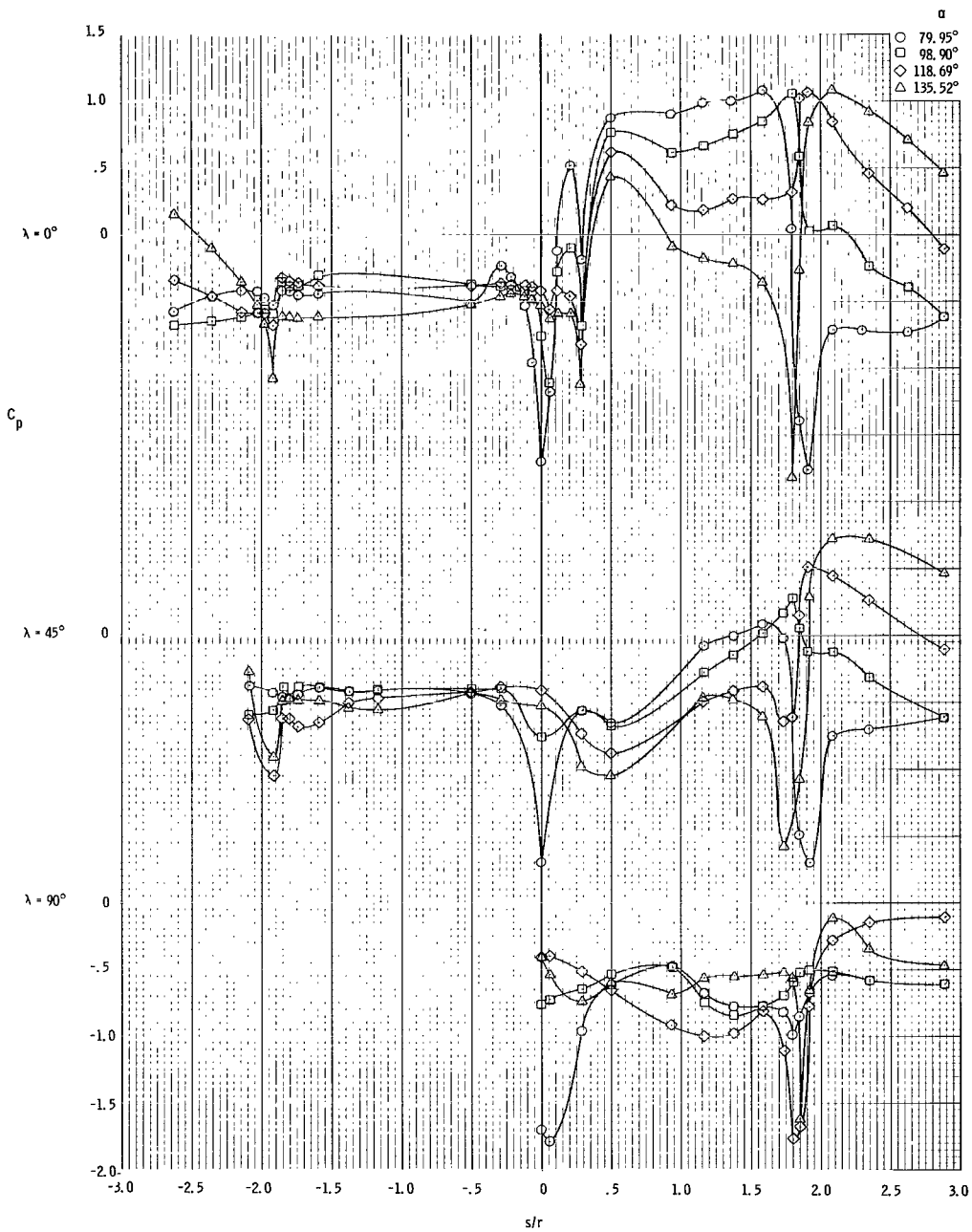

(c) α range is from 80° to 136°.

Figure 6. - Concluded.

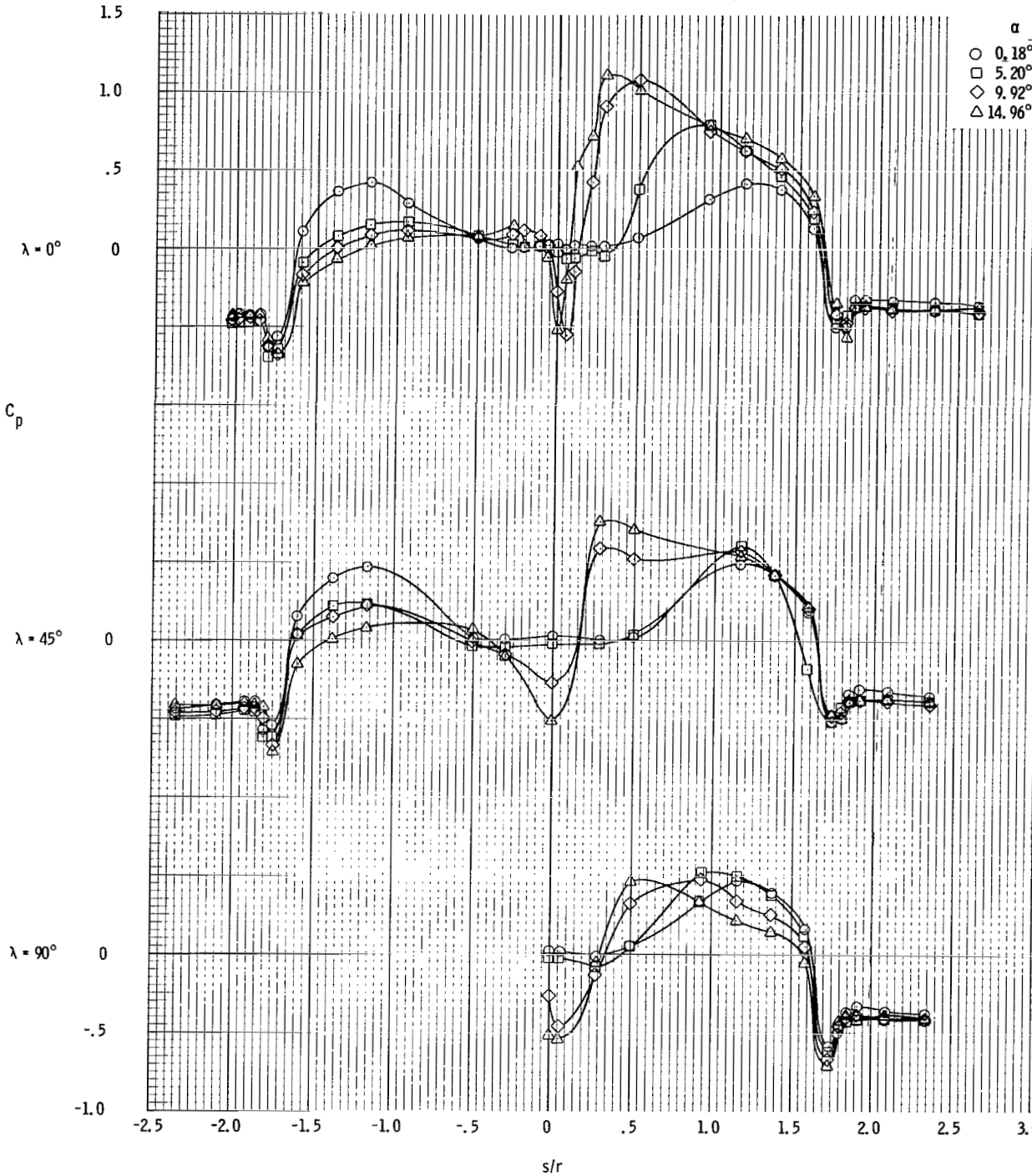

(a) α range is from 0° to 15°.

Figure 7. - Variation of C_p with increasing α at $\lambda = 0°$, $\lambda = 45°$, and $\lambda = 90°$ at $M = 0.7$. Data are for the command module only, in the presence of the escape tower and the rocket.

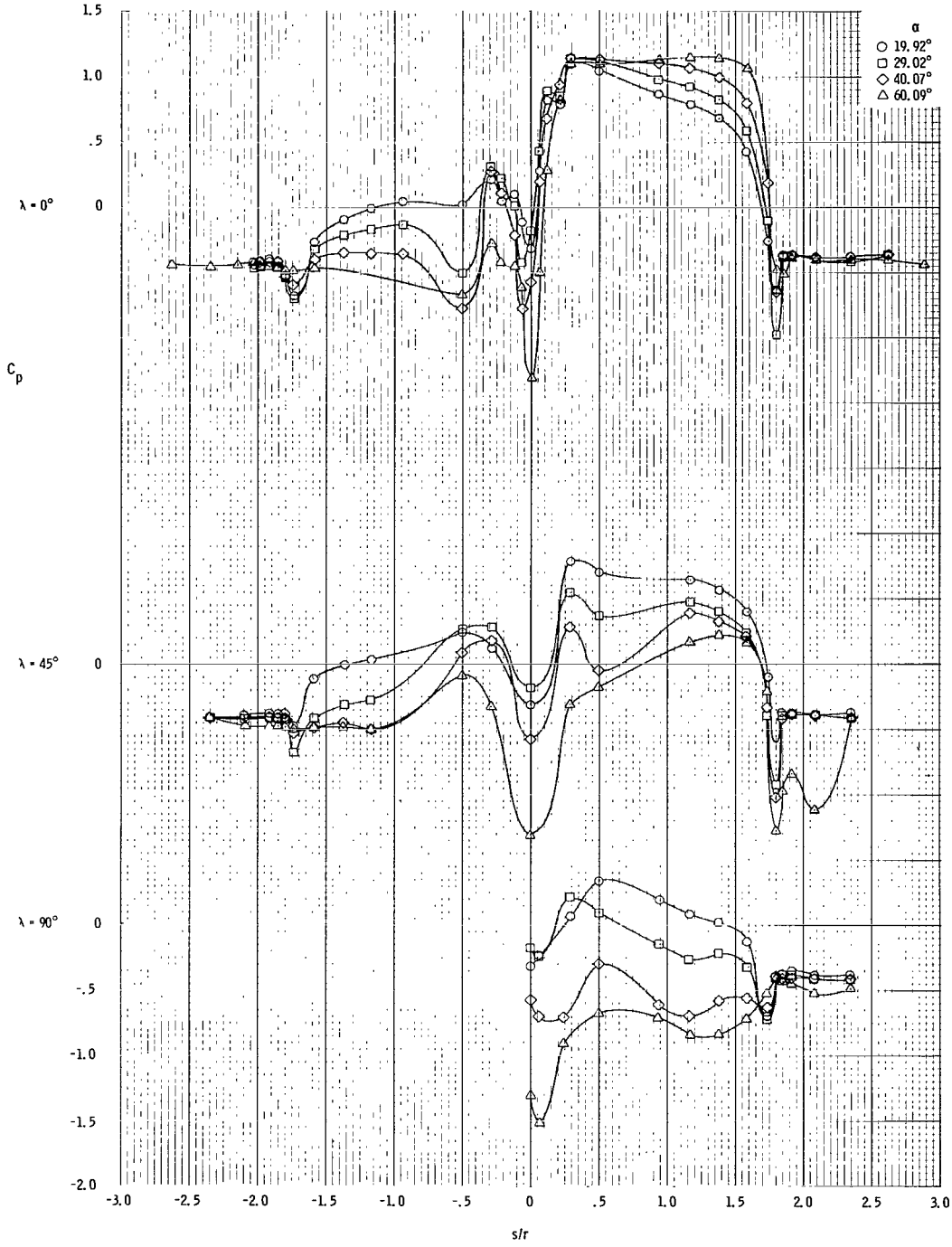

(b) α range is from 20° to 60°.

Figure 7. - Continued.

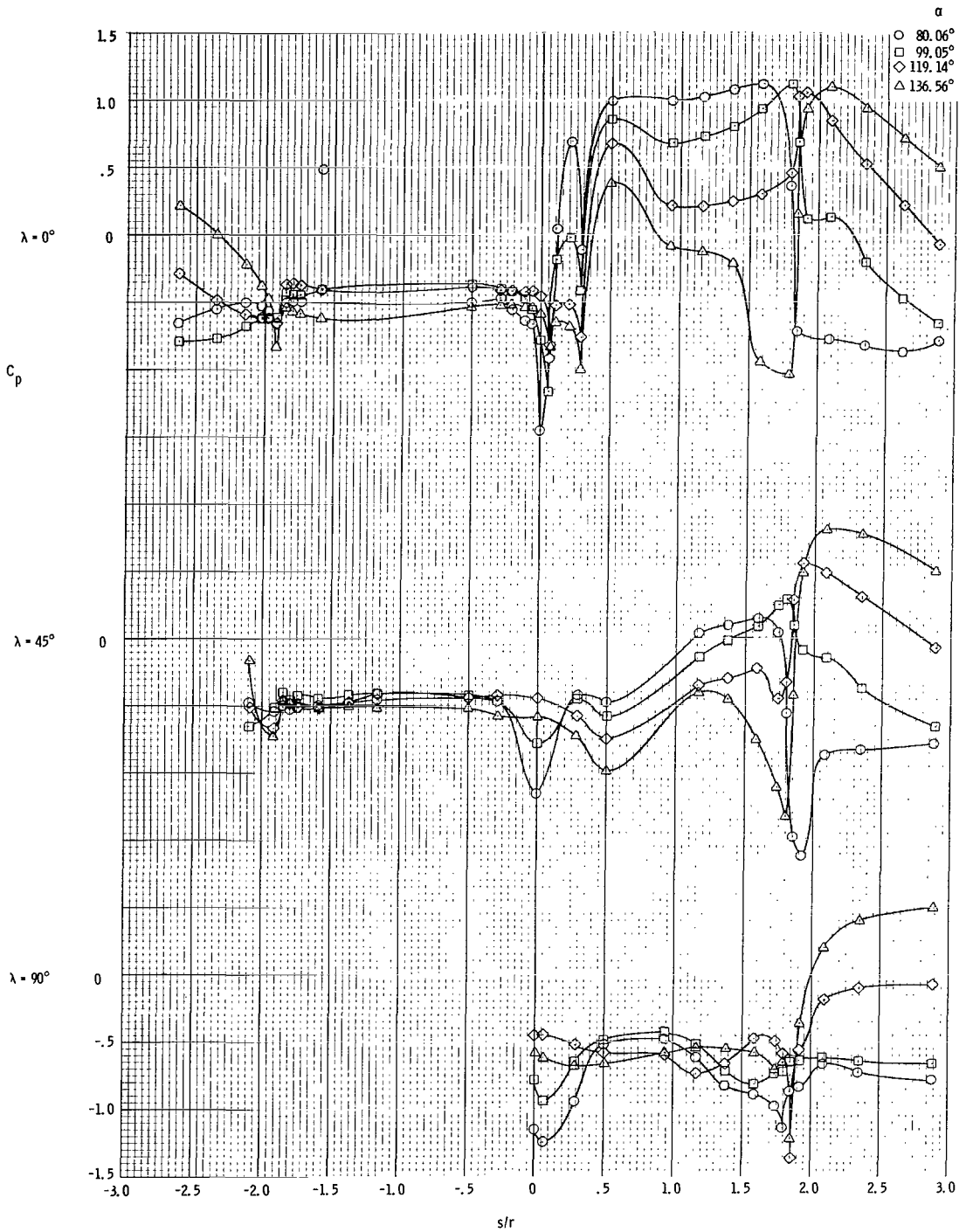

(c) α range is from 80° to 136°.

Figure 7. - Concluded.

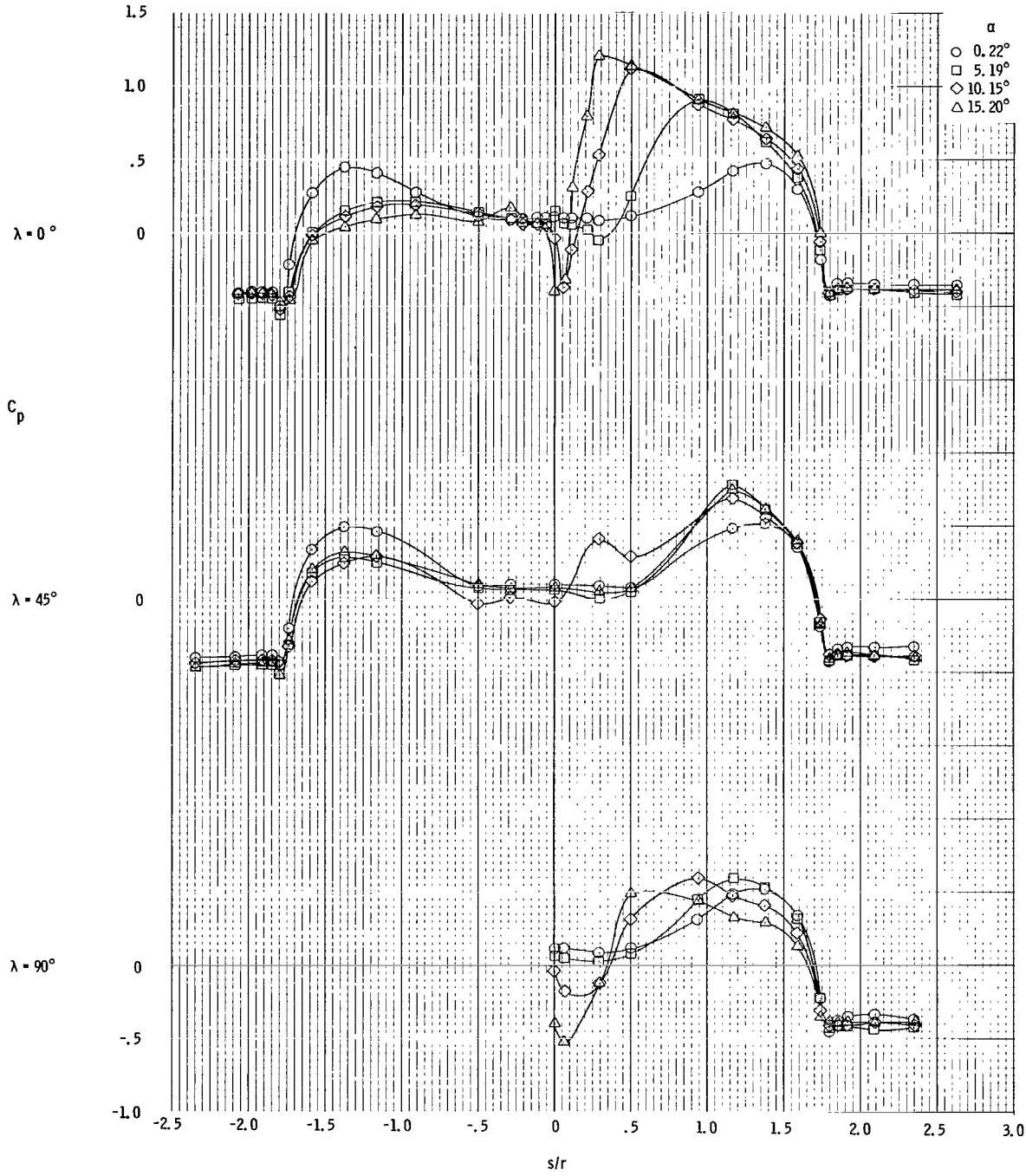

(a) α range is from 0° to 15°.

Figure 8. - Variation of C_p with increasing α at $\lambda = 0°$, $\lambda = 45°$, and $\lambda = 90°$ at $M = 0.9$. Data are for the command module only, in the presence of the escape tower and the rocket.

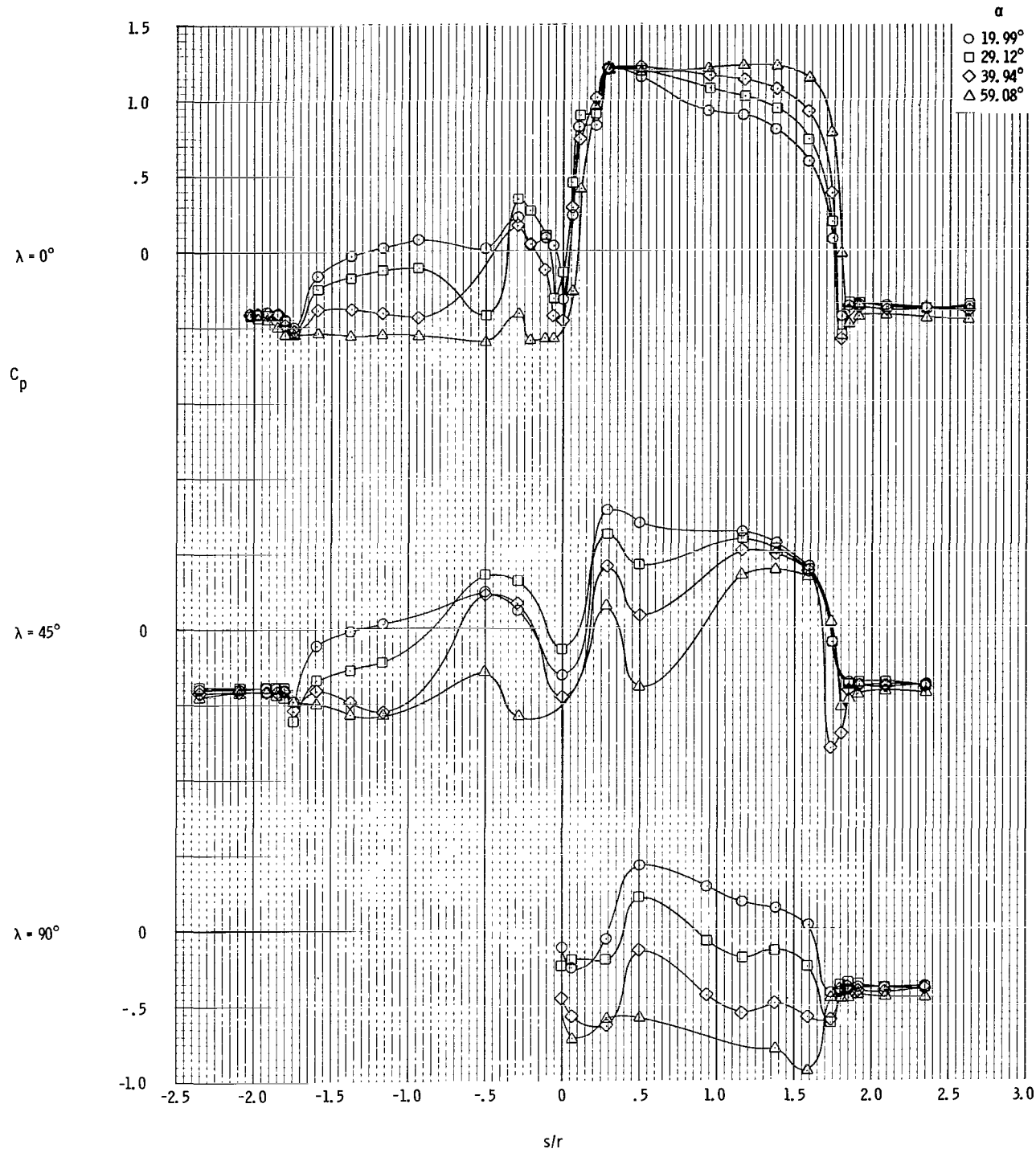

(b) α range is from 20° to 60°.

Figure 8. - Continued.

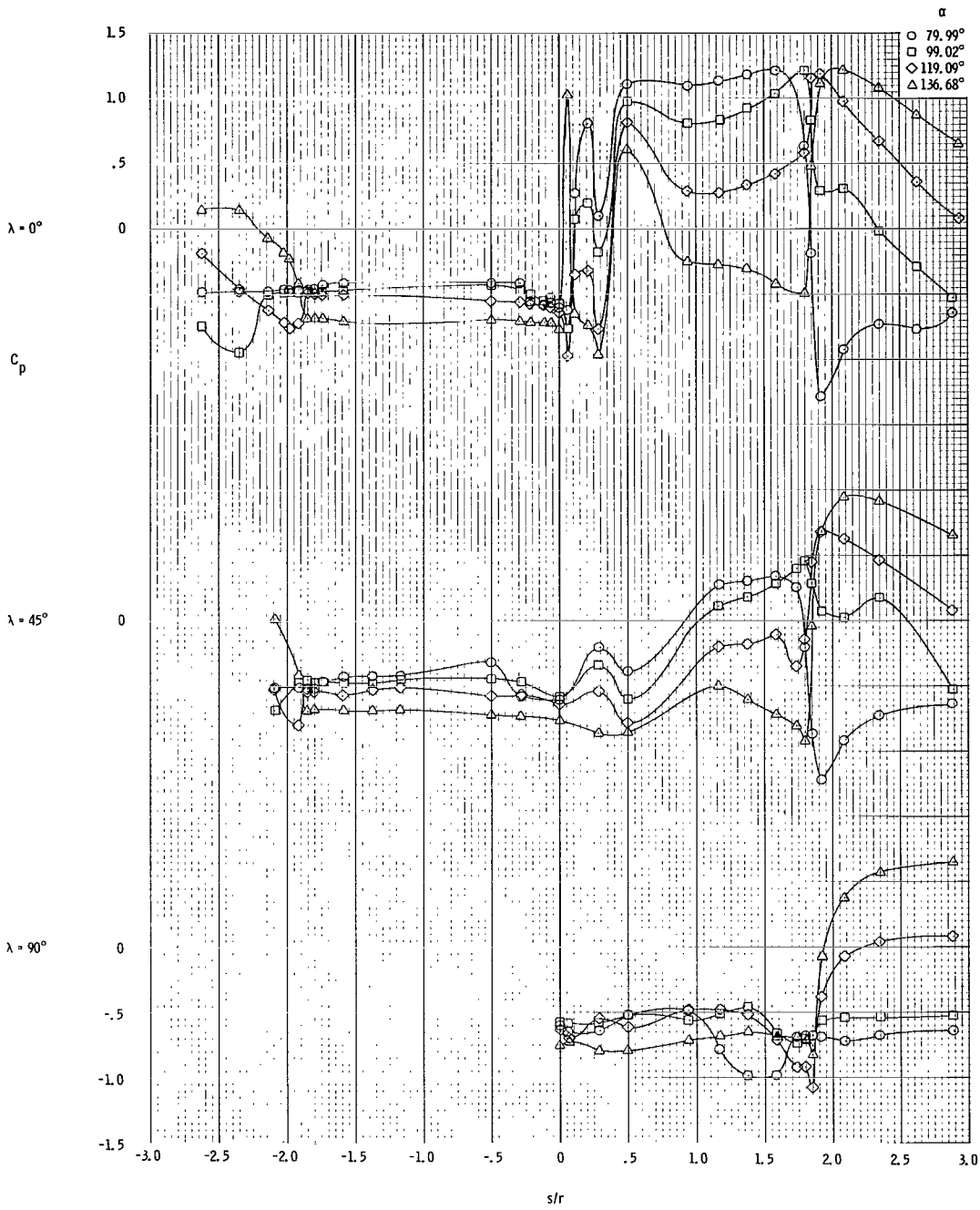

(c) α range is from 80° to 136°.

Figure 8. - Concluded.

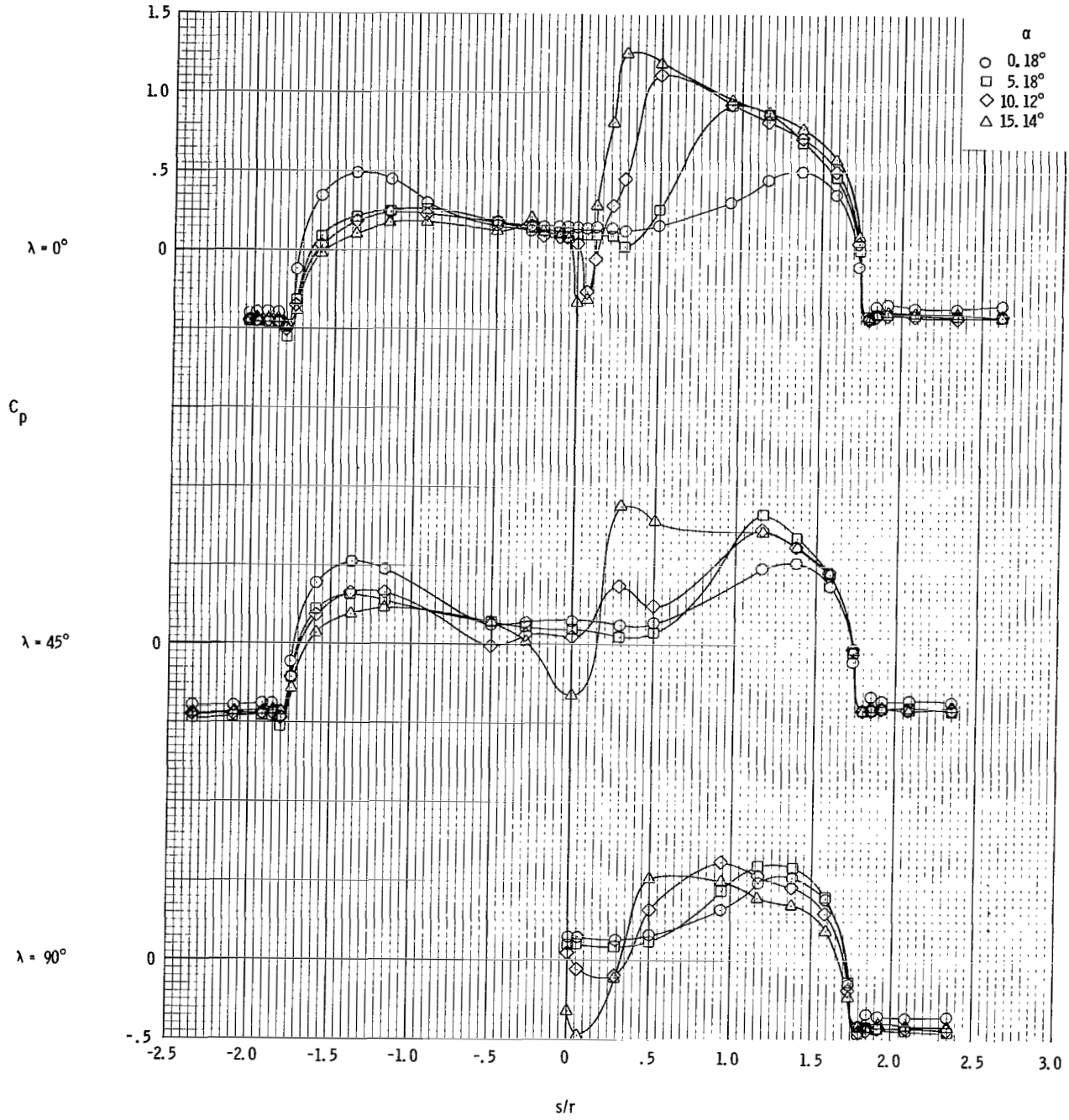

(a) α range is from 0° to 15°.

Figure 9. - Variation of C_p with increasing α at $\lambda = 0°$, $\lambda = 45°$, and $\lambda = 90°$ at $M = 0.95$. Data are for the command module only, in the presence of the escape tower and the rocket.

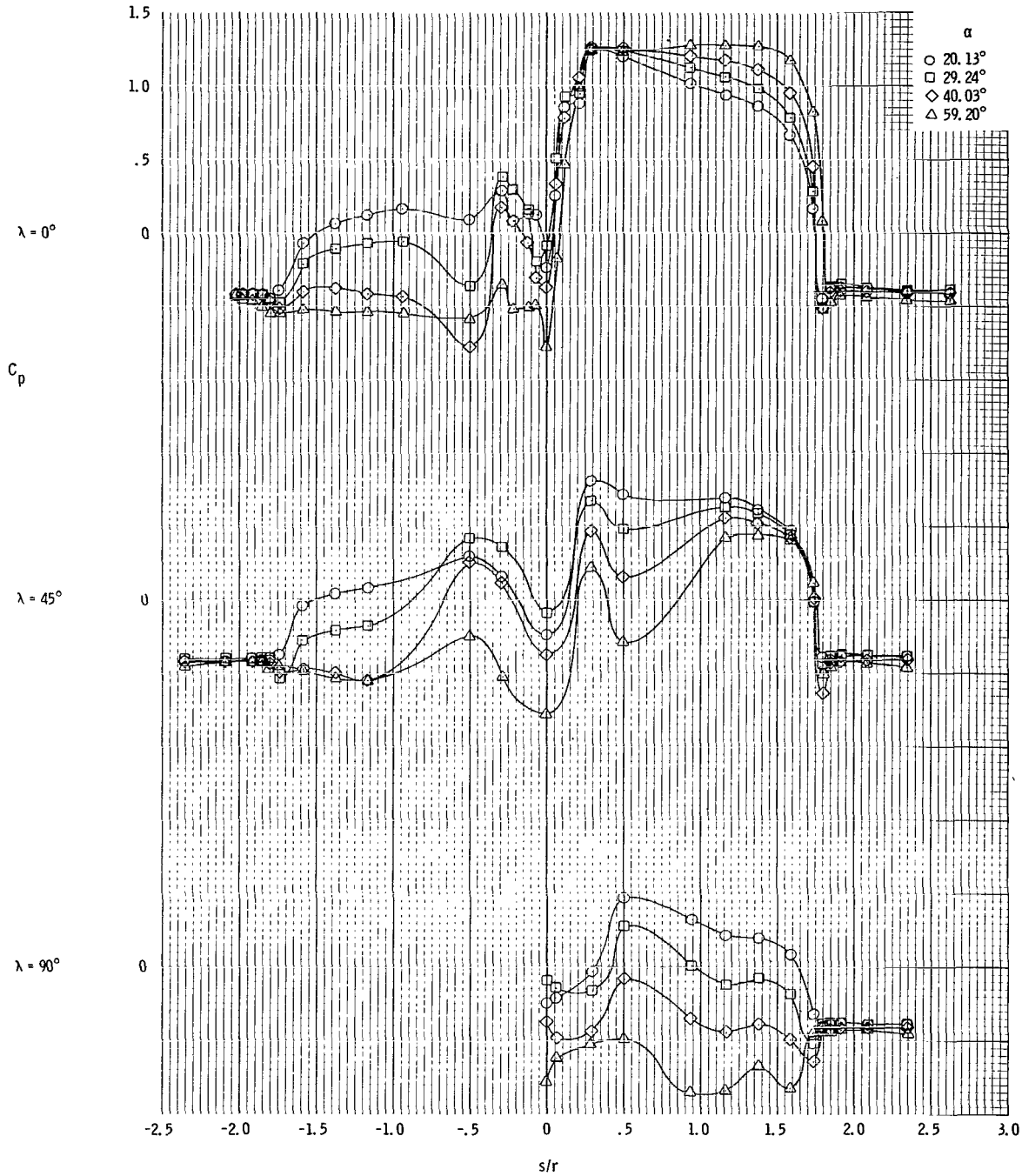

(b) α range is from 20° to 60°.

Figure 9. - Continued.

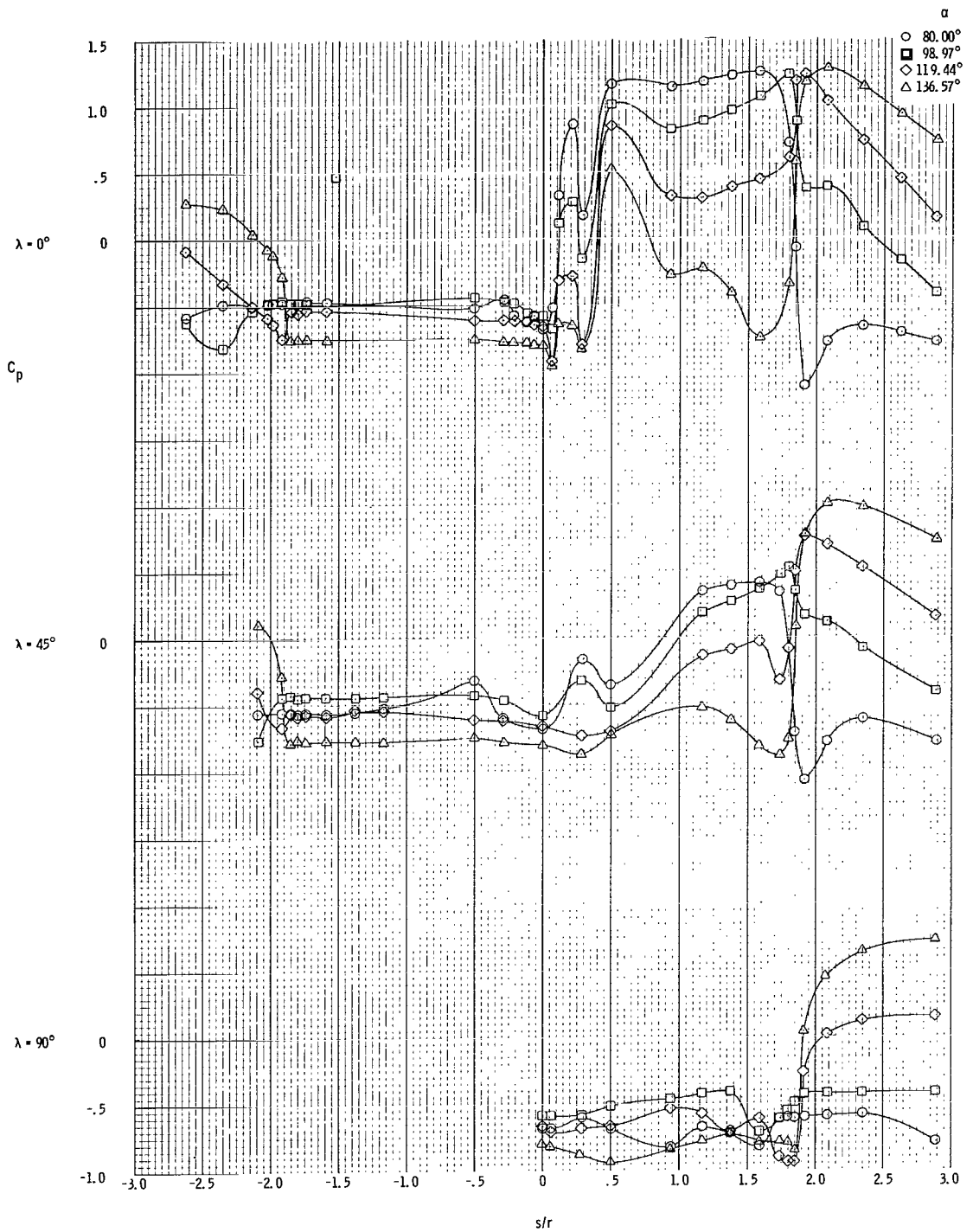

(c) α range is from 80° to 136°.

Figure 9. - Concluded.

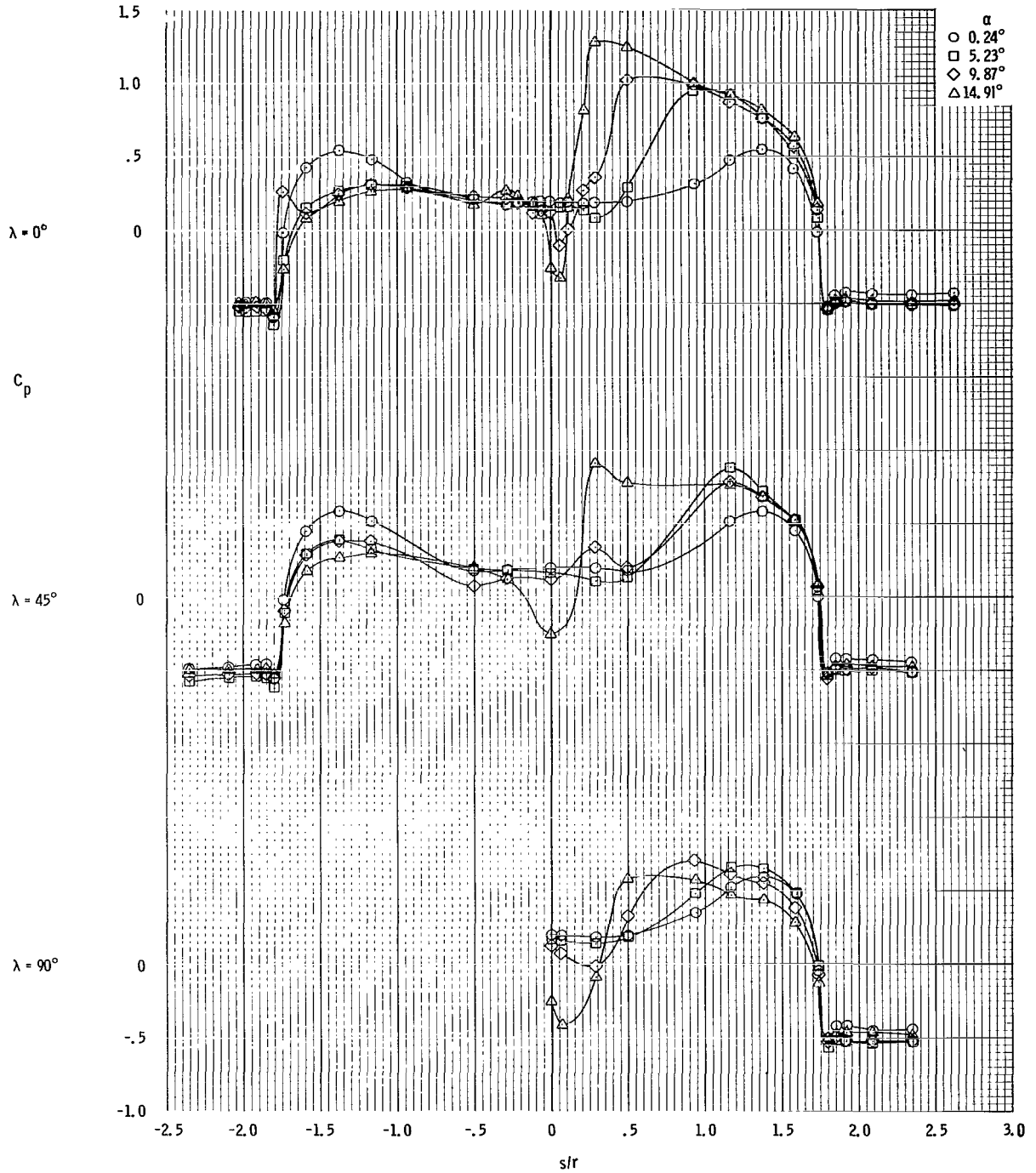

(a) α range is from 0° to 15°.

Figure 10. - Variation of C_p with increasing α at $\lambda = 0°$, $\lambda = 45°$, and $\lambda = 90°$ at $M = 1.05$. Data are for the command module only, in the presence of the escape tower and the rocket.

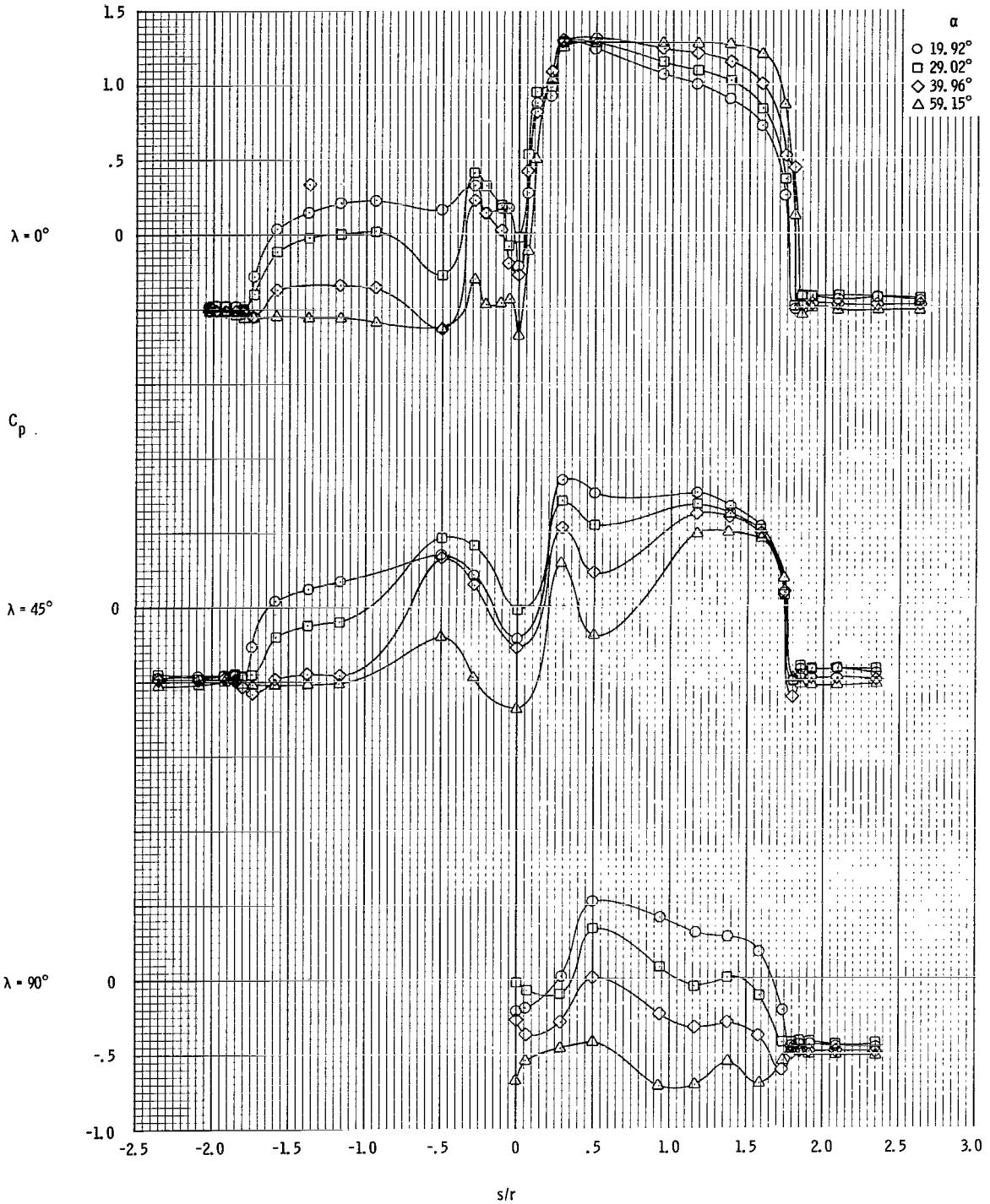

(b) α range is from 20° to 60°.

Figure 10. - Continued.

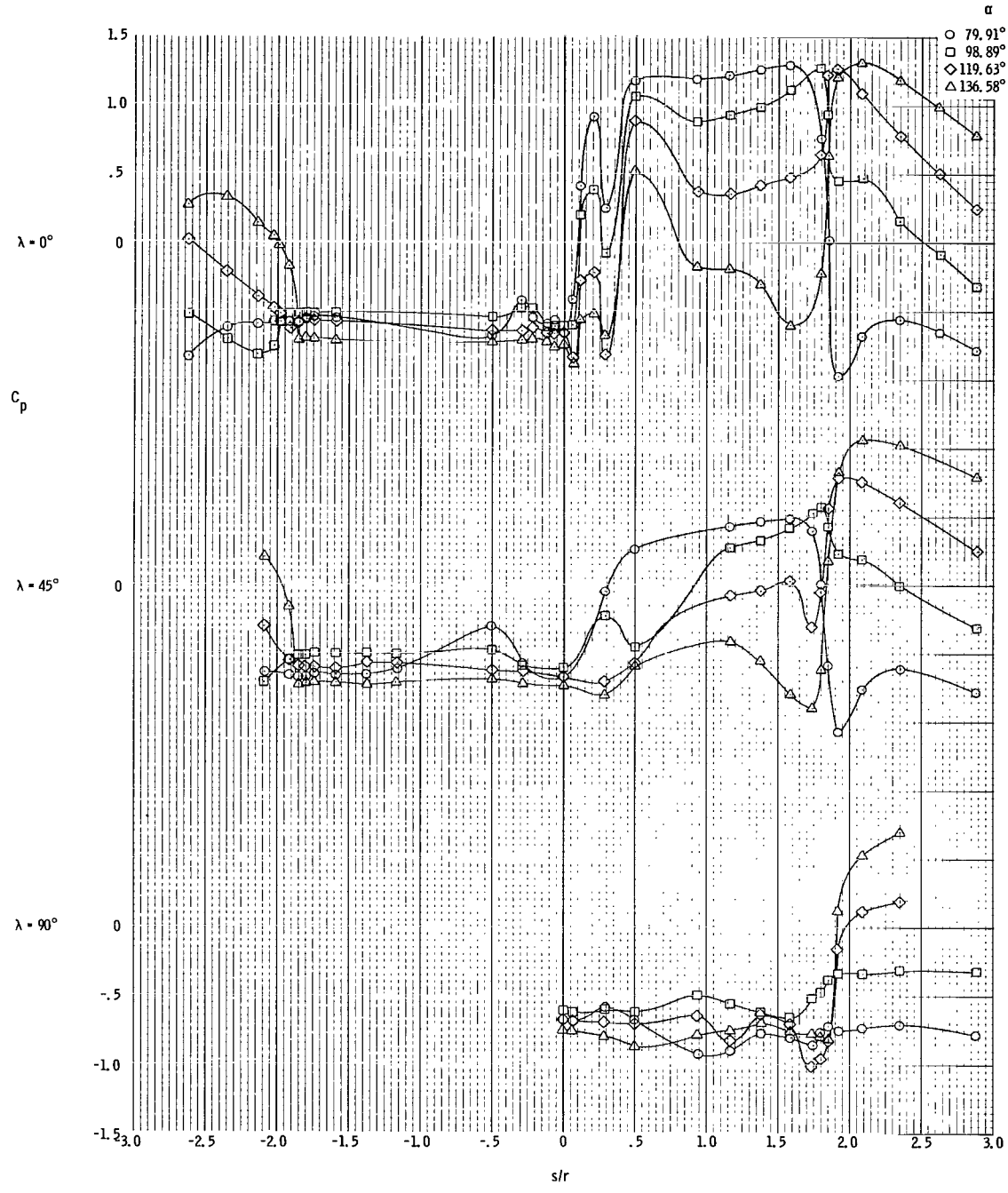

(c) α range is from 80° to 136°.

Figure 10. - Concluded.

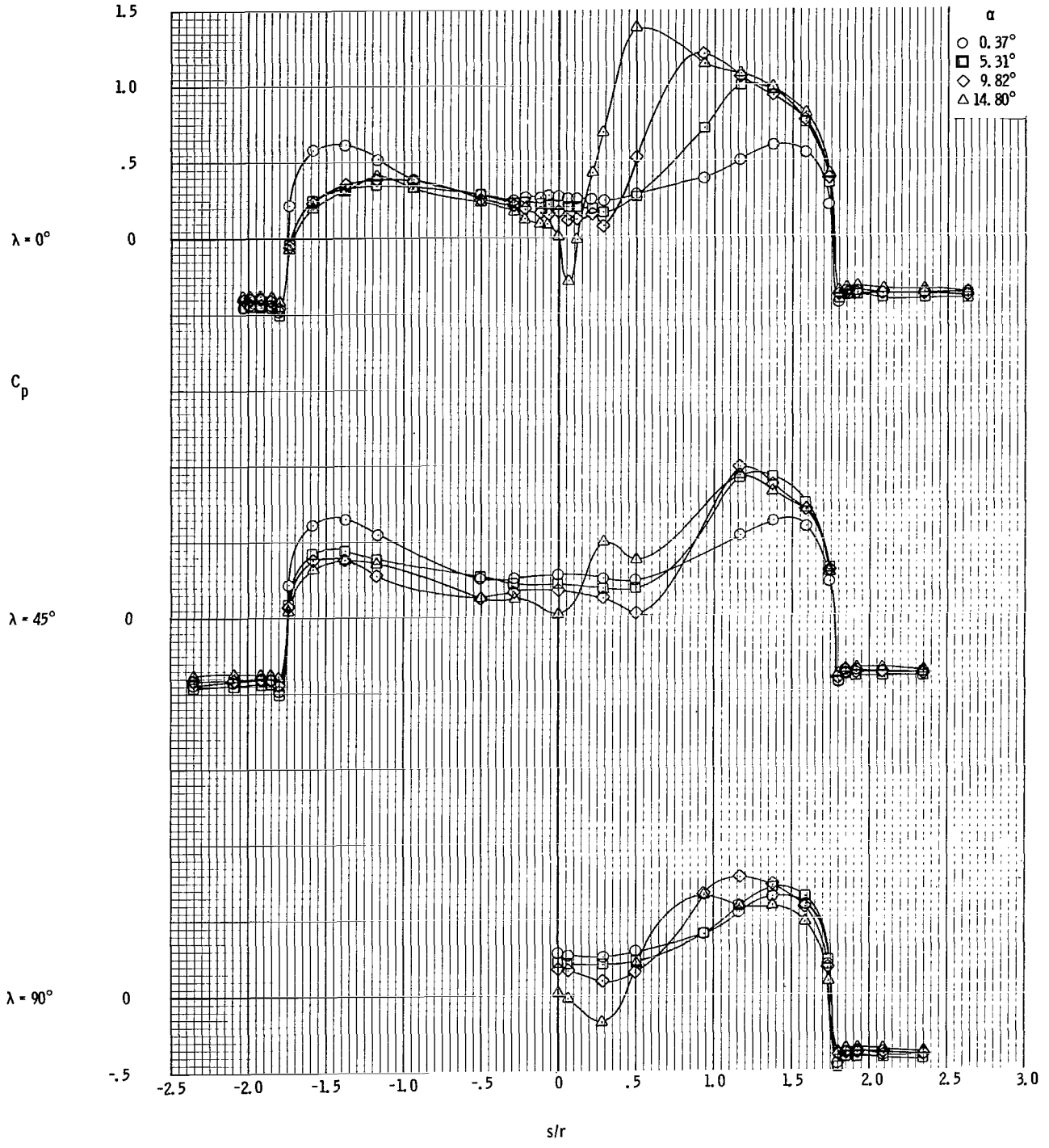

(a) α range is from 0° to 15°.

Figure 11. - Variation of C_p with increasing α at $\lambda = 0°$, $\lambda = 45°$, and $\lambda = 90°$ at $M = 1.20$. Data are for the command module only, in the presence of the escape tower and the rocket.

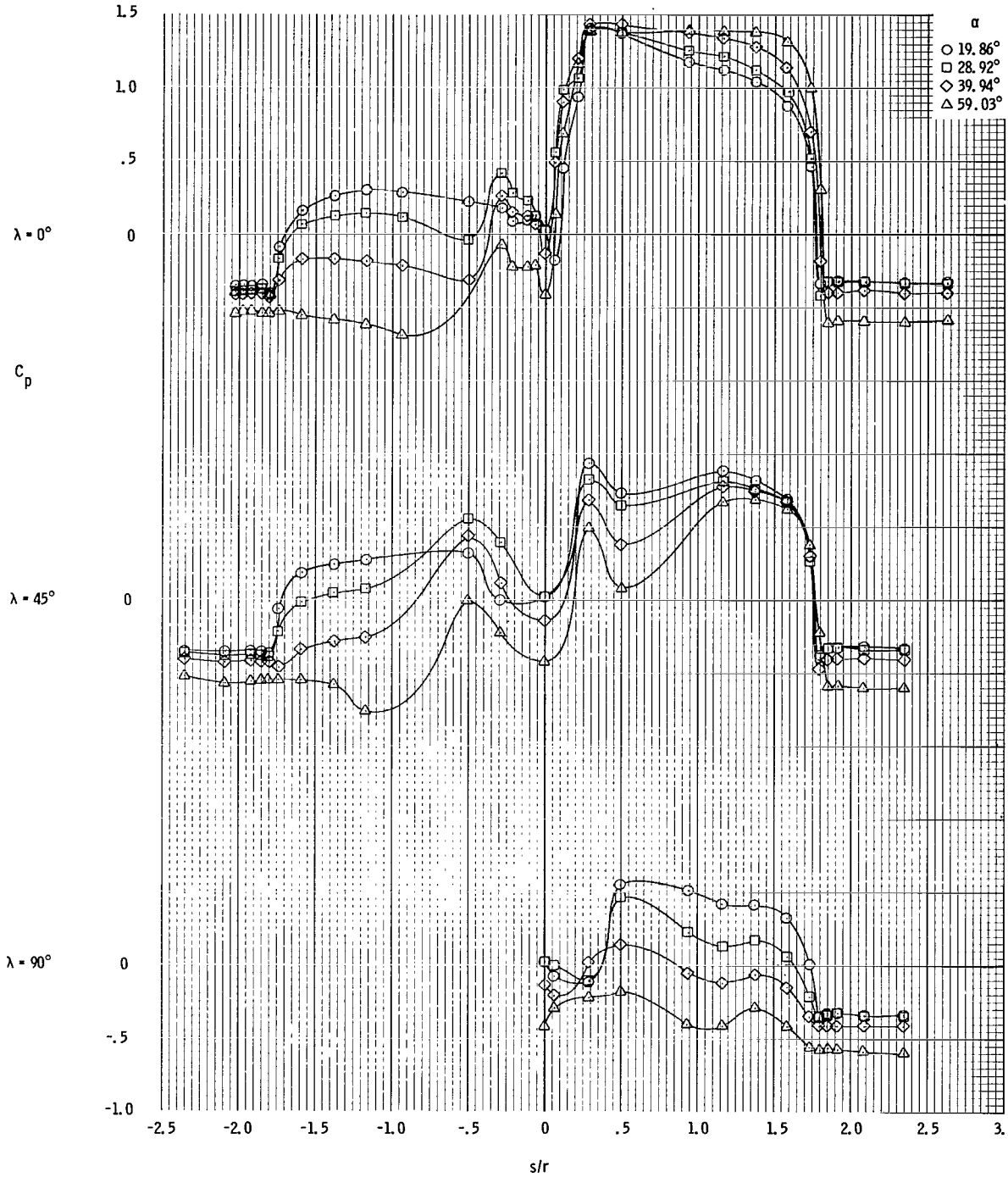

(b) α range is from 20° to 60°.

Figure 11. - Continued.

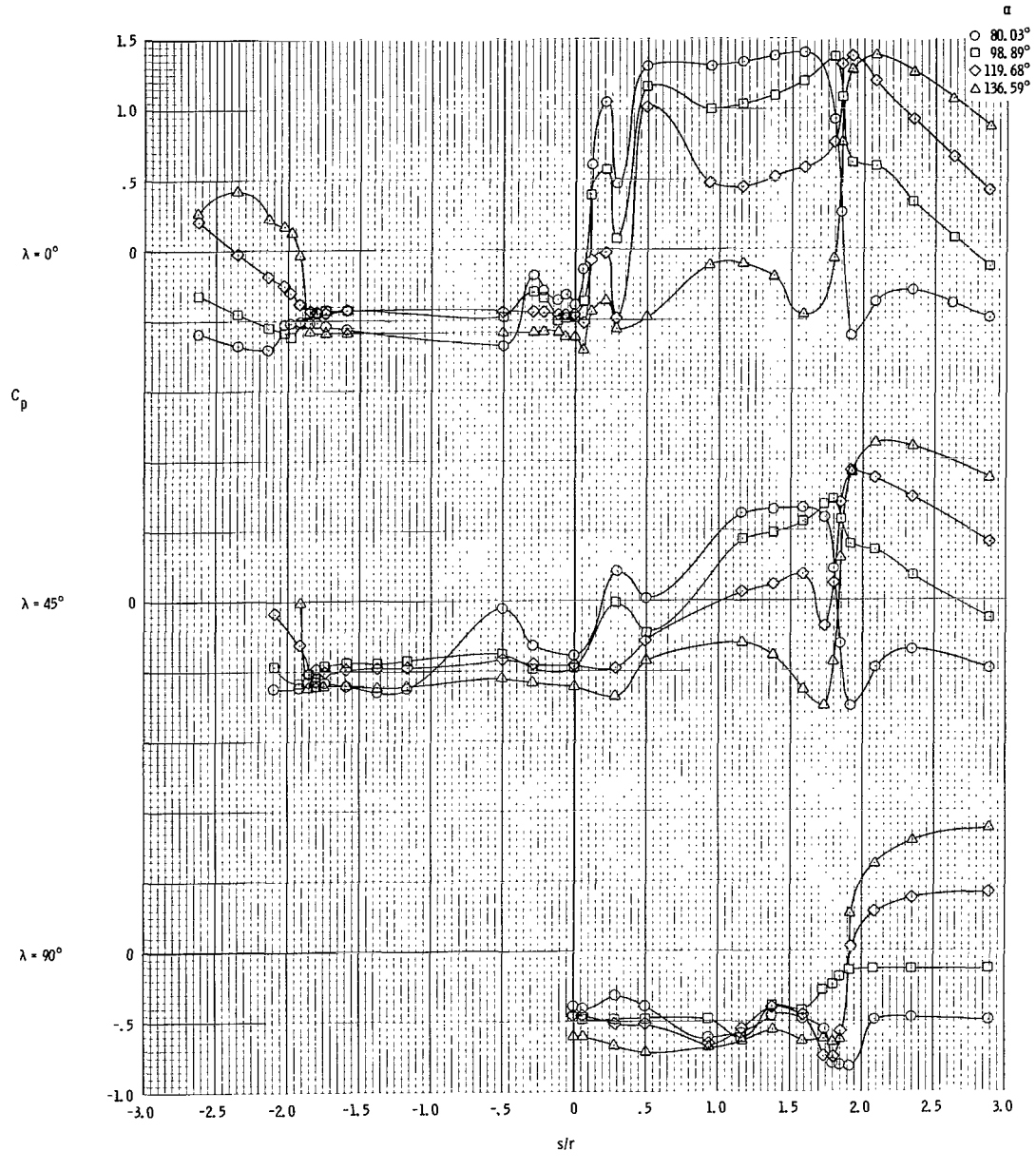

(c) α range is from 80° to 136°.

Figure 11. - Concluded.

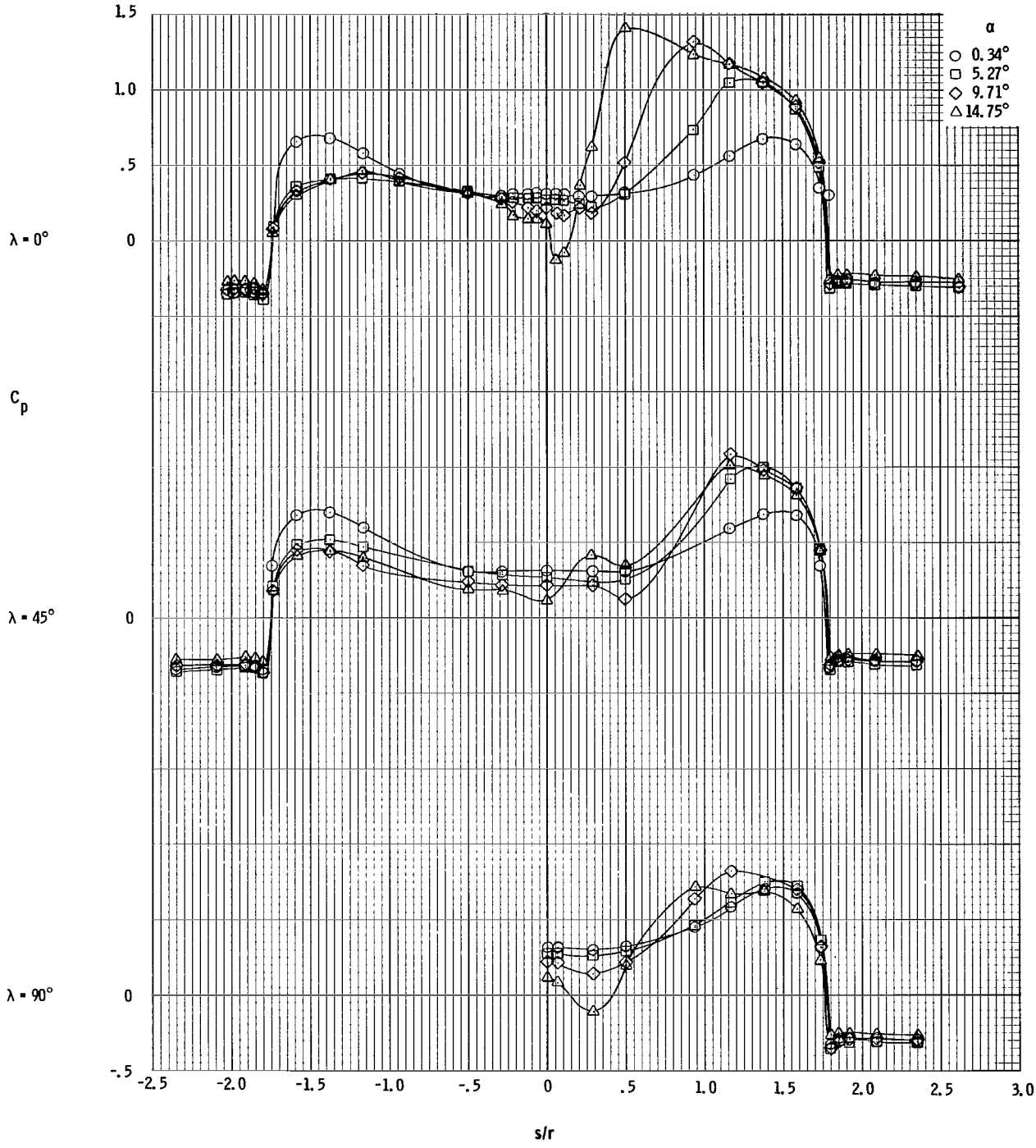

(a) α range is from 0° to 15°.

Figure 12. - Variation of C_p with increasing α at $\lambda = 0°$, $\lambda = 45°$, and $\lambda = 90°$ at $M = 1.34$. Data are for the command module only, in the presence of the escape tower and the rocket.

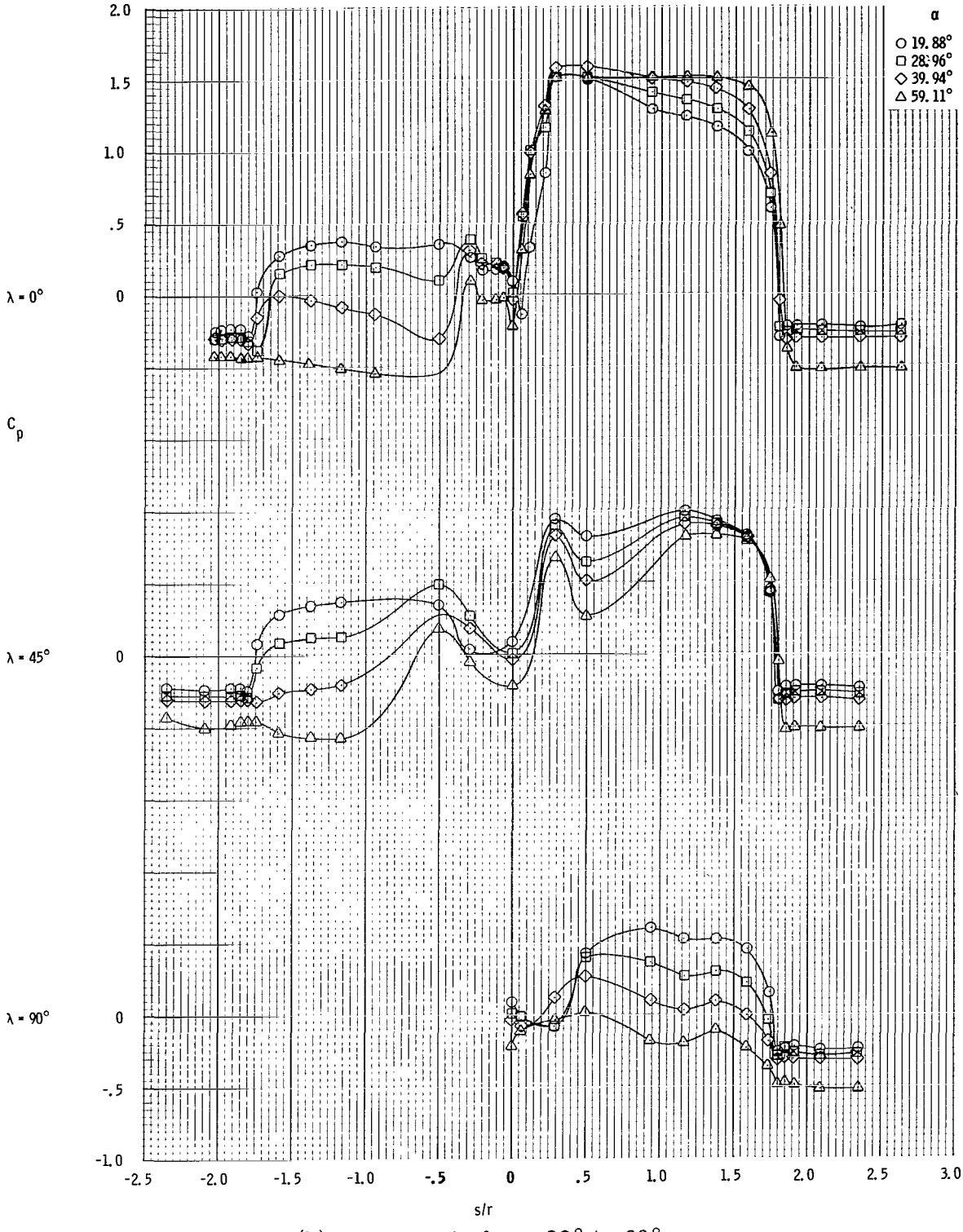

(b) α range is from 20° to 60°.

Figure 12. - Continued.

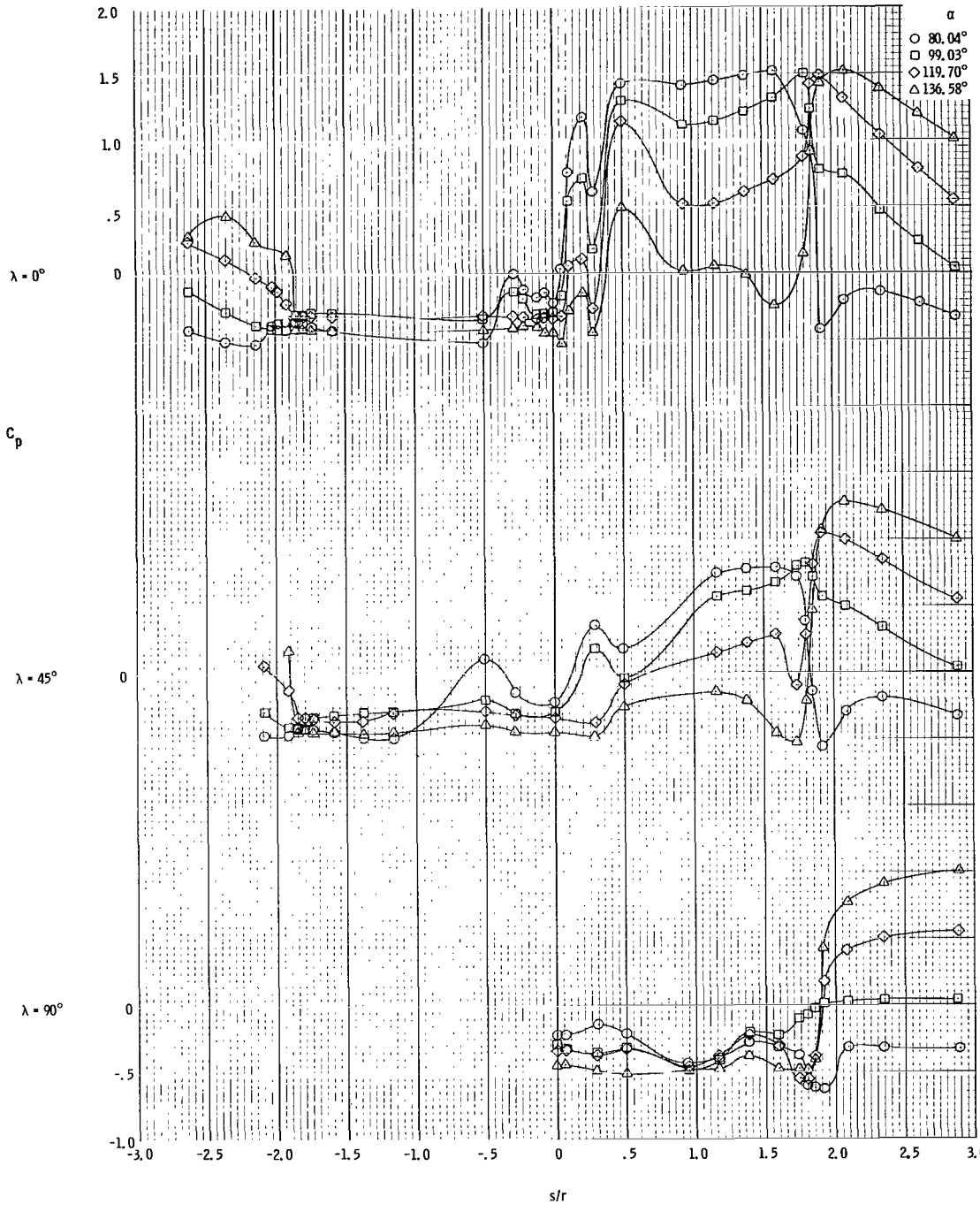

(c) α range is from 80° to 136°.

Figure 12. - Concluded.

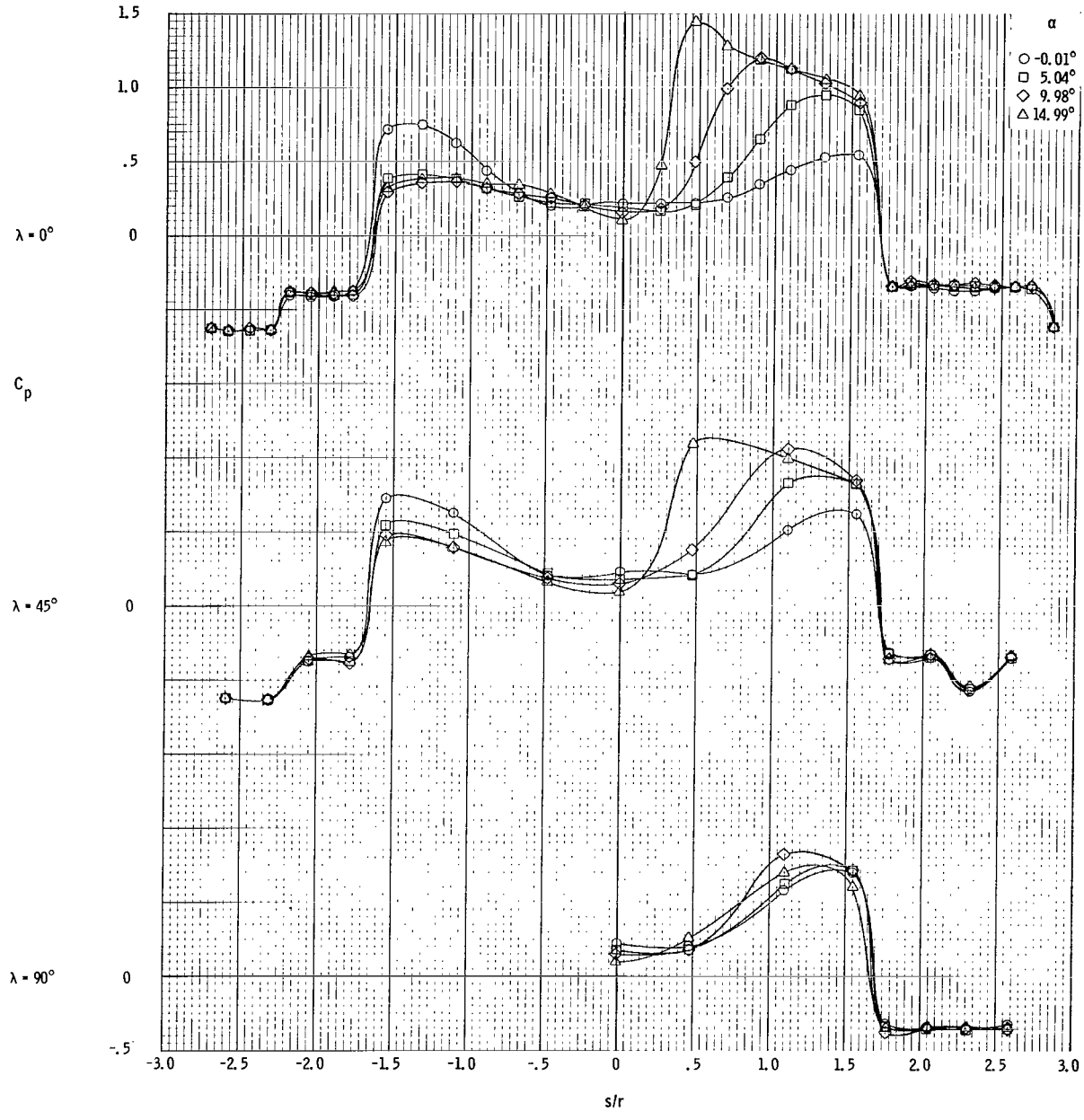

(a) α range is from 0° to 15°.

Figure 13. - Variation of C_p with increasing α at $\lambda = 0°$, $\lambda = 45°$, and $\lambda = 90°$ at $M = 1.48$. Data are for the command module only, in the presence of the escape tower and the rocket.

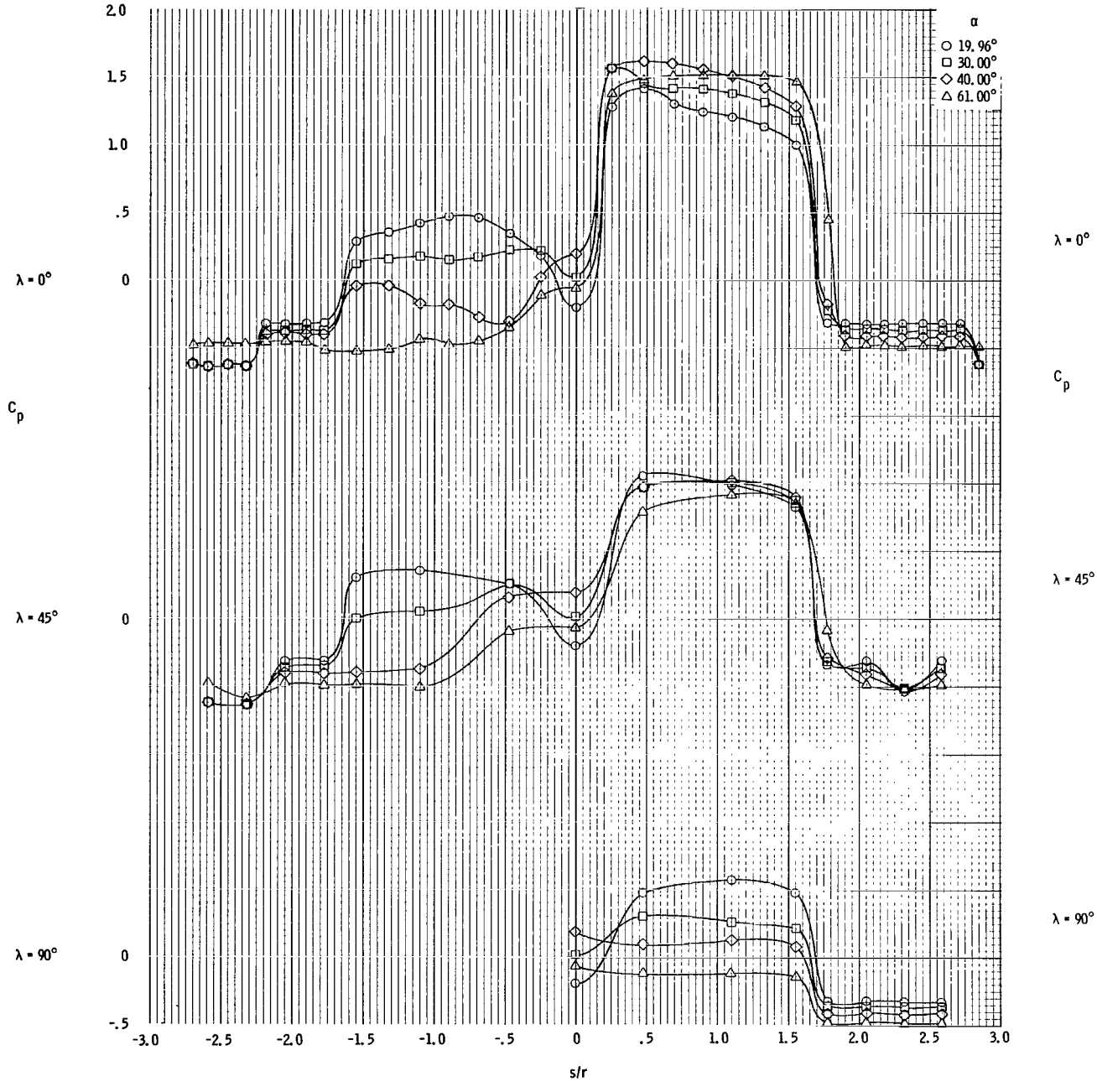

(b) α range is from 20° to 61°.

Figure 13. - Continued.

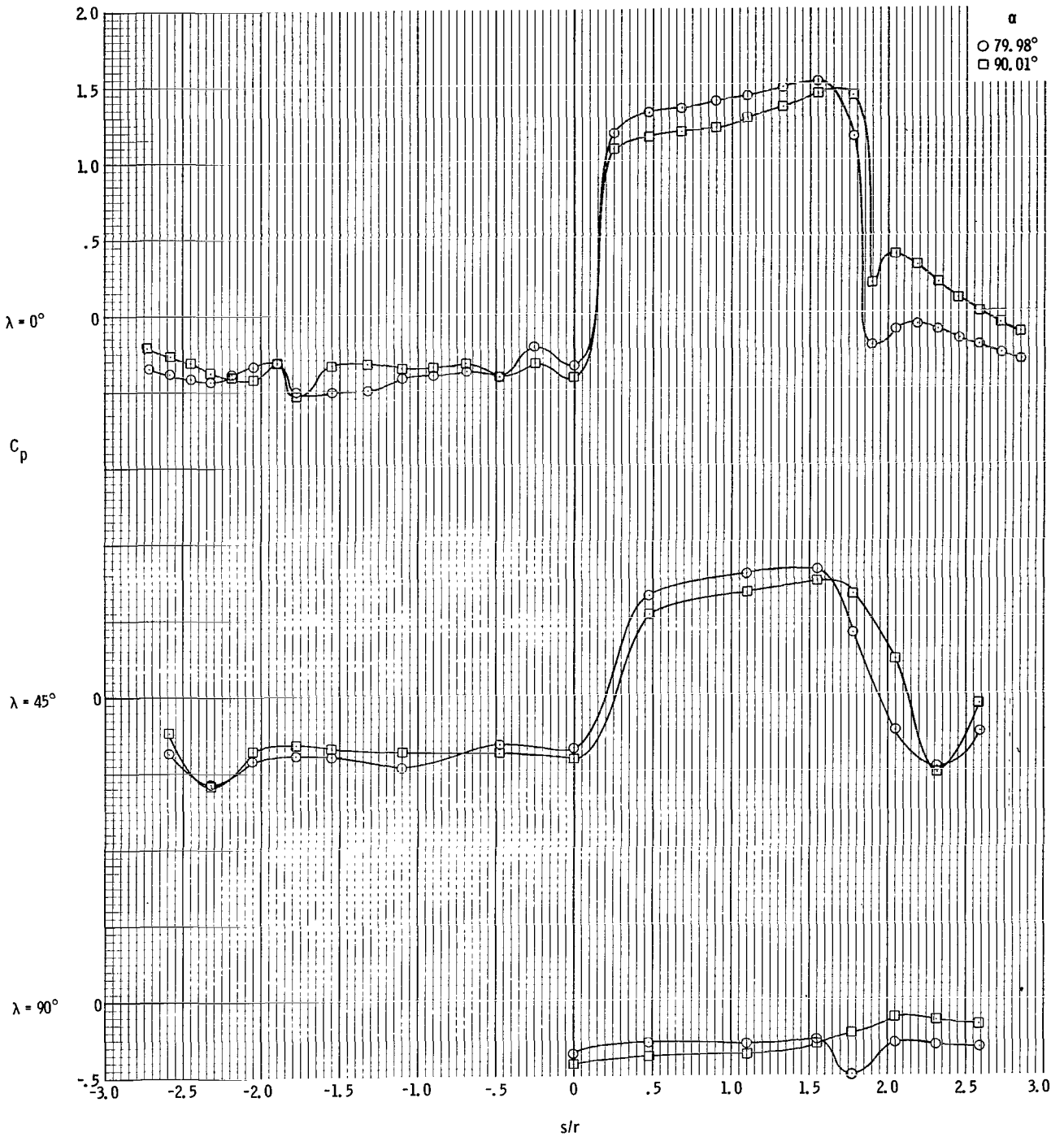

(c) α range is from 80° to 90°.

Figure 13. - Concluded.

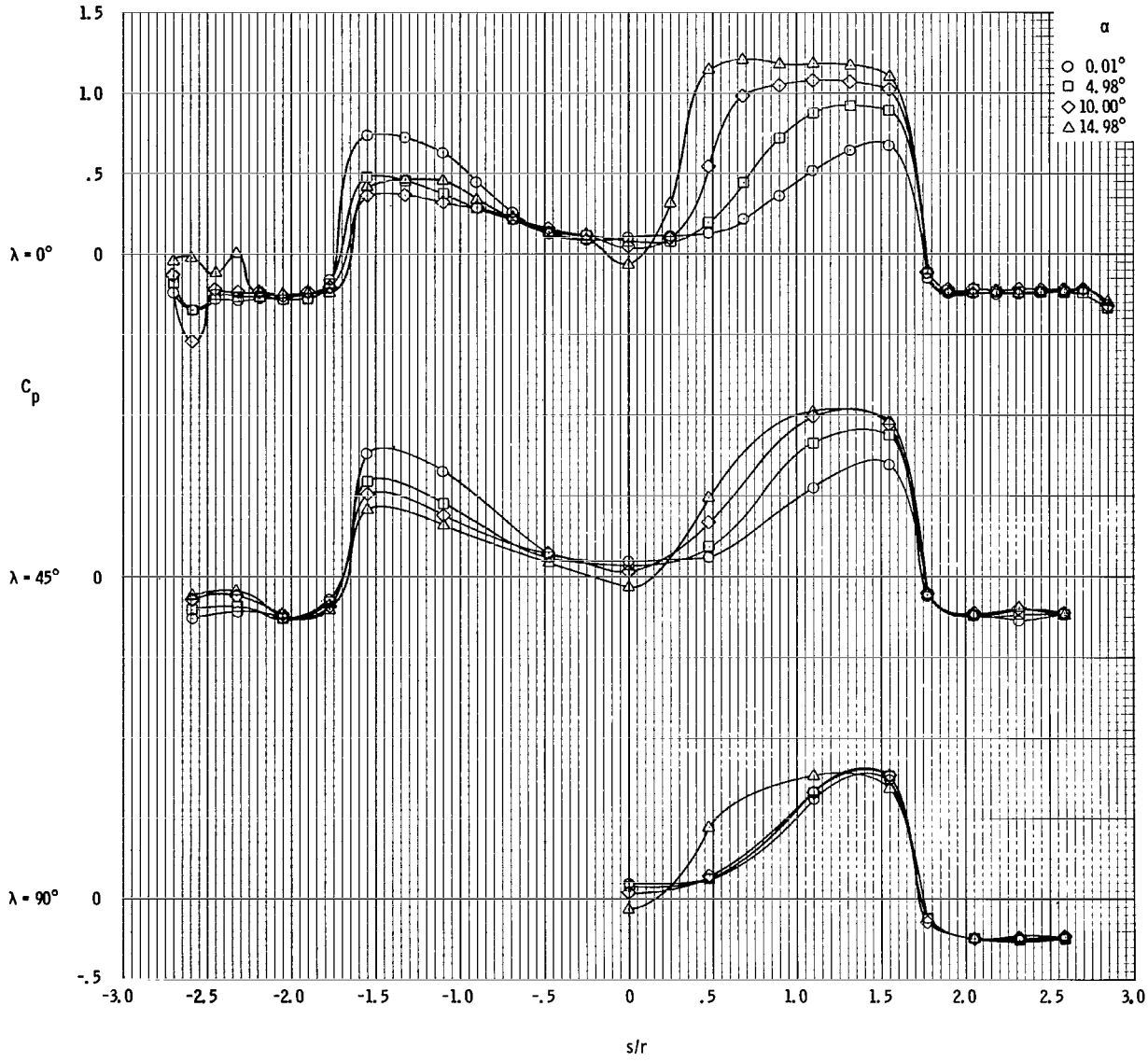

(a) α range is from 0° to 15°.

Figure 14. - Variation of C_p with increasing α at $\lambda = 0°$, $\lambda = 45°$, and $\lambda = 90°$ at M = 2.01. Data are for the command module only, in the presence of the escape tower and the rocket.

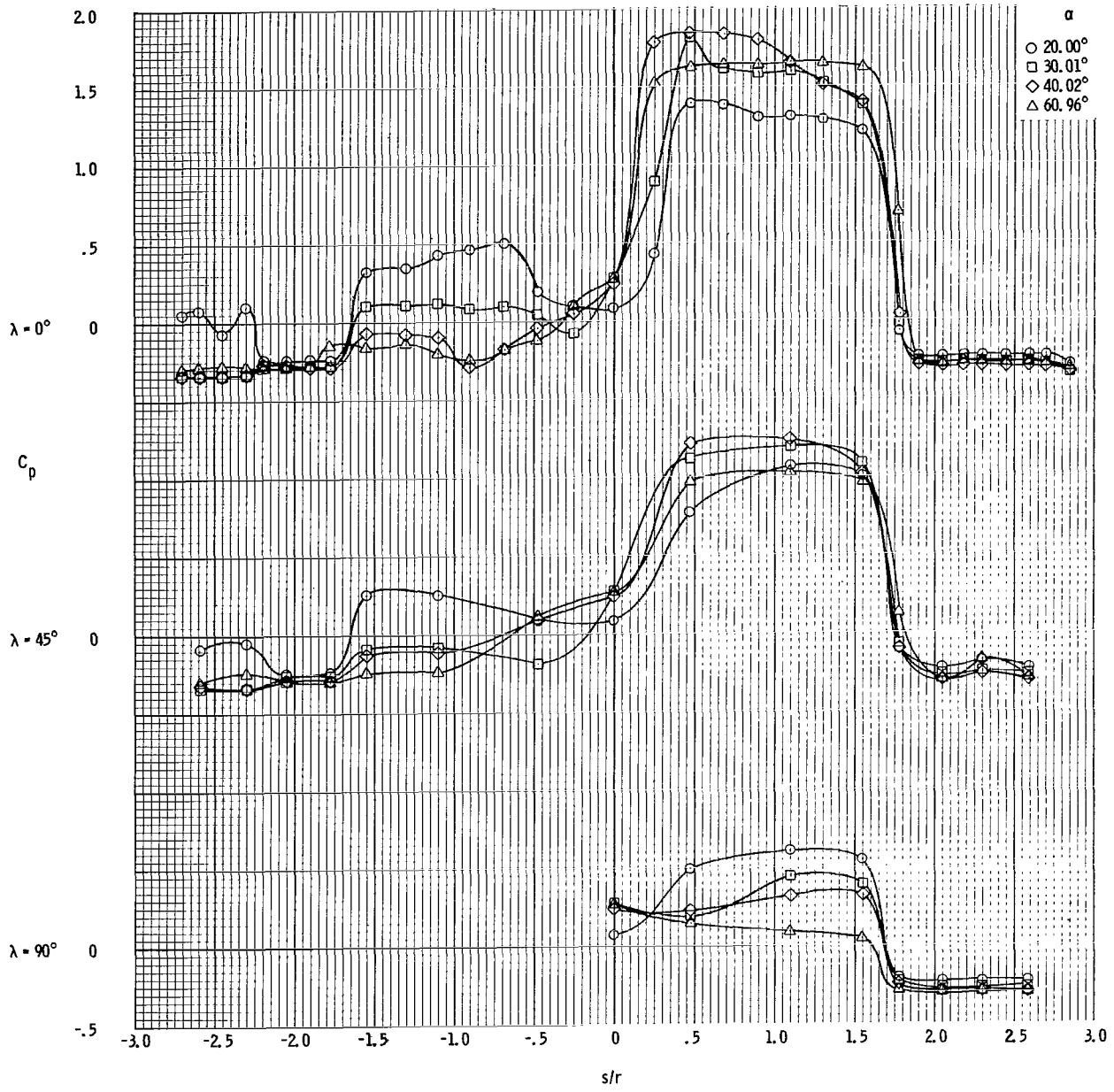

(b) α range is from 20° to 61°.

Figure 14. - Continued.

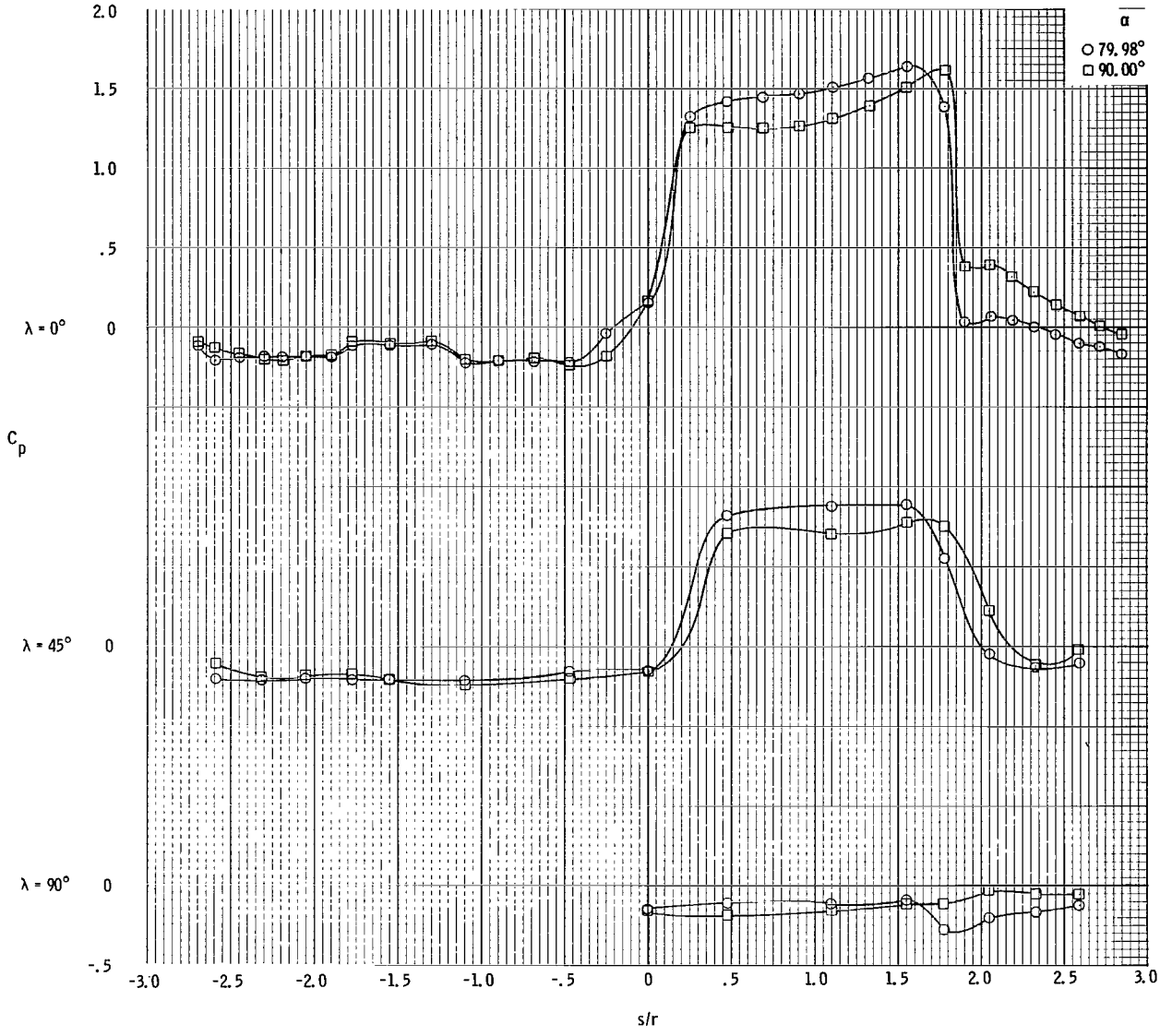

(c) α range is from 80° to 90°.

Figure 14. - Concluded.

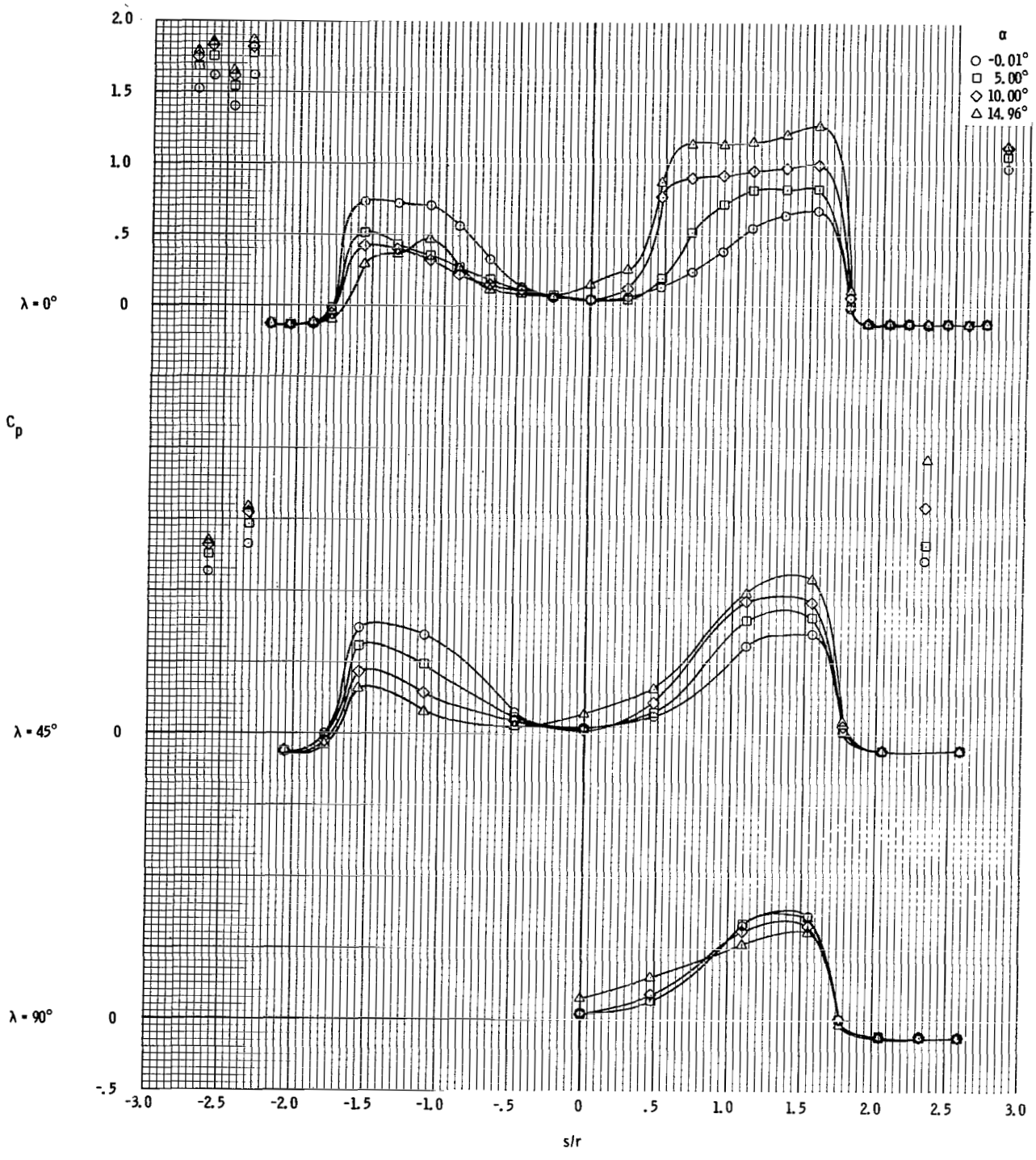

(a) α range is from 0° to 15°.

Figure 15. - Variation of C_p with increasing α at $\lambda = 0°$, $\lambda = 45°$, and $\lambda = 90°$ at M = 3.01. Data are for the command module only, in the presence of the escape tower and the rocket.

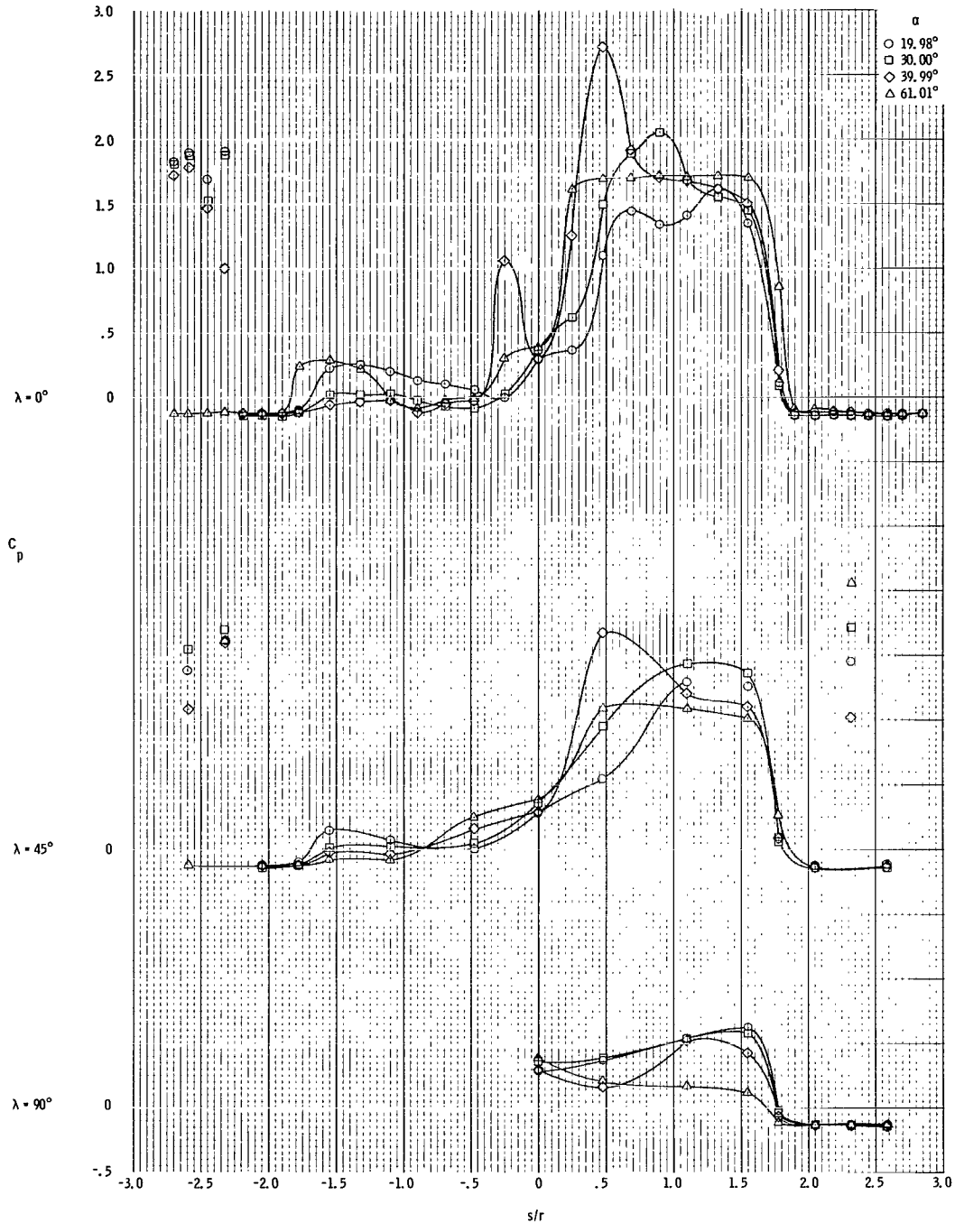

(b) α range is from 20° to 61°.

Figure 15. - Continued.

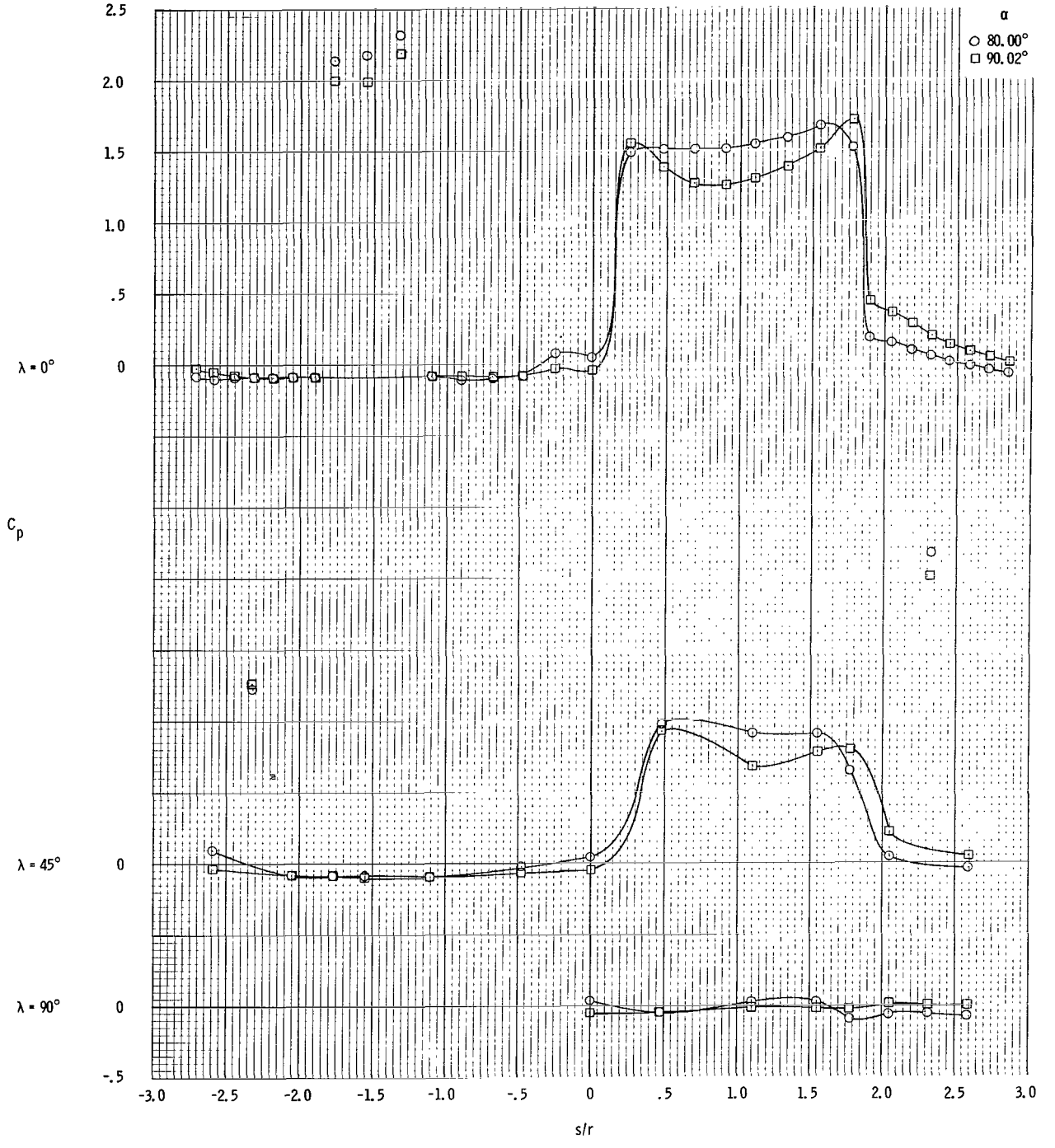

(c) α range is from 80° to 90°.

Figure 15. - Concluded.

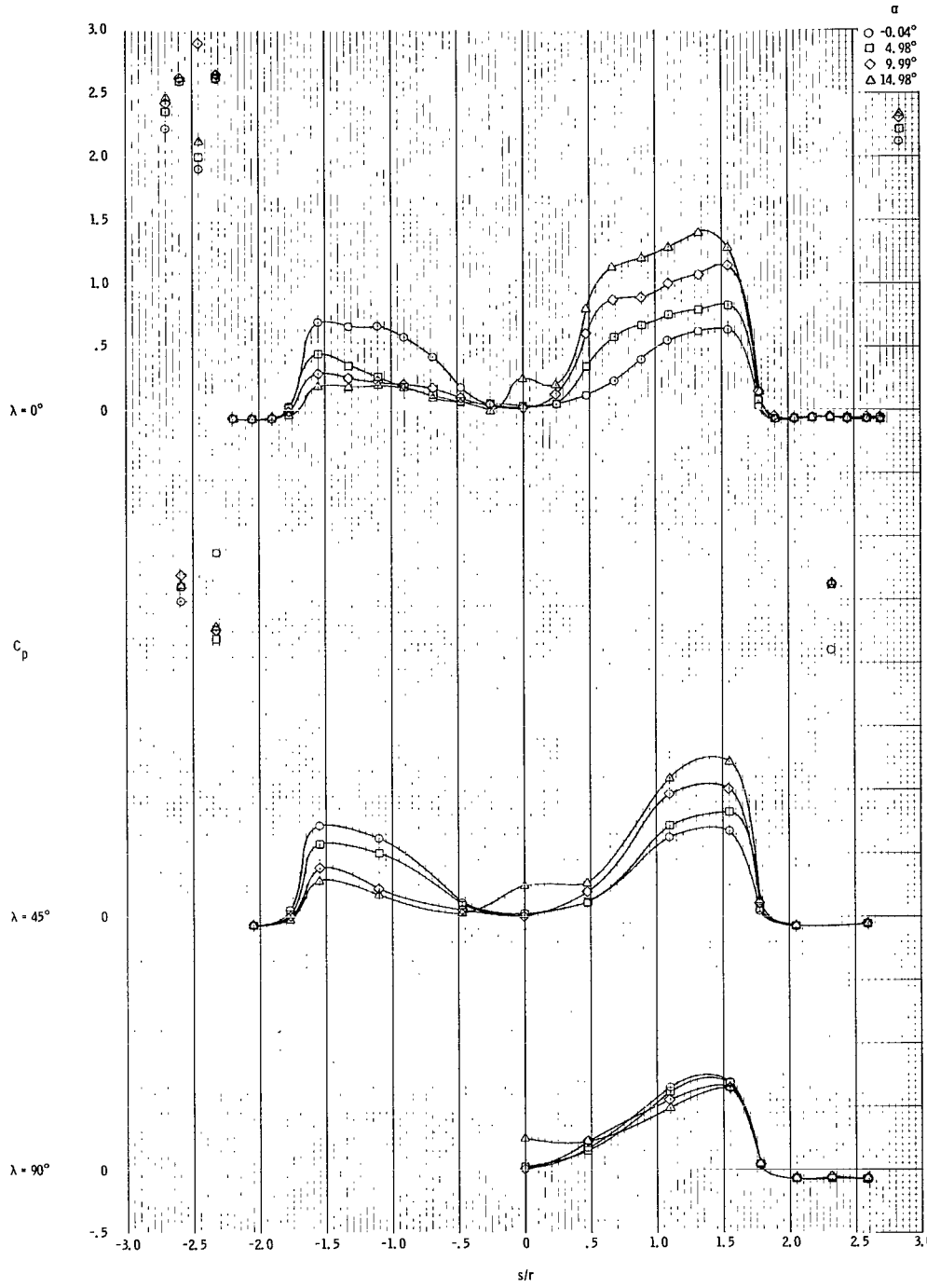

(a) α range is from 0° to 15°.

Figure 16. - Variation of C_p with increasing α at $\lambda = 0°$, $\lambda = 45°$, and $\lambda = 90°$ at $M = 3.99$. Data are for the command module only, in the presence of the escape tower and the rocket.

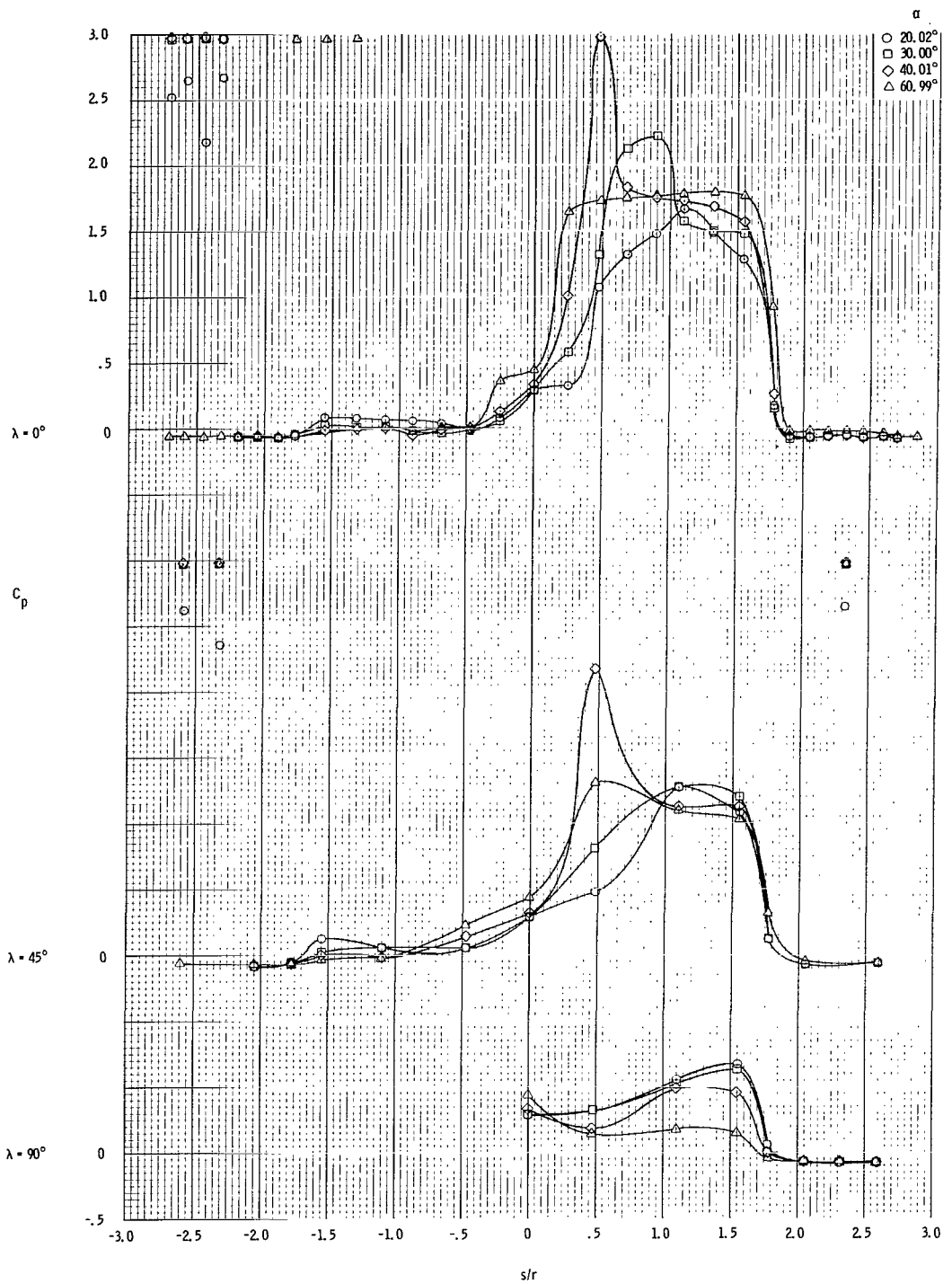

(b) α range is from 20° to 61°.

Figure 16. - Continued.

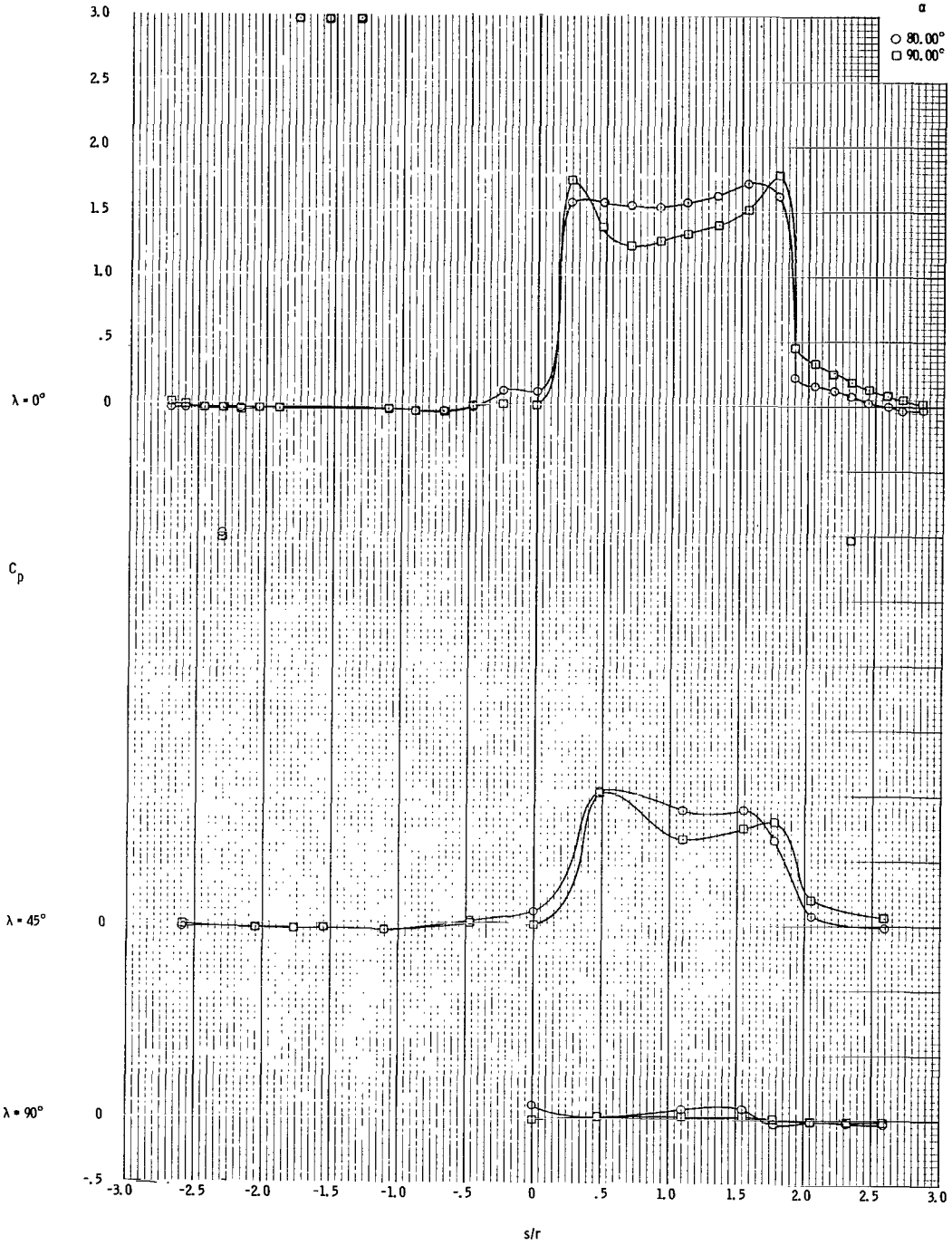

(c) α range is from 80° to 90°.

Figure 16. - Concluded.

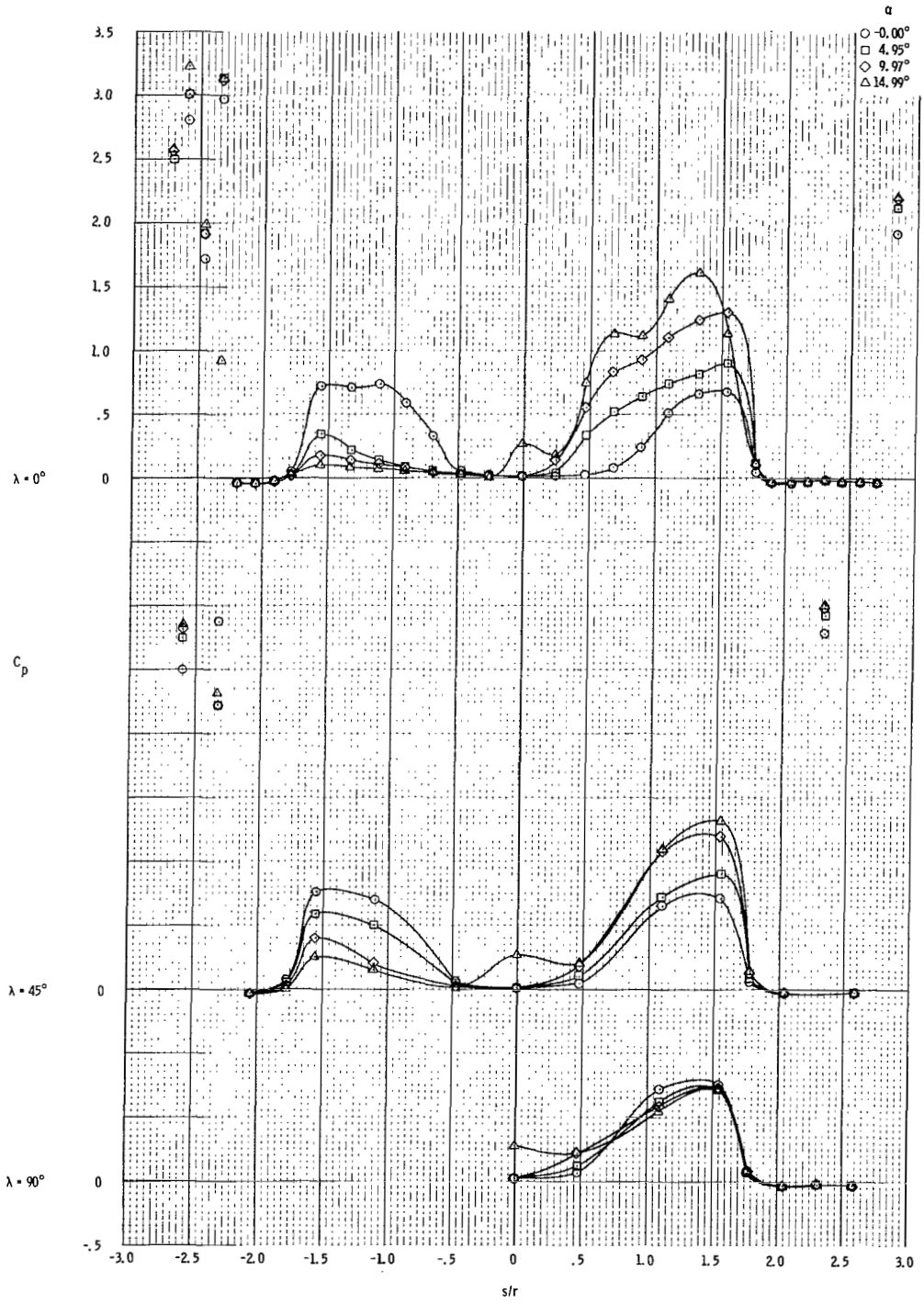

(a) α range is from 0° to 15°.

Figure 17. - Variation of C_p with increasing α at $\lambda = 0°$, $\lambda = 45°$, and $\lambda = 90°$ at M = 5.01. Data are for the command module only, in the presence of the escape tower and the rocket.

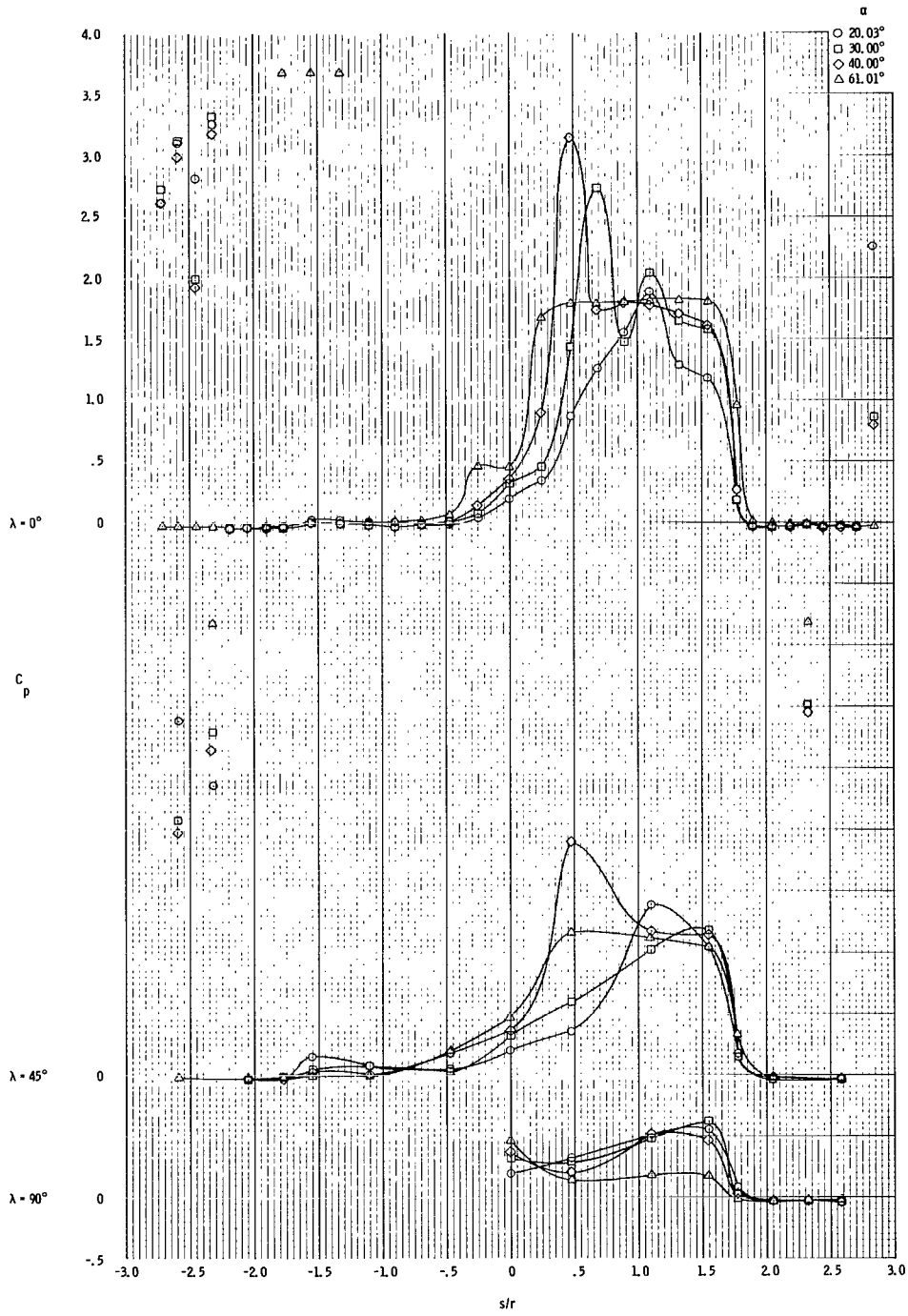

(b) α range is from 20° to 61°.

Figure 17. - Continued.

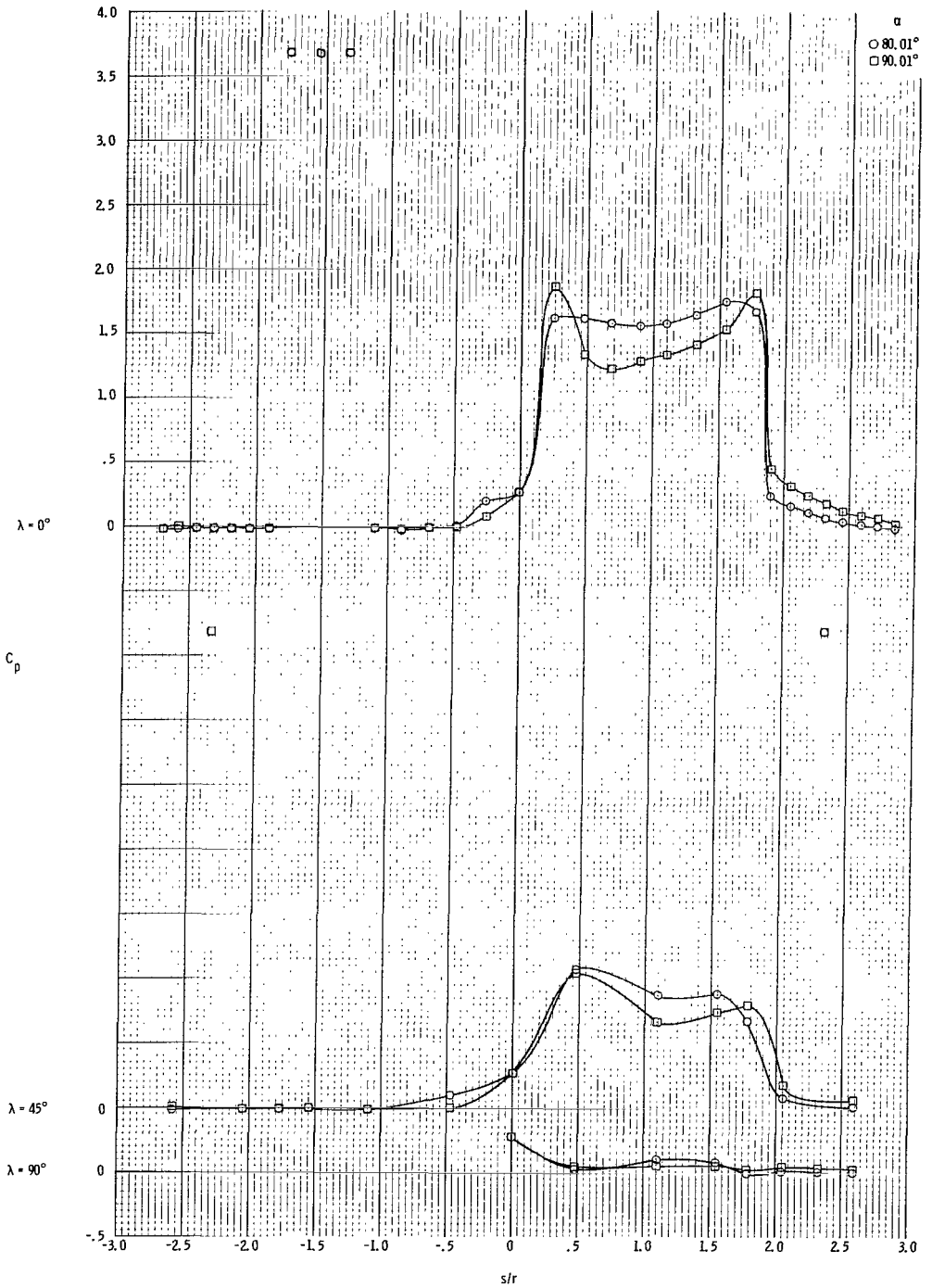

(c) α range is from 80° to 90°.

Figure 17. - Concluded.

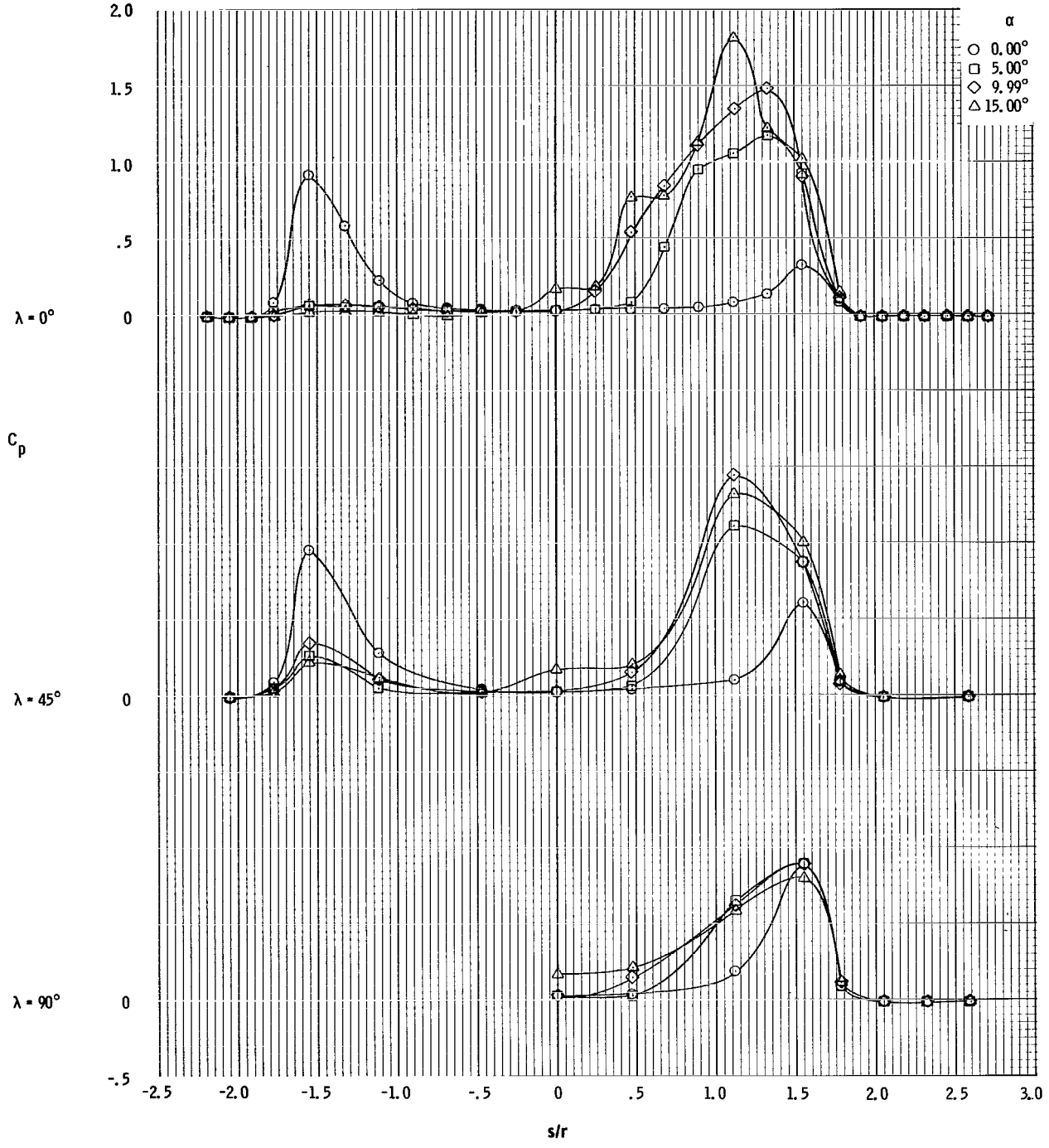

(a) α range is from 0° to 15°.

Figure 18. - Variation of C_p with increasing α at $\lambda = 0°$, $\lambda = 45°$, and $\lambda = 90°$ at M = 7.35. Data are for the command module only, in the presence of the escape tower and the rocket.

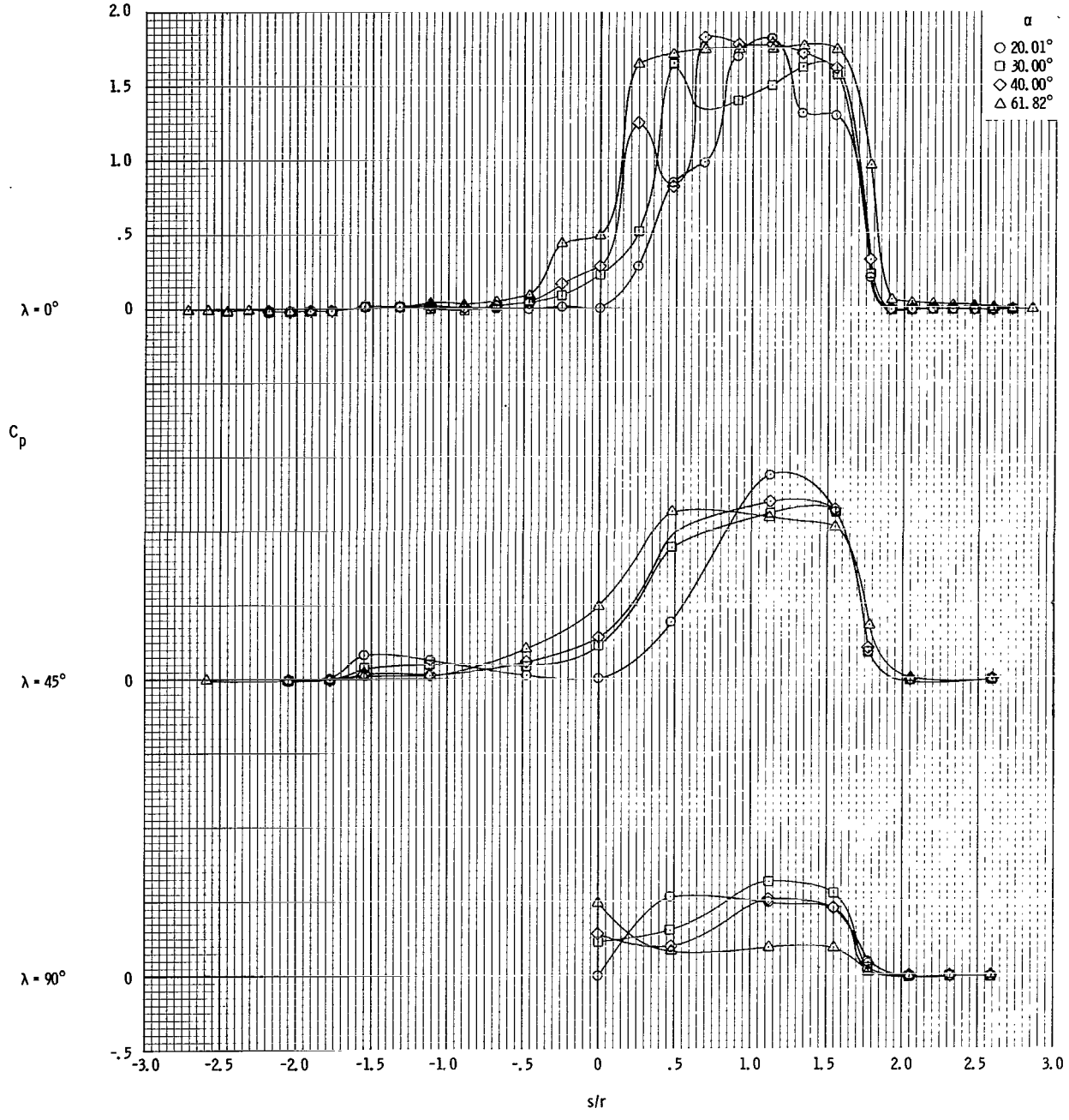

(b) α range is from 20° to 61°.

Figure 18. - Continued.

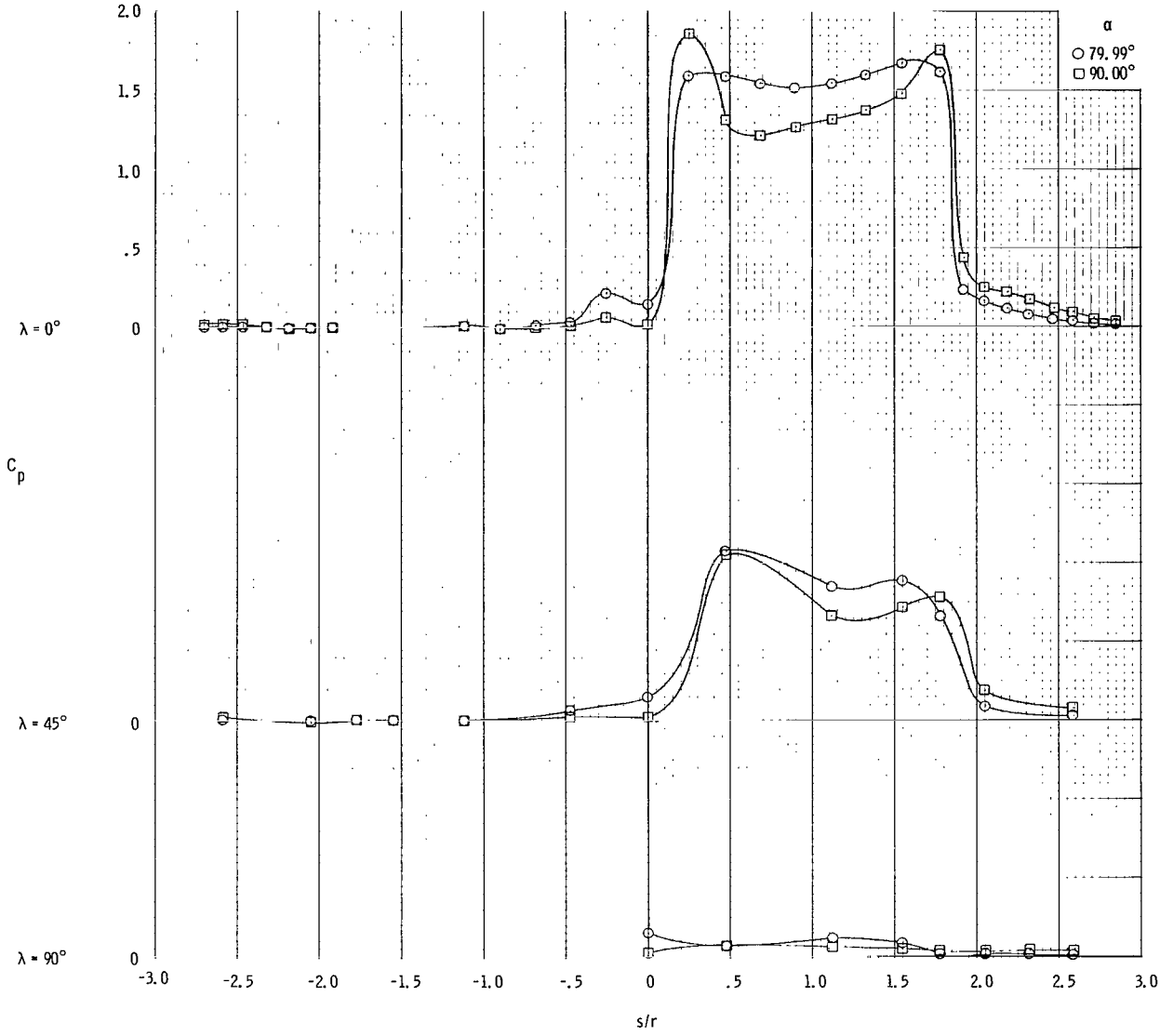

(c) α range is from 80° to 90°.

Figure 18. - Concluded.

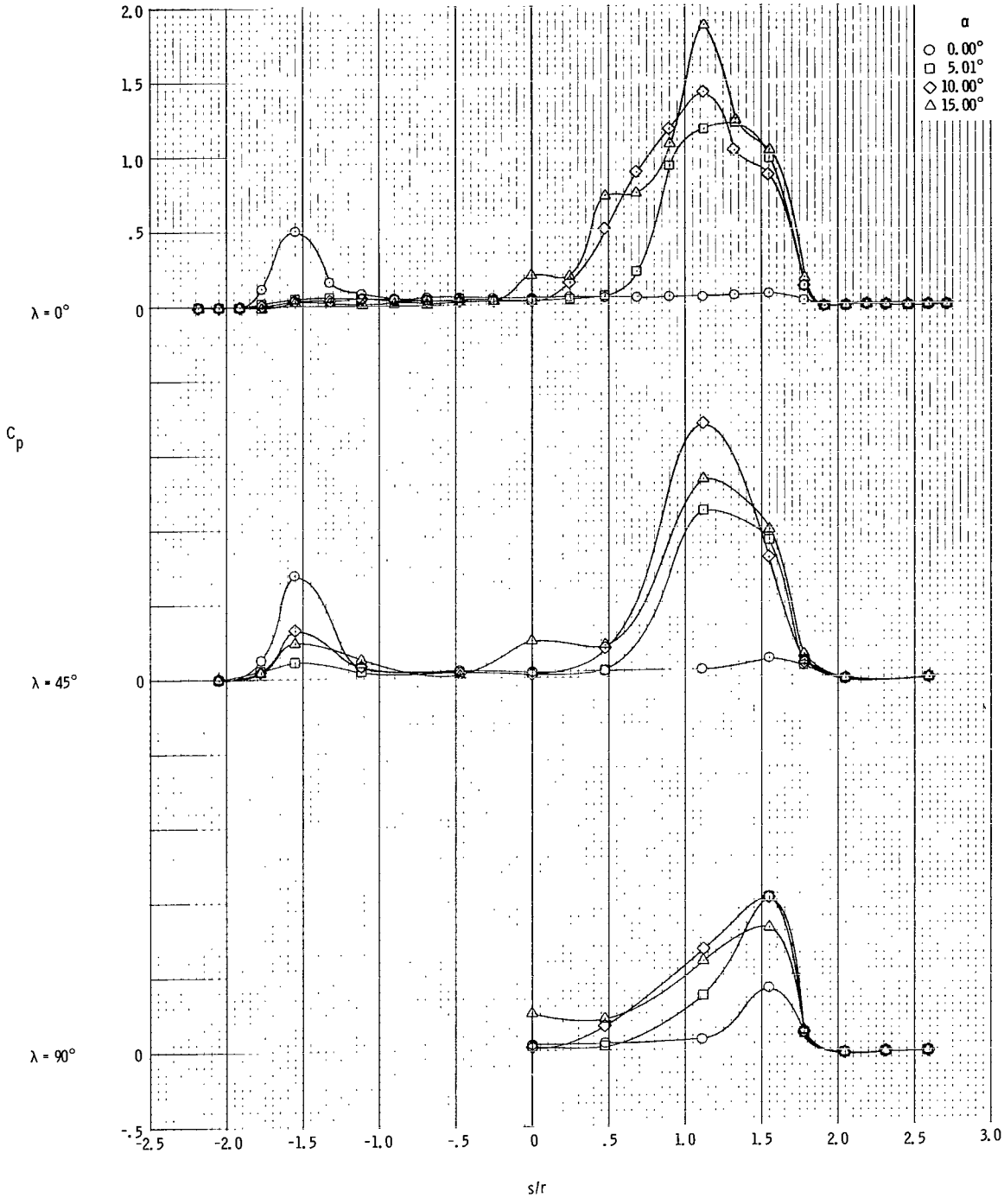

(a) α range is from 0° to 15°.

Figure 19. - Variation of C_p with increasing α at $\lambda = 0°$, $\lambda = 45°$, and $\lambda = 90°$ at M = 9.08. Data are for the command module only, in the presence of the escape tower and the rocket.

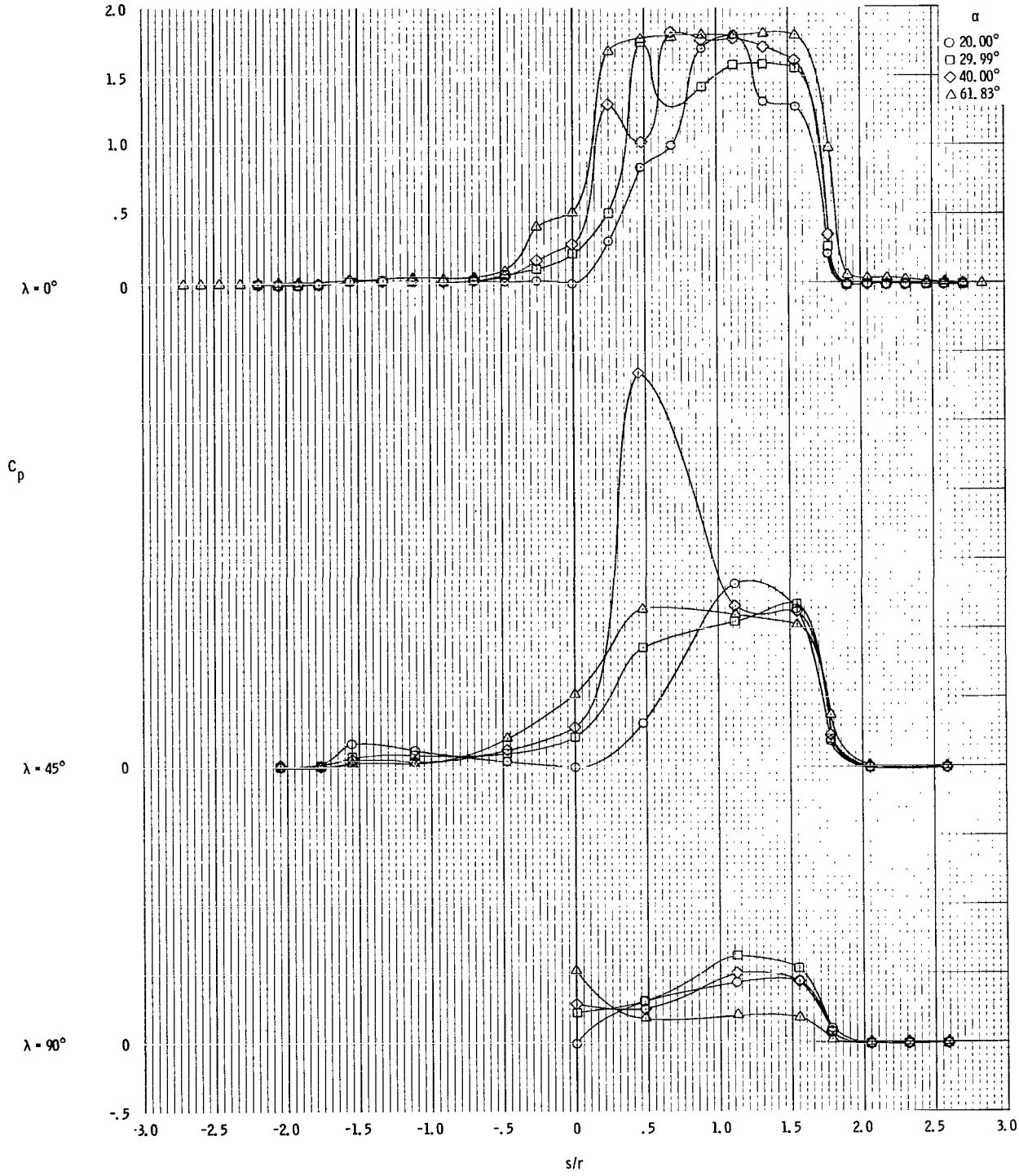

(b) α range is from 20° to 61°.

Figure 19. - Continued.

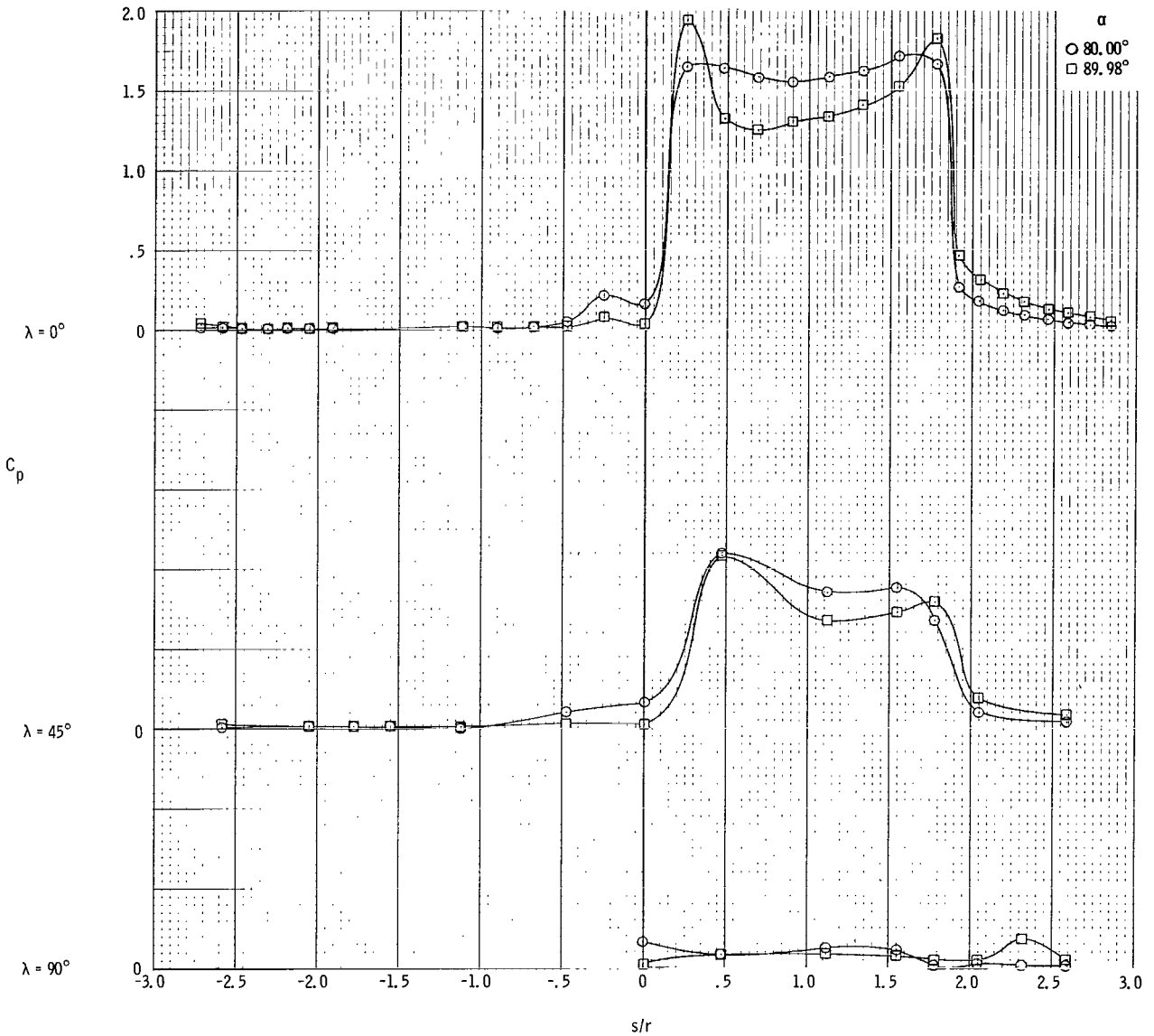

(c) α range is from 80° to 90°.

Figure 19. - Concluded.

NASA-Langley, 1970 —— 1 S-230